

**Preparative Chromatographic Separation of Ternary
Mixtures - Analysis of Fractionation Times and Novel
Concepts**

Dissertation

zur Erlangung des akademischen Grades

Doktoringenieur

(Dr.-Ing.)

von: M.Sc. Balamurali Sreedhar

geboren am: 12. Februar 1982

in: Thiruvalla (Kerala, Indien)

genehmigt durch die Fakultät für Verfahrens- und Systemtechnik
der Otto-von-Guericke Universität Magdeburg.

Gutachter Prof. Dr.-Ing. habil. Andreas Seidel-Morgenstern

Prof. Dr. habil. Atilla Felinger

Prof. Dr.-Ing. habil. Evangelos Tsotsas

eingereicht am: 4. Oktober 2010

Promotionskolloquium am: 17. Dezember 2010

Acknowledgments

This thesis originated during my tenure as a research assistant at the Max Planck Institute for Dynamics of Complex Technical Systems in Magdeburg.

My deepest sense of gratitude goes to my supervisor, Prof. Andreas Seidel-Morgenstern, who at the first place gave me a chance to work at the Max Planck Institute Magdeburg and to utilize its excellent research platform. I am immensely thankful to him for the endless support and encouragement I received since beginning, which enabled me to enhance my knowledge in the field greatly. In addition, working under Prof. Seidel-Morgenstern also enabled me to explore the local culture and customs in great depth, which I have always cherished.

I am sincerely thankful to Prof. Atilla Felinger and Prof. Evangelos Tsotsas for reviewing this thesis.

I am indebted to Dr. Annegret Wagler for all the mathematical knowhow, which forms an integral part of this work. Her constant supervision and cheerful support are greatly appreciated. I am also thankful to Dr. Malte Kaspereit for all the valuable discussions. I would also like to thank Dr. Barbara Witter for the support provided.

Help from the members of the Physical and Chemical Fundamentals of Process Engineering group, especially Jacqueline Kaufmann is very much appreciated. This thesis would not have been possible without the funding from Max Planck Gesellschaft, International Max Planck Research School, Magdeburg and the state of Saxony-Anhalt. I would also like to thank Bischoff Chromatography, Leoneberg, Germany for the generous gift of a POPLC Kit.

I am also very grateful to all my friends who made life in the institute and Magdeburg in general a pleasurable experience. Finally, I want to thank my wife Meera for all the patience and support.

Abstract

Preparative chromatographic techniques are widely employed today in pharmaceutical and biochemical industries. Optimal isolation of a target component with high purity is of significant importance in a sector with continuously increasing quality standards. The components of interest are often part of complex mixtures. Over the years, preparative batch chromatography has been successfully used to isolate target components from multi-component mixtures. It has been demonstrated frequently that by exploiting certain additional operational aspects, the separation performance of classical methods could be further enhanced. In this thesis, novel operating modes derived from classical schemes are evaluated focusing on the optimal separation of specific target components from multi-component mixtures.

Initially, a general framework has been provided for finding the critical fractionation or cut-times required to evaluate performance. New strategies were developed to find the cut-times based on a discrete and a continuous approach. The efficiency of these methods was compared with that of a widely implemented algorithm based on the evaluation of local purities. The robustness of the methods was analyzed using two theoretical case studies.

In the next part, the separation potential of a new scheme involving an initial solvent gradient and closed-loop recycling has been evaluated. Using specific objective functions, the separation performance of this new concept was compared with those of conventional operational modes. The new scheme showed an enhanced separation performance when the selectivities of the target component with respect to the neighboring components decreased with increase in elution strength.

In the final part, a concept of coupling chromatographic segments with different stationary phases has been extended to preparative applications using a theoretical study. The relative lengths and order of the segments were found to have a significant influence on the performance of separating an intermediately eluting component. Extending this concept to a mixed mode configuration resulted in an improved separation performance. The trends seen in the theoretical study were demonstrated experimentally using a test system. Adsorption isotherm data was measured and later used to quantify the sensitivity of optimal relative segment lengths on isotherm non-linearities. Rather than the factors inducing non-linearities themselves, their differences were found to have a larger influence on optimal separation.

Zusammenfassung

Die präparative Chromatographie ist heutzutage eine weit verbreitete Technik in der pharmazeutischen und biochemischen Industrie. Eine optimale Isolation von Zielkomponenten mit hoher Reinheit ist aufgrund stetig steigender Qualitätsstandards von großer Bedeutung. Erschwerend ist die Tatsache, dass das gewünschte Produkt meist in einem komplexen Gemisch vorliegt. Bislang konnte die präparative Batch-Chromatographie erfolgreich zur Isolierung von Zielsubstanzen aus Gemischen mehrerer Stoffe eingesetzt werden. Es wurde jedoch häufig gezeigt, dass neben der Änderung üblicher Parameter eine Verbesserung der Trennleistung klassischer Methoden zusätzlich durch Variation weiterer Prozessparameter erreicht werden kann. In dieser Arbeit werden auf der Grundlage klassischer chromatographischer Prozessführungen neuartige Konzepte untersucht. Hierzu steht die optimale Abtrennung einer bestimmten Zielsubstanz aus einem Mehrkomponentensystem im Mittelpunkt.

Zunächst wurde ein verallgemeinerter theoretischer Ansatz formuliert auf dessen Grundlage neue Strategien zur Ermittlung kritischer Fraktionierungszeiten entwickelt wurden. Diese sind notwendig zur Bestimmung der Leistungsindizes. Die Effizienz der untersuchten Methoden wurde durch einen Vergleich mit den Ergebnissen eines weit verbreiteten, auf der Auswertung lokaler Reinheiten basierenden Algorithmus bewertet. Anhand zweier theoretischer Fallbeispiele wurde die Robustheit der neuen Methoden analysiert.

Im zweiten Teil dieser Arbeit wurde das Trennpotenzial einer neuen Verfahrensvariante untersucht, die Gradientenchromatographie mit „Closed-Loop Recycling“ kombiniert. Die Trennleistung des neuen Konzeptes wurden unter Verwendung spezifischer Zielfunktionen mit der konventionellen Betriebsweise verglichen. Die neuartige Betriebsweise zeigte eine verbesserte Trennleistung für den Fall einer Abnahme der Selektivitäten der Zielkomponente zu den benachbarten Substanzen bei zunehmender Elutionsstärke.

Der letzte Teil befasst sich zunächst mit einer theoretischen Studie, um das Konzept gekoppelter Segmente mit unterschiedlichen stationären Phasen auch für den präparativen Maßstab nutzbar zu machen. Es konnte gezeigt werden, dass die relative Länge sowie die Reihenfolge der einzelnen Segmente einen großen Einfluss auf die Trennleistung eines intermediär eluierenden Stoffes haben. Eine Erweiterung dieses Konzeptes stellt das homogene Vermischen verschiedener stationärer Phasen dar, wodurch die Trennleistung weiter erhöht werden konnte. Die in der theoretischen Betrachtung auftretenden Tendenzen wurden durch Untersuchungen mit einem Testsys-

tem experimentell bestätigt. Adsorptionsisothermen wurden gemessen und anschließend für die Quantifizierung der Sensitivität der optimalen relativen Segmentlängen hinsichtlich der Nichtlinearität der Isotherme verwendet. Dabei konnte u.a. gezeigt werden, dass nicht die Faktoren, die für die Nichtlinearität verantwortlich sind, sondern deren Differenzen einen Einfluss auf die optimale Trennleistung haben.

Contents

1	Introduction	1
1.1	Background	2
1.2	Principle of chromatography	2
1.3	Recycling chromatography	4
1.4	Gradients in chromatography	5
1.4.1	Solvent gradients	5
1.4.2	Chromatography using multiple stationary phases	7
1.5	Modeling, performance evaluation and optimization	8
2	Scope of the thesis	11
3	Theory	13
3.1	Modeling chromatographic processes	13
3.1.1	Craig model	14
3.1.2	Ideal and equilibrium dispersive models	15
3.2	Model parameters	17
3.2.1	Column porosities and efficiency	17
3.2.2	Adsorption isotherms	19

3.2.3	Determination of adsorption isotherms	21
3.2.3.1	Frontal analysis	22
3.2.3.2	Perturbation method	23
3.2.3.3	Elution by characteristic point	25
3.2.3.4	Inverse method	25
3.3	Numerical solution of model equations	25
3.4	Performance parameters	27
3.5	Optimization of parameters	28
3.5.1	Optimizers	30
4	Optimization of cut-times in preparative chromatography	33
4.1	Approaches to find cut-times	33
4.1.1	Discrete cut-time optimization	35
4.1.1.1	By evaluating local purities	35
4.1.1.2	Optimization using binary variables	36
4.1.2	Continuous cut-time optimization	38
4.2	Comparison of methods	39
4.2.1	Symmetric case	39
4.2.2	Non-linear case	42
4.3	Conclusions	46
5	Theoretical study using closed-loop recycling with an initial	

gradient	47
5.1 Introduction	47
5.2 Closed-loop recycling with an initial gradient	49
5.3 Adsorption equilibria	51
5.4 Column model and numerical solution	53
5.5 Operating parameters and objective functions	54
5.6 Optimization	56
5.7 Results and discussion	57
5.7.1 <i>Convergent-convergent</i> case	57
5.7.2 Comparison in a wider parameter range	62
5.7.2.1 Role of regeneration time	63
5.7.3 <i>Convergent-divergent</i> case	64
5.7.4 <i>Divergent-convergent</i> case	67
5.8 Conclusions	68
6 Theoretical study of ternary separations using multiple stationary phases	71
6.1 Introduction to the separation problem	71
6.2 Theory	72
6.2.1 Column model and isotherm parameters	73
6.2.2 Objective functions and operating parameters	75
6.2.3 Parametric study and optimization	76

6.3	Results and discussions	77
6.3.1	<i>Case I</i>	77
6.3.2	<i>Case II</i>	81
6.3.3	<i>Case III</i>	83
6.4	Mixed mode operation	87
6.5	Role of selectivity reversals	88
6.6	Conclusions	91
7	Experimental demonstration and illustration of theoretical tools	93
7.1	Introduction	93
7.2	Experimental system	93
7.3	Demonstration of trends	94
7.4	Quantitative analysis	97
7.4.1	Adsorption isotherms	97
7.4.2	Application of adsorption isotherm parameters to determine sensitivity to non-linearities	101
7.5	Conclusions	103
8	Summary and conclusions	107
A	Detector calibration and peak deconvolution	111
A.1	Detector calibration	111

A.2 Finding calibration factors	111
A.3 Peak deconvolution	112

References	115
-------------------	------------

List of Figures

1.1	Principle of chromatography	3
1.2	The principle of closed-loop isocratic recycling; (a) Elution mode : Valves V1 and V2 in open loop configuration to facilitate one pass elution (b) Recycle mode : V1 and V2 switched to realize closed-loop formation	4
1.3	Simulated column outlet concentration profiles for isocratic elution of a ternary mixture (dashed lines) compared to elution with a linear solvent gradient (solid lines), the modifier concentration changes between $t_{g,start}$ and $t_{g,end}$ from $C_{mod,start}$ to $C_{mod,end}$	6
3.1	Craig model: step 1) solute injected into first stage. Step 2) after equilibration, v_m amount of liquid transferred into next stage, same amount removed from last stage. Step 3) process repeated until all solutes have left the column	15
3.2	a) Single component Langmuir adsorption isotherm b) Resulting linear and non-linear concentration profiles	20
3.3	Illustration of a typical frontal analysis experiment for Cyclopentanone on a ProntoSIL C18 [80x3mm] column. Mobile phase : 35/65 Methanol/Water, $\dot{V}_f=0.5$ ml/min.	23
3.4	An example of perturbation method with a ternary mixture	24
3.5	Fractionation of the intermediately eluting component ($i=2$) from a ternary mixture	27
3.6	Different optimization approaches for a PDE constrained problem [78, 79]	29

4.1	Contours of the objective function (thick lines) and the purity constraint (thin line), corresponding to the chromatogram in figure 3.5	34
4.2	Local purity (Pu_{loc}) of the target component against time. $t_1^0 - t_2^0$: interval in which $Pu_{loc} \geq Pu_{lim}(0.99)$	35
4.3	Trajectory taken by the algorithm when expanding in both directions (thick gray line). Dashed segment : terminal step when $Pu_{des,2} < Pu_{lim} = 0.99$	36
4.4	Symmetric chromatograms with middle component as target (thick line) generated by the Lorentzian function 4.8. Parameters from table 4.1	39
4.5	Influence of the degree of discreteness on the performance of different optimization approaches	42
4.6	Sample preparative chromatograms simulated with $a_1 = 13.33$, $a_2 = 20.00$, $a_3 = 30.00$. Other parameters from table 4.2. Time discretization points of the chromatogram (numerical solution of ED model, see section 3.3) changed by varying the Courant number between 1.5 and 2.5	44
4.7	Influence of the degree of discreteness (N_t) on the performance of different optimization approaches, using an asymmetric overloaded chromatogram (figure 4.6)	45
5.1	Simulated concentration profiles for a closed-loop recycling configuration (see figure 1.2). The intermediate part of the profiles containing the second (target) component is recycled until the required purity and yield are achieved	48
5.2	Simulated concentration profiles at the outlet of the column for closed loop recycling with initial gradient (CLR-G) using 4 cycles (Conditions : $L_{f,tot} = 18$, $G = 3$ %/min, other parameters from Table 5.2).	50
5.3	Dependencies of adsorption isotherm parameter a_i (equations 3.28 and 3.29) on modifier volume fraction C_{mod} ; <i>convergent-divergent</i> case, (parameters from Table 5.1)	53

5.4	Illustration of linear modifier gradients with different slopes (G in %/min)	55
5.5	Optimal front plot: Pr_2 v/s Y_2 ; Convergent - convergent case	58
5.6	Decision variables corresponding to the optimal front plot (figure 5.5) for the <i>convergent-convergent</i> case	59
5.7	Elution profiles at the column outlet for the four operation modes considering the <i>Convergent-convergent</i> case with optimized parameters corresponding to a yield around 99.5%; enlarged squares in figures 5.5 and 5.6 (other standard parameters from table 5.2)	61
5.8	Comparison of CLR-ISO and CLR-G schemes; production rates (solid lines) and number of cycles required (dashed lines) for the <i>convergent-convergent</i> case: CLR-ISO with $C_{mod} = 44$ (black) and CLR-G with $G = 2.5$ (gray) , other parameters from Table 5.2	62
5.9	Dependence of production rate on the regeneration factor (r_f); in accordance with equations 3.37,5.10 and 5.11	63
5.10	Optimal fronts plot: Pr_2 v/s Y_2 ; Convergent - convergent case; isocratic modes without regeneration ($r_f=0$) and gradient modes with longer regeneration time ($r_f=5$)	64
5.11	Optimal fronts plot: Pr_2 v/s Y_2 ; Convergent - divergent case .	64
5.12	Decision variables corresponding to the optimal fronts plot (Figure 5.11) for the <i>convergent-divergent</i> case	66
5.13	Optimal fronts plot: Pr_2 v/s Y_2 ; Divergent - convergent case .	67
5.14	Decision variables corresponding to the optimal fronts plot (Fig. 5.13) for the <i>divergent-convergent</i> case	68
6.1	Preparative isolation of a target component by serially coupling two chromatographic segments.	72

6.2	Scheme representing preparative separation of a ternary mixture for two cases of different adsorption isotherm sets (a and b).	73
6.3	<i>Case I</i> : Pr_2Y_2 plot in $V_{inj} - x_A$ space for the two segment orders, other parameters from Tables 6.1 and 6.3	77
6.4	<i>Case I</i> : Elution profiles for the optimal parameters (see Table 6.5)	80
6.5	Effective separation factors of the serial assembly as a function of relative segment lengths, equation (6.3). Optimal values of $\alpha_{i,k,eff}$ for preparative case ($x_A = 0.3132$ for A-B and $x_A = 0.4626$ for B-A) different from that of analytical case ($x_A = 0.4260$)	81
6.6	<i>Case II</i> : Pr_2Y_2 plot in $V_{inj} - x_A$ space for the segment order A-B, other parameters from Tables 6.1 and 6.3	82
6.7	Linear case: elution profile of the 7 components in the linear range for both segment orders, with $b_{i,j} = 0$ l/g, $V_{inj} = 0.01$ ml and $x_a = 0.5$. Other parameters from Tables 6.2 and 6.3	83
6.8	<i>Case III</i> : Pr_2Y_2 plot in $V_{inj} - x_A$ space for both segment orders, other parameters from Tables 6.2 and 6.3	84
6.9	<i>Case III</i> : Elution profiles of order A-B for the optimal case (component 2) in Table 6.7, $V_{inj} = 0.0090$ ml, $x_A = 0.0686$ with $Pr_2Y_2 = 93.6668$ $\mu\text{g}/\text{cm}^2$ min. Parameters from Tables 6.2 and 6.3	85
6.10	<i>Case III</i> : Pr_3Y_3 plot in $V_{inj} - x_A$ space for both segment orders, other parameters from Tables 6.2 and 6.3	86
6.11	<i>Case III</i> : Elution profiles of order A-B for the optimal case (component 3) in Table 6.8, $V_{inj} = 0.0090$ ml, $x_A = 0.1599$ with $Pr_3Y_3 = 51.9097$ $\mu\text{g}/\text{cm}^2$ min. Parameters from Tables 6.2 and 6.3	87
6.12	Mixed mode with <i>Case I</i> : Pr_2Y_2 plot in the $V_{inj} - y_A$ space with maximum $Pr_2 = 6506.58$ $\mu\text{g}/\text{cm}^2\text{min}$ and $Y_2 = 0.9437$. Other parameters from tables 6.3 and 6.4).	88

6.13	Influence of selectivity reversals: (a) <i>Case I-A</i> : serial coupling A-B (b) <i>Case I-A</i> : mixed mode (c) <i>Case I-B</i> : serial coupling A-B (d) <i>Case I-B</i> : mixed mode	90
6.14	Example of extreme selectivity reversal: (a) serial coupling A-B (b) mixed mode. For $a_{2,A}, a_{2,B} = 5$, $\alpha_{1,2,A}=\mathbf{0.7}$, $\alpha_{2,3,A}=2.0$, $\alpha_{1,2,B}=2.0$ and $\alpha_{2,3,B}=1.1$	91
7.1	Separation of a small ($V_{inj}=2\mu\text{l}$, black lines) and overloaded ($V_{inj}=30\mu\text{l}$, gray lines) injection sample using C18 and EPS segments	95
7.2	Separation of a small ($V_{inj}=2\mu\text{l}$, black lines) and overloaded ($V_{inj}=30\mu\text{l}$, gray lines) injection sample using C18 and EPS segments. Solid lines: segment order C18-EPS, dashed lines: segment order EPS-C18. Total segment length = 8 cm.	96
7.3	Breakthrough curve for C6 to determine initial values of q_{sat}	99
7.4	Evaluation of isotherm parameters by inverse method: fit of experimental and simulated detector response for a flowrate of $\dot{V}_f=0.5\text{ ml/min}$	100
A.1	Single component pulse injection responses for calculating $k_{f,i}$ on EPS column	112
A.2	Calibration curves at different wavelengths	112
A.3	An example of deconvolution of concentration profiles (three components) from total detector response	114

List of Tables

4.1	Parameters used for the chromatograms given in figure 4.4 . . .	40
4.2	Parameters used to simulate the preparative chromatogram in figure 4.6	44
5.1	Adsorption isotherm parameters of equations 3.28 and 3.29, for three different cases (see Figure 5.3 for illustration)	52
5.2	Parameters of the chromatographic system analyzed	53
5.3	Degrees of freedom considered for the four operational modes (fixed: $C_{mod,start}$, $C_{mod,end}$, $t_{g,start}$)	57
6.1	Adsorption isotherm parameters of equation (6.2), for ternary mixtures of <i>case I</i> and <i>case II</i> , see Fig. 6.14 for illustration . .	74
6.2	Adsorption isotherm parameters of equation (6.2), a 7 component mixture <i>case III</i> , $a_{i,j}$ values from Nyiredy et al. [50] and calculated $b_{i,j}$ values for $q_{sat} = 50$ [g/l]	75
6.3	Parameters of the chromatographic system analyzed	76
6.4	Solver settings used for MATLAB Genetic Algorithm Toolbox	77
6.5	<i>Case I</i> : Optimal values of Pr_2Y_2 for the combination and individual segments ($x_A \in \{0, 1\}$), along with the resulting parameters. Optimized using GA Toolbox (settings from Table 6.4)	78
6.6	<i>Case II</i> : Optimal values of Pr_2Y_2 for the combination and individual segments ($x_A \in \{0, 1\}$), along with the resulting parameters. Optimized using GA Toolbox (settings from Table 6.4)	82

6.7	<i>Case III</i> , component 2 : Optimal values of Pr_2Y_2 for the combination and individual segments ($x_A \in \{0, 1\}$), along with the resulting parameters. Optimized using GA Toolbox (settings from Table 6.4)	85
6.8	<i>Case III</i> , component 3 : Optimal values of Pr_3Y_3 for the two segment orders and the resulting parameters, using GA Toolbox (settings from Table 6.4)	86
6.9	Isotherm parameters for minor selectivity reversals	89
7.1	Retention parameters of C6, Ph and C7 from single component injections on C18 and EPS stationary phases at $\dot{V}_f=0.5$ ml/min	98
7.2	Saturation capacity (q_{sat}) estimates [mg/ml] for initial values in the inverse method	99
7.3	Parameters determined by the inverse method, corresponding to figure 7.4, with $b_i = a_i/q_{sat}$	101
7.4	Isotherm parameter b_i [ml/mg] and chromatogram non-linearity parameter ($\bar{\lambda}_i$) of the ternary system for $C_{inj,i} = 20$ mg/ml . .	102
7.5	Dependency of optimal $Pr_{Ph}Y_{Ph}$ [$\mu\text{g}/\text{cm}^2\text{min}$], V_{inj} [ml], x_{C18} and segment order isotherm non-linearities (q_{sat}). Light gray cells : $q_{sat,C18}/q_{sat,EPS} = 2$. Dark gray cells : $q_{sat,C18}/q_{sat,EPS} = 0.5$. See table 7.4 for the corresponding b_i values and chromatogram non-linearity parameters ($\bar{\lambda}_i$).	104

Notations

a_{1i}	Adsorption isotherm parameter in equation (3.28) [/ % C_{mod}]
a_{2i}	Adsorption isotherm parameter in equation (3.28)
A_{col}	Cross sectional area of the column [cm ²]
a_{cou}	Courant number
a_i	Henry coefficient of component i
b_{1i}	Adsorption isotherm parameter in equation (3.29) [1/g % C_{mod}]
b_{2i}	Adsorption isotherm parameter in equation (3.29)
b_i	Langmuir adsorption isotherm parameter of component i [1/g]
$C_{inj,i}$	Injected concentration of i [g/l]
C_i	Concentration of the i^{th} component in the mobile phase [g/l]
$C_{mod,end}$	Modifier volume fraction at gradient end [%]
$C_{mod,start}$	Modifier volume fraction at gradient start [%]
C_{mod}	Modifier volume fraction in an isocratic case [%]
C_{thr}	Threshold concentration for fractionation [mg/ml]
$D_{app,i}$	Axial dispersion of component i [cm ² /min]
d_c	Inner diameter of the column [cm]
F	Phase ratio
G	Gradient slope, see equation (5.7) [%modifier /min]
HETP	Height equivalent theoretical plate [cm]
h_i	Height of the peak i in Lorentzian function, equation (4.8)
k	Number of exchange steps in Craig model
L	Total length of the chromatographic column [cm]
$L_{f,i}$	Loading factor of component i [%]

$L_{f,tot}$	Total loading factor	[%]
l_j	Length of segment j , $j \in A, B$, chapter 6	[cm]
m_i	Amount of i collected	[mg]
N	Number of theoretical plates or stages	
N_c	Number of components	
N_t	Number of time steps	
N_{cyc}	Number of cycles	
Pr_i	Production rate of i	[mg/cm ² min]
$Pu_{loc,i}^k$	Local purity of component i at time step k	
Pu_i	Purity of component i	
Pu_{lim}	Purity limit constraint e.g equation (4.2)	
q_i	Concentration of the i^{th} component in the stationary phase	[g/l]
q_{sat}	Saturation capacity of the stationary phase	[g/l]
r_f	Regeneration factor, see equation (5.11)	[-]
S	Total detector response	[mAU]
t	Time	[min]
t_0	Dead time of the column	[min]
t_1	Cut-time start	[min]
t_2	Cut-time end	[min]
$t_{cut1,r}$	First fractionation point of the r^{th} cycle	[min]
$t_{cut2,r}$	Second fractionation point of the r^{th} cycle	[min]
t_{cyc}	Cycle time	[min]
t_{dead}	Dead time of the plant	[min]
$t_{g,end}$	Gradient end time	[min]
$t_{g,start}$	Gradient start time	[min]
$t_{inj,end,j}$	Injection end time for segment j , chapter 6	[min]
$t_{inj,end,r}$	Injection end time for the r^{th} cycle, chapter 5	[min]

$t_{inj,start,j}$	Injection start time for segment j , chapter 6	[min]
$t_{inj,start,r}$	Injection start time for the r^{th} cycle, chapter 5	[min]
t_{inj}	Injection time (of a pulse)	[min]
$t_{r,i}$	Retention time of component i	[min]
t_{rec}	Residence time in the recycle loop	[min]
t_{reg}	Regeneration time	[min]
u	Interstitial mobile phase velocity	[cm/min]
u_c	Velocity of a component associated with a given concentration	[cm/min]
\dot{V}_f	Volumetric mobile phase flow rate	[ml/min]
v_{col}	Column volume	[ml]
v_{inj}	Volume injected	[ml]
v_m	Interstitial volume	[ml]
v_{pore}	Pore volume in a particle	[ml]
v_{st}	Volume of porous stationary phase	[ml]
v_s	Volume of solid	[ml]
$w_{1/2,i}$	Width of the peak at half height	[min]
X	Vector of design variables	
x^k	Binary variable ($x^k \in \{0, 1\}$), see section 4.1.1.2	
x_j	Relative length of segment j , $j \in \{A,B\}$, see section 6.2.2	
Y_i	Recovery yield of i	
y_j	Mix ratio of segment j , $j \in \{A,B\}$, see section 6.4	
z	Space co-ordinate	[cm]

Greek symbols

$\alpha_{i,j}$	Separation factor between components i and j	
Δt	Time step length	[min]
Δz	Space step length	[min]

ϵ	Total porosity of the column
ϵ_{int}	Interstitial porosity of the column
$\bar{\lambda}_i$	Chromatogram non-linearity parameter of component i
λ	Wave length
σ_i	Peak breadth parameter for i , equation (4.8) [min]

Superscripts

k	Time index
k_1	Time index corresponding to t_1
k_2	Time index corresponding to t_2
max	Maximum value

Subscripts

exp	Experimental
i	Component index
j	Stationary phase index
p	Space index
r	Cycle index
sim	Simulation

List of abbreviations

B-G	Batch gradient elution
B-ISO	Batch isocratic elution
C6	Cyclohexanone
C7	Cycloheptanone
CLR-G	Closed-loop recycling with an initial gradient
CLR-ISO	Isocratic close-loop recycling
ContOpt	Continuous optimization scheme for finding cut-times
EPS	Enhanced polar stationary phase
HETP	Height equivalent theoretical plate
HILIC	Hydrophilic interaction liquid chromatography
IEX	Ion exchange chromatography
LocPur	Cut-times finding algorithm based on the evaluation of local purities
MeOH	Methanol
MINLP	Cut-times finding algorithm based on Mixed Integer Non-linear Programming
NP	Normal phase
Ph	Phenol
RP	Reversed phase
SEC	Size exclusion chromatography

Chapter 1

Introduction

Chromatography in its current form originates from the separation experiments conducted by the Russian botanist M. Tswett in the early 1900s. He used a glass tube filled with calcium carbonate and organic solvents flowing through it to separate chlorophylls and carotenoids [1]. Since then, chromatography has evolved into an indispensable segment of separation sciences. In the course of the last century, the evolution of the technique saw emergence of many outstanding analytical methods based on the same principle, including gas chromatography and capillary electrophoresis. The most relevant advance with regard to this study has been the development of so called reversed phase (RP) and its implementation in the form of high performance liquid chromatography (HPLC) in the 1970s. Advancement to RP led to the use of aqueous mobile phases. In addition, use of small and uniform RP particles led to considerable reductions in the analysis time besides providing good reproducibility [2].

The focus of this study is to isolate an intermediately eluting target component from a complex multi-component mixture using non-continuous preparative chromatographic methods. In reality, many such problems can be envisaged as a ternary separation with the middle component forming the target. Hence, most of the separation problems considered in this study involve only three components. The fundamentals of different preparative chromatographic operation modes commonly used are explained in this chapter, followed by the scope of the thesis in chapter 2. More details about column modeling, adsorption isotherms, objective functions, formulation of optimization problems and their solutions are discussed in the theoretical chapter 3. An important aspect when calculating performance parameters in preparative chromatography is the identification of cut-times for the target component. A generalized approach to find optimal target cut-times from a multi component chromatogram is illustrated in chapter 4 along with a comparison of different approaches. The robustness and universal applicabilities of the methods are discussed. This is followed in chapter 5 by results from a new approach of combining closed-loop recycling with solvent gradient for the preparative ternary separation. In chapter 6, the potential of using multiple stationary phases in order to solve a separation problem is analyzed

theoretically. The final chapter discusses the experimental validation of using multiple stationary phases in the serially coupled configuration.

1.1 Background

The goal of isolating a target component from a multi-component mixture in larger (preparative) amounts can be achieved using a multitude of chromatographic methods. The choice usually depends on the complexity of the separation problem and the economic viability of the mode of operation under consideration. This chapter explains the fundamental chromatographic methods which form the basis of the more complex schemes used in the chapters to follow. The first section explains the fundamental concept behind a chromatographic separation in a classical batch operation mode. This is followed by the introduction of more advanced mode of implementing periodic operation to the system in the form of recycling chromatography. The concept of varying the solvent properties and the stationary phases to improve the separation performance are introduced in the last section.

1.2 Principle of chromatography

In the most basic setup, a typical chromatographic separation unit consist of a solid matrix which remains fixed or stationary. A solvent or mobile phase is continuously passed through this stationary phase at a constant velocity [3]. In liquid chromatography (LC), the mobile phase typically consists of a mixture of different solvents with varying polarities. Additionally, depending on the complexity of the separation problem and the objective, small quantities of other (separation) performance enhancing substances may be present in the mobile phase [4, 3]. On the other hand, in most of the LC applications, the stationary phase consists of spherical particles (size 2-50 μm depending on the application area [5]) packed into stainless steel tubes (called columns) of varying lengths and diameters. In the usual form of operation, the mixture of substances to be separated is dissolved in the mobile phase and are injected into the mobile phase stream over a fixed period of time at the column inlet. This sort of operation is called pulse injection.

The core separation principle behind any chromatographic separation is the differences in the degree of interaction between the components and the stationary phase in the presense of the corresponding mobile phase. As components move in the column with the mobile phase, due to the interaction differences, differences in their migration velocities arise. This in fact results in the separation of individual component bands or peaks. This basic operation mode with two components is illustrated in Figure 1.1

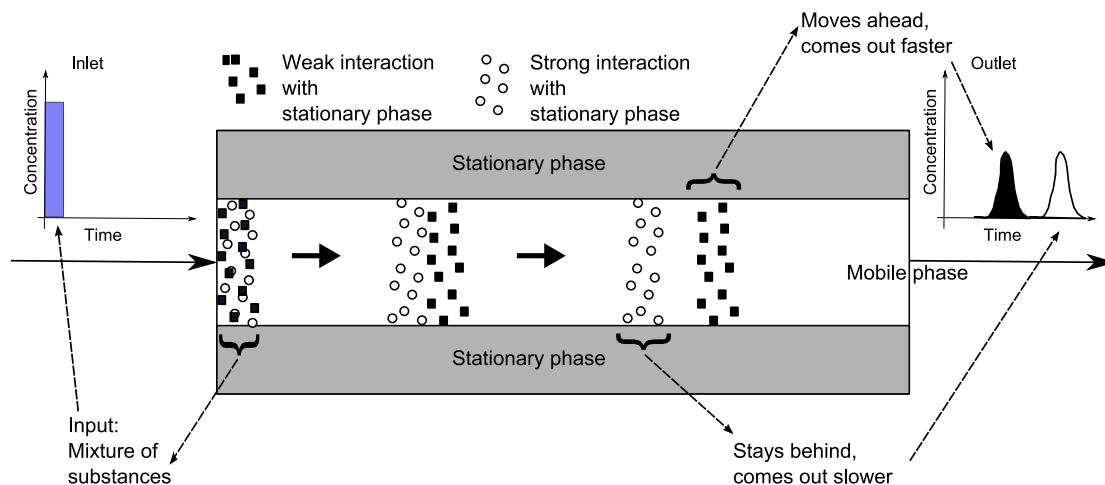


Figure 1.1: Principle of chromatography

As the components migrate through the column, those with strong interactions stay behind, whereas the others with lower interactions move faster. If this differences in speed is sufficient enough, the individual components can be collected at the outlet of the column at different time intervals. This mode of operation is known by the name batch elution or simply elution chromatography and the resulting concentration vs time data is known as the chromatogram or elution profile. It is also worth noting that in the process of elution, the components disperse in the column, resulting in lower concentration at the column outlet [6]. The degree of dispersion depends on a number of factors and its characterization, and estimation are discussed in the chapters to follow.

Based on the separation problem considered and the type of "interactions" involved, LC can be classified into many sub categories. A good review on the classification can be found in [3]. In the framework of this study, the focus will be on the widely applied category of adsorption chromatography employing the reversed phase (RP). RP chromatography employs a stationary phase usually made of silica particles with hydrophobic ligands grafted to the residual silanol group. With the stationary phase being non-polar, such a modification facilitates the use of an aqueous or polar mobile phase [7]. Irrespective of the type, the interaction between solute and the stationary phase in the given mobile phase environment can be characterized by adsorption isotherms. They quantify the relationship between the amount of components distributed between mobile and stationary phases. Moreover, adsorption isotherms of the components in a given stationary - mobile phase system form the primary knowledge base required to predict the migration and separation of the components. They are discussed in detail in chapter 4.

1.3 Recycling chromatography

Using conventional batch chromatography, the achievable separations are often insufficient. One trivial option to improve the separation is to increase the column length. This however also increases the amount of stationary phase needed and the pressure drop. For a given chromatographic set-up, there exists a finite maximum allowable pressure drop. A change in column dimension or flowrates has to respect this constraint.

An often practiced workaround for the problem of insufficient separation involves repeated recycling of certain fractions containing the target component until the required separation is reached. This mode of operation is called closed-loop recycling chromatography [8, 9]. Fig. 1.2 shows a schematic illustration of the concept implemented commonly today [10].

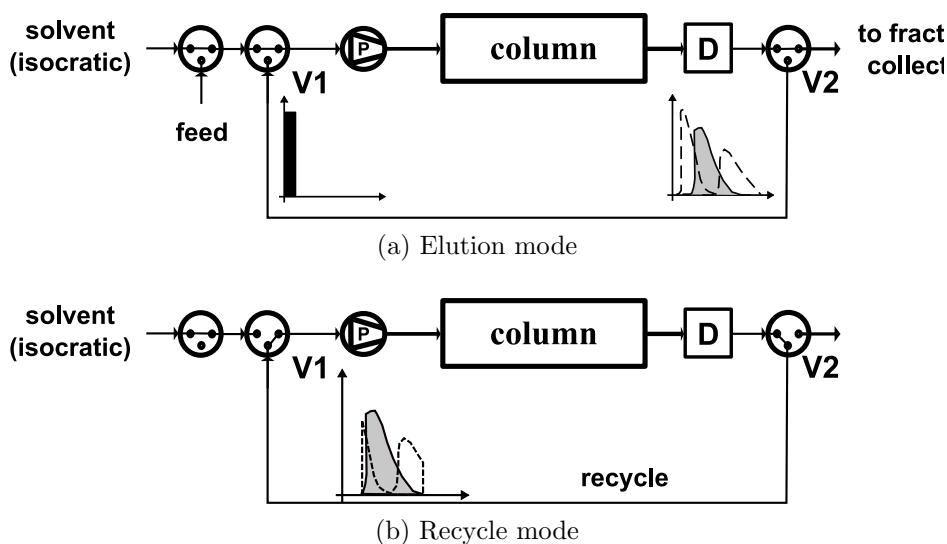


Figure 1.2: The principle of closed-loop isocratic recycling; (a) Elution mode : Valves V1 and V2 in open loop configuration to facilitate one pass elution (b) Recycle mode : V1 and V2 switched to realize closed-loop formation

The closed-loop recycling principle was successfully implemented based on isocratic conditions for example by Bombaugh and Levangie [8] and Biesenberger et al. [11]. Duvdevani et al. [12] suggested the principle of "alternate pumping and recycling" to avoid the periodic destruction of achieved separation by repeatedly transporting the recycle fraction through the pump. The key advantage of closed-loop recycling relies on the fact, that the available number of theoretical plates can be increased, i.e. additional separation could be achieved without increasing the actual length of the chromatographic column [9, 13, 14, 15]. Bailly and Tondeur [16, 17] and Crary et al. [18] simulated recycling chromatography using the ideal model of chromatography considering also injections of fresh feed in every cycle. This operation in-

volving periodic fresh feed injection evolved as the steady state recycling (SSR) chromatography [19]. Over the years, SSR chromatography has been implemented mainly for binary separations in a multitude of ways based on how the fresh feed is injected into the system [20, 21, 22, 23]. Recently, this concept was analyzed for a ternary separation involving nucleosides by Lee and Wankat [24].

Another significant advantage of recycling chromatography is that no fresh solvent is required during the recycling periods, offering the potential to reduce the overall solvent consumption [25]. Later in this study, the performance of closed-loop recycling operation in separating a ternary mixture is compared with other operation modes including the batch and gradient elution modes (see chapter 5).

1.4 Gradients in chromatography

The chromatographic separations discussed until now were explained considering a mobile phase with unchanged characteristics or properties. Such an operation under a constant 'elution strength' is called an isocratic operation. During such an operation, for a given system, components injected in small amounts migrate in the column with a constant speed. This characteristic however can be manipulated in our favor by changing a multitude of factors such as temperature, pH, mobile phase composition etc. The most prominent parameters among them when using RP chromatography is the solvent composition. The organic modifier content in the mobile phase stream can be varied with time to improve the separation performance. This kind of an operation is designated as solvent gradient. Another more recent and lucrative option is to use multiple stationary phases to achieve similar objectives.

1.4.1 Solvent gradients

Frequently encountered problems in chromatographic processes are high retention factors of some of the components and thus long overall retention times. In this context, solvent gradients can be effectively used, which lower the retention times gradually by a monotonic increase of the elution strength [26, 27]. This change of elution strength can be implemented by mixing two or more solvents with different polarities. The most frequently used type of solvent gradient is a binary gradient (mixing two solvents) because of its simplicity. However it is also possible to construct ternary, quaternary or relay gradients (several subsequent steps with many mobile phase changes) [28].

The basic principles of solvent gradient chromatography were in place

even before the advent of reverse phase chromatography [29, 30]. Over the years, several research groups have been studying the potential of changing solvent strength during the chromatographic process. Specifying a gradient time interval and solvent composition bounds, changes in elution strength can be carried out in many different ways. Most of the investigations evaluated linear or step gradients, e.g. [31, 32, 33]. Jandera [34] optimized general shapes of gradients using flexible functions. Shan and Seidel-Morgenstern [35] compared linear, non-linear and step gradients for the preparative isolation of the middle component from a ternary mixture. In the initial part, a weak mobile phase (low elution strength) is used to provide sufficient retention time for weakly retaining components. The later period includes an increase of elution strength to reduce the retention time towards the end of the gradient run.

Fig. 1.3 illustrates a typical scenario where a linear solvent gradient is used to accelerate elution. The required change in the elution strength of the mobile phase is typically achieved by varying the volume fraction of a modifier from a certain lower starting value ($C_{mod,start}$) at $t_{g,start}$ to a higher value ($C_{mod,end}$) at the gradient end time ($t_{g,end}$). After the elution of the components, typically the column is regenerated rapidly to bring it back to the starting state.

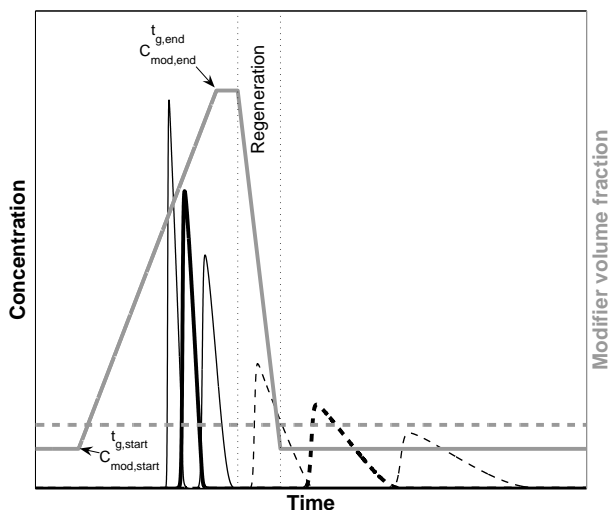


Figure 1.3: Simulated column outlet concentration profiles for isocratic elution of a ternary mixture (dashed lines) compared to elution with a linear solvent gradient (solid lines), the modifier concentration changes between $t_{g,start}$ and $t_{g,end}$ from $C_{mod,start}$ to $C_{mod,end}$.

By varying the solvent strength, the slowly migrating components can be speeded up. In analytical chromatography, this often helps to increase the peak capacity (number of components which can be separated in a sin-

gle run) and resolution (quantitative measure for the distance between two adjacent peaks) [36, 28]. On the other hand, faster elution makes way for more frequent sample injections and thereby better productivity in preparative chromatography. In addition to shorter cycle times, gradient elution also allows for higher product concentrations compared to isocratic elution. These improvements in performance however come at the cost of an additional regeneration time, required to return the columns to their initial state before the next sample can be injected.

1.4.2 Chromatography using multiple stationary phases

Unlike changing the strength of the mobile phase in solvent gradient chromatography, the stationary phase itself can be arranged in a manner to favorably improve the separation performance. This idea has been widely practiced in analytical separations. Numerous separation problems have been already studied and solved exploiting differences in the interactions between a set of components and different stationary phases. In principle, all established interaction mechanisms applied in chromatography (e.g. normal phase (NP), reverse phase (RP), ion exchange (IEX), size exclusion (SEC), hydrophilic interaction (HILIC)) could be combined and utilized, either in a single or in multiple columns. A single, more sophisticated stationary phase providing two or more retention mechanism is often referred to as a mixed mode phase. This configuration today is widely implemented today in a HPLC format for separation of peptides and small proteins [37]. Mixed HILIC and IEX mode is a popular and successful combination in this category. Since its introduction in the early nineties [38], the technique has been used to separate numerous peptide mixtures [39, 40]. In multi-dimensional chromatography, columns packed with multiple stationary phases are coupled with dedicated switching and intermediate sample storage mechanisms. An early implementation of this concept was proposed by Erni and Frei [41], using a 10-port valve and two loops allowing the collection of a fraction of the eluent in between two columns for further injection in a second column. Using multiport valves and sample loops in between stationary phases offers in possibilities to operate each column with different mobile phases, velocities and temperatures. The techniques exploiting 2 stationary phases are called often 2D chromatography, which again can be used to enhance peak capacities [42]. In the so called comprehensive 2D chromatography, all components from the first column (first dimension) are collected and sent to the second column (second dimension) [43]. A modification of this technique is the heart cut 2D chromatography, where only a particular fraction containing selected components is passed from a first on to a second column [44].

Among the 2D concepts, combinations of IEX and RP are widely used pairs of columns capable to separate mixtures of peptides [45]. For example

in [46], peptide mixtures were initially captured in an IEX column, followed by stepwise salt gradients, allowing to gradually elute the components into a RP column, where the peptides and salt are separated with or without the help of a linear gradient. Typically, gradients in RP are achieved by changing the composition of an organic modifier, e.g. acetonitrile. Whereas, IEX chromatography is conducted using different concentrations of salts such as sodium chloride or ammonium acetate [47]. One key advantage the 2D method is that, there is an additional degree of freedom to manipulate the mobile phase compositions independently in each segments [48]. This however comes at the cost of using more sophisticated instrumentation and sample loops in between.

Faster and easier options not relying on storage in between two subsequent columns can be achieved by directly coupling chromatographic segments filled with different stationary phases. However, by such coupling, the possibility of manipulating the mobile phases in between the segments is lost. This introduces severe constraints and allows combining only stationary phases that can be operated with a common mobile phase. This loss of freedom however, can be eventually compensated by a less sophisticated and more robust separation. Applications of this kind of a solid gradient concept are seen for example in the combination of various RP materials characterized by certain difference in end capping or length of alkyl chains. Such a multi-segment technique has been recently evaluated for analytical separations of multi-component mixtures [49, 50] using segment coupling techniques with minimal dead volume in between the segments [51]. In a part of this study, the concept will be extended to preparative separations with the objective of isolating a target component with maximum productivity and yield. Related theoretical investigations and subsequent experimental results are described in detail in chapters 6 and 7.

1.5 Modeling, performance evaluation and optimization

In contrast to analytical chromatography, the main goal of preparative chromatography is the separation of one or more components from a complex mixture in large quantities. It is much easier to predict the outcome of an analytical separation with the knowledge of few basic parameters. The peaks are almost always near gaussian in shape and the presence of one component does not influence the migration properties of other components [52, 53, 54]. This however is no longer the case when columns are overloaded with higher feed concentrations or volumes in a production oriented approach. The overloaded component peaks are generally non-symmetric and far away from ideal. Thus, to analyze and compare different strategies in preparative chro-

matography, more complex mathematical models and more parameters are required in preparative chromatography to predict the propagation of concentration profiles.

Once the profiles at the outlet of the column are known for a given separation problem, the efficiency and quality of separation could be measured by deducing certain performance parameters. The elution profiles may be the outcome of an experiment or the solution of a suitable mathematical model. As explained before, typical performance parameters in the analytical case include capacities and resolution. In contrast, typical objective function in preparative chromatographic separations are recovery yield, production rate etc. [5].

The performance parameters can be effectively used as a reference value to compare different chromatographic operating modes or configurations. The comparison is usually done with optimized values of the objective functions. The maximization or minimization of the indices can be done by an array of techniques. The choice usually depends on the complexity of the problem in hand. Calculation of the objective functions in analytical chromatography is often straight forward and the resulting optimizations generally converge rather quickly. However, optimizations involving the solution of preparative separation problems in most of the cases are constrained by complex partial differential equations, hence they are by nature more computational resource intensive. More about various mathematical models, parameters and typical optimization strategies used are explained in detail in chapter 3.

Chapter 2

Scope of the thesis

The goal of preparative isolation of a target component from a multi-component mixture has been traditionally carried out using conventional batch elution under isocratic conditions. However, it has been demonstrated frequently, that classical elution is not always the most attractive mode of operation [52]. This thesis illustrates the efforts made to improve the separation performance of the target component using alternative operation modes and their combinations described in the previous chapter.

In any performance evaluations using the typical preparative chromatographic performance parameters (e.g. production rate and yield, see chapter 3), a central task is to accurately determine fractionation or cut-times. For a given chromatogram, these cut-times can be calculated by maximizing the amount of the target collected with respect to a purity constraint. The initial quest was to analyze existing cutting strategies and systematically categorize suitable methods. In chapter 4, a general cut-time finding framework was to be proposed with insights into solving such problems using continuous and discrete algorithms.

The main focus in chapter 5 was to combine recycling chromatography with gradient elution in the first cycle and analyze its potential on the separation performance. In a theoretical case study, it was to be evaluated whether the combined operation mode has the potential to outperform the batch modes of operation and closed-loop recycling.

The next goal in chapter 6 was to employ multiple stationary phases to solve a separation problem. Using a theoretical study to analyze the effect of coupling two different segments with different stationary phases, one of the task was to evaluate whether the segment order had an impact on separation performance. The relative lengths of the individual segments had to be optimized for optimal separation. This concept was to be also extended to a mixed mode configuration.

The final objective in chapter 7 was to experimentally demonstrate the

trends seen in the theoretical study exploiting a serial coupling of stationary phases. A ternary system was to be identified which exhibited selectivity differences on two different types of stationary phases.

All together, various valuable insights into the potential of improving the separation performance of multi-component mixtures using alternative chromatographic techniques (closed-loop recycling, solvent and stationary phase gradients) are highlighted in this thesis. The theoretical fundamentals required are explained in the next chapter.

Chapter 3

Theory

As outlined in the introductory chapter, few alternate variations of batch and recycling chromatographic operation modes were suggested and analyzed for the preparative isolation of a target component. For a qualitative comparison, mathematical models of the process are required to predict the migration behavior of the components in the column. This chapter gives an insight into the theory behind and the tools used in this work. Common models used to describe the process are explained in the first section. The estimation and characteristics of the underlying parameters are illustrated in the following sections.

3.1 Modeling chromatographic processes

The existing chromatographic separation models can be broadly classified into three main categories, namely the discrete plate models, continuous models based on differential equations and statistical variants [52].

Plate models assumes that a column of length L can arbitrarily divided into a finite number of well mixed stages of equal length in series, with the mobile phase passing through each of these stages. The second assumption being that complete equilibrium is achieved between mobile and stationary phases in each stages. The two most prominent examples in this category include the "tanks in series" model of Martin and Synge[55] and the model proposed by Craig[56].

The second branch of modeling approach arises from differential mass balance of the solute in a slice of the column, which leads to a set of partial differential equations. Solution to which describes the migration of components in the column. The kinetics of mass transfer in the column may or may not be incorporated with varying degrees of complexity. The simplest of these include the ideal model, in which all sorts of mass transfer kinetics are neglected. However, their solvability is limited to few components with rather non-complex isotherm models and boundary conditions.

Continuous models once again can be classified into many categories based on the degree to which mass transfer effects are incorporated. The most elaborate model is the general rate model which uses two mass balance equations, one for the mobile phase outside the stationary phase particles and the other for the stagnant and adsorbed mobile phase inside particles. The two concentrations are coupled using a mass transfer flux term through the particle boundary. This model can be further simplified by assuming very fast kinetics inside the particle, leading to the lumped pore model. For system with still faster kinetics, transport inside particle could be disregarded, resulting in the lumped kinetic model. If the mass transfer is infinitely fast between the mobile phase and the particle, all mass transfer effects can be lumped into one single dispersion term, resulting in the equilibrium dispersive (ED) model. A good summary and comparison of all these models can be found for example in [52, 57].

The third category of modeling approach involves the application of statistical methods. These models are based on various probabilistic approaches. The original idea involved the definition of a probability density function for solute molecules in time and space [58, 59]. A detailed discussion on this topic is beyond the scope of this study. A good overview can be found for example in [60].

In the framework of this study, the Craig model has been used to model chromatographic modes involving solvent gradients. Otherwise, the equilibrium dispersive model has been extensively used because of its relative simplicity, accuracy and fast solution capability. The following subsections explain the Craig model, ideal and equilibrium dispersive models.

3.1.1 Craig model

As highlighted before, the Craig model uses a series of stages or tanks in series assuming equilibrium at each stage. It can be differentiated from the classical Martin and Synge model by the fact that the latter uses a differential mass balance around each stage assuming a continuous flow. In contrast, the Craig model uses a discrete shifting of the mobile phase from stage to stage. In terms of predictability, both stage models are very similar and the differences in resulting solutions vanish when the stage numbers involved are sufficiently high [54].

Figure 3.1 shows a schematic implementation of the Craig model. In this case, the column is divided into N discrete stages. Each stage has a mobile and stationary phase volumes of v_m and v_s respectively. Initially, only the first stage has all off the solutes injected and is allowed to reach the equilibrium. In the next step, the liquid fraction from the last stage (stage

N) is withdrawn, and the liquid fractions in each of these stages are shifted in the direction of fluid flow by one stage. Fresh mobile phase (or sample) is introduced into the first stage. This procedure is repeated until all of the solute has left the last stage.

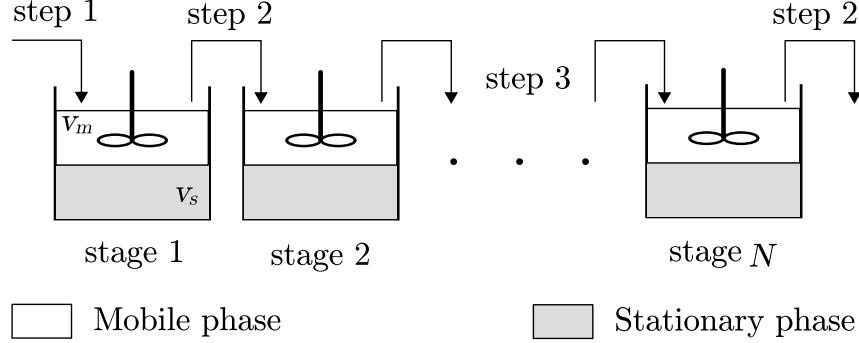


Figure 3.1: Craig model: step 1) solute injected into first stage. Step 2) after equilibration, v_m amount of liquid transferred into next stage, same amount removed from last stage. Step 3) process repeated until all solutes have left the column

The mass balance equations of the Craig model for a certain stage p and a component i can be expressed as [61]:

$$C_{i,p}^k + \left(\frac{1 - \epsilon}{\epsilon} \right) q_{i,p}^k = \frac{1 - \epsilon}{\epsilon} q_{i,p}^{k-1} + C_{i,p-1}^{k-1} \quad i = 1, \dots, N_c \quad p = 1, \dots, N \quad (3.1)$$

here $C_{i,p}$ and $q_{i,p}$ represents the liquid and solid phase concentration at step k or $k - 1$, with N_c being the total number of components. ϵ in this case represents the volume fraction of the mobile phase in each stage. In the above equations, the equilibrium relationship

$$q_{i,p} = q_{i,p}(C_{1,p}, C_{2,p}, \dots, C_{N_c,p}) \quad (3.2)$$

is provided by the adsorption isotherms, more of which is explained in section 3.2.2.

3.1.2 Ideal and equilibrium dispersive models

In contrast to the discrete models, the simplest version of a continuous model is the ideal model, represented by [53]:

$$\frac{\partial C_i}{\partial t} + F \frac{\partial q_i}{\partial t} + u \frac{\partial C_i}{\partial z} = 0 \quad (3.3)$$

$$q_i = f(C_1, \dots, C_{N_c}) \quad (3.4)$$

where, z and t are the space and time co-ordinates. The interstitial or linear velocity of the mobile phase is given by u . The ratio between stationary and liquid phase here is represented by the phase ratio, $F = \left(\frac{1-\epsilon}{\epsilon}\right)$.

The ideal model is an obvious tool when looking for analytical solutions and often gives good insights into the separation problems. For a pulse injection, the ideal model can be solved using the following inlet conditions:

$$C_i|_{z=0} = \begin{cases} C_{inj,i} & \text{for } 0 \leq t \leq t_{inj} \\ 0 & \text{for } t > t_{inj} \end{cases} \quad (3.5)$$

For a component i , equation 3.3 can be re-arranged as [54, 61]:

$$\frac{\partial C_i}{\partial t} + \frac{u}{1 + F \frac{dq_i}{dC_i}} \frac{\partial C_i}{\partial z} = 0 \quad (3.6)$$

Based on the equation above (3.6), the velocity associated with each solute concentration can be defined as :

$$u_{c,i}(C_i) = \frac{u}{1 + F \left. \frac{dq_i}{dC_i} \right|_{C_i}} \quad (3.7)$$

This equation gives very valuable information about the migration properties of the components in a chromatographic column. For a single component with a given concentration, the associated velocity u_c as per equation 3.7 is a constant [54]. Alternately, the constant time taken for a concentration to reach the length L of a column can be re-written from equation 3.7 as :

$$t_{r,i}(C_i) = t_0 \left(1 + F \left. \frac{dq_i}{dC_i} \right|_{C_i} \right) \quad (3.8)$$

with

$$t_{r,i} = \frac{L}{u_{c,i}} \quad \text{and} \quad t_0 = \frac{L}{u} \quad (3.9)$$

In reality, a column exhibits a finite amount of dispersion resulting from various mass transfer kinetics. In this regard, the equilibrium dispersive model can be represented by adding a dispersive term to equations 3.3 and 3.4, resulting in :

$$\frac{\partial c_i}{\partial t} + F \frac{\partial q_i}{\partial t} + u \frac{\partial c_i}{\partial z} = D_{app,i} \frac{\partial^2 C_i}{\partial z^2} \quad (3.10)$$

The dispersive term with the empirical coefficient $D_{app,i}$ accounts for all mass transfer effects. The advantage of using ED model is that, very fast and sufficiently accurate numerical solution could be achieved by using an algorithm proposed by Rouchon et al. [62]. Numerical solution of the underlying mass balance equations used in this study are explained in section 3.3.

3.2 Model parameters

In order to solve the mathematical models described in the previous sections, knowledge of the underlying parameters is necessary. The first set includes the column void fraction or porosity (ϵ) and the apparent dispersion coefficients ($D_{app,i}$). The next set of parameters arise from the adsorption isotherm model $q_i = f(C_1, \dots, C_{N_c})$ in consideration.

3.2.1 Column porosities and efficiency

For any solution based on the mathematical models above, the role of porosity is very significant. Additionally, porosity estimation the basis for many of the parameter determination that follows (e.g. Adsorption isotherms). The total volume of a given column is composed of the interstitial volume occupied by the mobile phase (v_m) and the stationary phase volume (v_{st}) (total volume of all porous particles for example). v_{st} again contains the solid volume (v_s) and the volume of the pores (v_{pore}). Thus the total volume of the column becomes :

$$v_{col} = v_m + v_s + v_{pore} \quad (3.11)$$

Based on the volumes involved, two types of porosities can be defined, namely the interstitial porosity (ϵ_{int}) and total porosity (ϵ), given by [5]:

$$\epsilon_{int} = \frac{v_m}{v_{col}} \quad (3.12)$$

$$\epsilon = \frac{v_m + v_{pore}}{v_{col}} \quad (3.13)$$

$$\text{with } v_{col} = \frac{\pi d_c^2}{4} L \quad (3.14)$$

The choice of porosities depends on the question as to which volumes are accessible to the components. For example internal pore volumes are inaccessible for very large molecules and in such cases ϵ_{int} should be used. Irrespective of the volumes considered, the basic principle behind the estimation of porosities is the same. A non adsorbing tracer component is injected into the column and the resulting peak is analyzed to determine its first absolute moment :

$$t_0 = \frac{\int_0^\infty C_i t dt}{\int_0^\infty C_i dt} \quad (3.15)$$

where t_0 is called the dead time of the column. This value could differ based on the tracer used. If a large molecule is used to estimate the v_m and ϵ_{int} , the resulting t_0 would be smaller compared to the value obtained for a small molecules that penetrates into the pores. Once the dead time is estimated,

calculating the corresponding porosity is quite straight forward. The total porosity can be for example calculated from a dead time obtained for a pore penetrating tracer as :

$$\epsilon = \frac{t_0 \dot{V}_f}{v_{col}} \quad (3.16)$$

where \dot{V}_f is the actual volumetric flow rate of the mobile phase. Through out this study, the total porosity given by equation (3.16) was considered.

Another important separation parameter that characterizes separation efficiency is the number of theoretical plates (N). The higher the value of N , the lower the dispersion due to flow non idealities and mass transfer effects. The number of theoretical plates are related to the chemical engineering concept of height equivalent to a theoretical plate (HETP) as:

$$\text{HETP} = \frac{L}{N} \quad (3.17)$$

For uniformly packed columns with incompressible fluid flow and for an analytical peak with near gaussian shape, N can be estimated as [3]:

$$N = 5.54 \left(\frac{t_{r,i}}{w_{1/2,i}} \right)^2 \quad (3.18)$$

where $t_{r,i}$ is the first absolute moment of the component peak (equation (3.15)) and $w_{1/2,i}$ is the width of the peak at half height. The number of theoretical plates again is a measure of the degree of the dispersion involved and for large N , it is co-related to axial diapersion term $D_{app,i}$ introduced previously (equation (3.10)) as [54]:

$$D_{app,i} = \frac{uL}{2N} \quad (3.19)$$

Additionally, it is worth noting that the theoretical plate numbers are significantly influenced by the linear velocity u . The so called van Deemter equation is given by [63]:

$$\text{HETP} = \tilde{A} + \frac{\tilde{B}}{u} + \tilde{C}u \quad (3.20)$$

In the above equation, the first term \tilde{A} accounts for the flow mal-distributions resulting from packing imperfections, broad particle size distributions etc.. The second term represents the influence of axial diffusion of the molecules, which often can be neglected provided the velocity is high enough. The last term shows a linear dependence with interstitial velocity, where \tilde{C} quantifies the resistance to mass transfer at very high velocities.

3.2.2 Adsorption isotherms

Irrespective of the mathematical models involved, adsorption isotherms are an necessary to accurately predict the development of concentration profiles in chromatographic columns. These are functional relationships between the stationary and mobile phase concentrations in equilibrium at constant temperature and pressure. In literature there are a multitude of models derived for gas phase adsorption. More details can be found for example in [64, 52, 65]. Among many available isotherm models, the Langmuir isotherm is the most commonly applied variant in preparative chromatography, which is also used in this study.

In its most simplest form, the Langmuir type isotherm for a single component is based on the following assumptions :

- Adsorbent has a homogeneous surface, with adsorption sites that are energetically equal
- Adsorption of only one molecule per site
- Only monolayer formation
- Absence of lateral interactions between the adsorbed molecules

Based on the above assumptions, the Langmuir isotherm for a single component i can be formulated as :

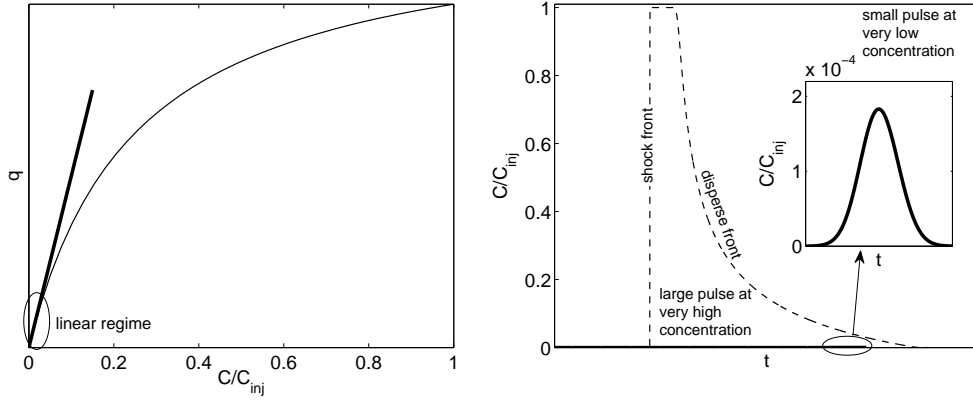
$$q_i = \frac{a_i C_i}{1 + b_i C_i} \quad (3.21)$$

where a_i characterizes the linear relationship between the concentration in two phases in a low concentration range, and is known as the Henry constant. Parameter b_i on the otherhand quantifies the non-linear influences and is related to the Henry constant through :

$$a_i = b_i q_{sat} \quad (3.22)$$

where q_{sat} represents the saturation capacity of the stationary phase.

The influence of linear and non-linear nature of the isotherms is depicted in Figure 3.2. At very low concentrations, the isotherm behaves linearly, characterized by the numerator of equation (3.21). Whereas, higher concentrations imply that the denominator gains importance, rendering the isotherm non-linear.



(a) Single component isotherm (thin line) with initial slope (thick line) (b) Resulting linear (inset) and non-linear (dashed line) chromatograms

Figure 3.2: a) Single component Langmuir adsorption isotherm b) Resulting linear and non-linear concentration profiles

The influence of these two regimes on the chromatogram is illustrated in figure 3.2b. A linear adsorption isotherm leads to a near gaussian peak (inset in figure 3.2b), whereas overloaded peaks are characterized by a sharp shock front and a dispersed tail. In the figure, the overloaded peak results from a highly concentrated pulse with sufficiently large injection volume to form a plateau after the shock front. This sort of non-linear behavior by the chromatogram can be explained by the equilibrium theory (equation 3.3). Front sharpening occurs due to the convex upward nature of the isotherm (figure 3.2a, equation 3.21). The retention time of the shock front depends on the chord drawn between the initial and plateau concentrations [66]. Based on equation 3.8, this results in :

$$t_{r,i}|_{shock} = t_0 \left(1 + F \frac{\Delta q_i}{\Delta C_i} \right) \quad (3.23)$$

Similarly, when the feed concentration is switched to initial concentration ($C_{init} = 0$ in the figure), the retention time of the resulting dispersed tail follows the local slope of the isotherm. The shape of the rear profile is thus governed by equation 3.8. The dynamics however are much simpler in the linear regime. A direct result is the formation near gaussian peak in this regime ($\left. \frac{dq_i}{dC_i} \right|_{C_i \Rightarrow 0} = a_i$). The resulting retention time of the peak can be written as :

$$t_{r,i} = t_0 (1 + F a_i) \quad (3.24)$$

Additionally, the non-linearity of a chromatogram is greatly influenced by the operating concentration and especially the isotherm parameter b_i (see equation 3.21). In this regard, the measure of non-linearity of a chromatogram can be characterized by a chromatogram non-linearity parameter

$\bar{\lambda}$, based on the injection concentration as :

$$\bar{\lambda}_i = \frac{b_i C_{inj,i}}{1 + b_i C_{inj,i}} \quad (3.25)$$

with a $\bar{\lambda}_i$ value less than 0.01 characterizing a linear chromatogram and a value above 0.1 for non-linear case.

Another useful parameter that characterizes the degree of separation between a pair of components in linear regime is the separation factor (α). Separation between two adjacent components i and j can be quantified by

$$\alpha_{i,j} = \frac{a_i}{a_j} \quad \text{with } a_j \geq a_i \quad (3.26)$$

Single component isotherms (equation (3.21)) are insufficient to describe multi-component injections. Typically, the presence of one component interferes with the adsorption of other components. The existing single component Langmuir isotherms can be modified to accommodate multiple components in the form

$$q_i = \frac{a_i C_i}{1 + \sum_{j=1}^{N_c} b_j C_j} \quad (3.27)$$

It is worth noting that in the above formulation, in order to fulfill thermodynamic consistency, the saturation capacity (equation (3.22)) has to be equal for all components, i.e. $q_{sat,1} = q_{sat,2} = \dots = q_{sat,N_c}$.

The isotherm parameters in the above equations can be influenced by several factors including temperature and pH. The most relevant factor with respect to this study is the modifier volume fraction (C_{mod}) introduced in section 1.4.1. The relationship between q_i and C_i is thus influenced also by C_{mod} . Several models have been suggested to correlate a_i and C_{mod} in normal and reverse phase analytical chromatography [36]. Similar correlations are often employed to describe the additional isotherm parameters required in non-linear models [67, 68]. In this study, the following semi-empirical relations [69] were used in all cases where gradient operations are encountered.

$$a_i = (a1_i C_{mod})^{a2_i} \quad \text{with } i = 1, \dots, N_c \quad (3.28)$$

$$b_i = (b1_i C_{mod})^{b2_i} \quad (3.29)$$

3.2.3 Determination of adsorption isotherms

There is a wide array of methods to determine parameters of the adsorption isotherms introduced in the previous section. Fundamentally, these methods can be classified into static and dynamic methods [66]. Methods in

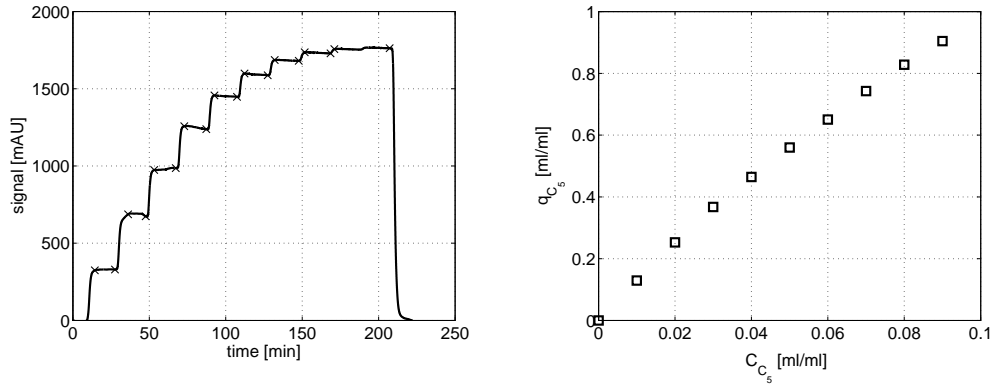
the former case are relatively cumbersome and are exclusively based on the mass balances alone. Dynamic methods on the other hand use extensively the concentration-time data and are far more accurate [5]. Hence only the dynamic methods are focused in this section. Most widely used dynamic methods to measure equilibrium data include the frontal analysis (FA), perturbation method, elution by characteristic point (ECP) and the inverse or peak fitting method.

3.2.3.1 Frontal analysis

FA is a standard and highly accurate method to determine single component isotherms. The basic principle involves injection of a very large pulse of the component of interest to get a breakthrough curve (typically a sharp front followed by a plateau, see figure 3.2b). The equilibrium loading for the corresponding plateau concentration can be calculated from the resulting retention time of the shock front (given by equation 3.23). Starting from an initial column loading, successive step changes (usually increasing) can be performed to evaluate a number of q values for respective concentrations [70].

FA is an excellent tool to find single component equilibrium data. For example, figure 3.3 shows FA steps constructed to measure single component adsorption isotherm of Cyclopentanone. Retention times of total of 9 sharp fronts can be deduced from Figure 3.3a, resulting in equal number of isotherm data points (in addition to $C_{init} = q_{init} = 0$, figure 3.3b).

This method can also be extended to multi-component mixtures, provided component specific detector response is available. The greatest advantage of FA is that it can be used for columns with low efficiencies [5]. Besides, as a by product of the breakthrough experiments, the detector calibration data is also obtained. The main drawback of the method however is the large sample requirement.



(a) Frontal analysis steps

(b) Resulting single component q vs C data

Figure 3.3: Illustration of a typical frontal analysis experiment for Cyclopentanone on a ProntoSIL C18 [80x3mm] column. Mobile phase : 35/65 Methanol/Water, $\dot{V}_f=0.5$ ml/min.

3.2.3.2 Perturbation method

This method is based on the analysis of the response to a small perturbation made to a system in equilibrium. The dynamics of the resulting response can be explained using the equilibrium theory. For a column equilibrated with a single component at a particular concentration, a sufficiently small concentration change introduced would result in a small peak that propagates with a velocity given by equation 3.7. Thus, the retention time of the disturbance would depend solely on the local slope of the isotherm at the equilibrium concentration ($\left. \frac{dq_i}{dC_i} \right|_{C_i}$).

The scenario changes when a multi-component equilibrium is considered. Perturbation made to a system with N_c components would result in an equal number of wave responses governed by local slopes ($\left. \frac{dq_i}{dC_i} \right|_{\bar{C}}$) of isotherms at that particular equilibrium concentration vector \bar{C} [54]. The characteristic retention time of each wave or pulse is given by [66]:

$$t_{r,i}^j(\bar{C}_i) = t_0 \left(1 + F \left. \frac{dq_i}{dC_i} \right|_{\bar{C}} \right) \quad \text{with } i, j = 1, \dots, N_c \quad (3.30)$$

with the local slopes of the isotherms given by :

$$\left. \frac{dq_i}{dC_i} \right|_{\bar{C}} = \sum_{k=1}^{N_c} \left. \frac{\partial q_i}{\partial C_k} \right|_{\bar{C}} \left. \frac{dC_k}{dC_i} \right|_{\bar{C}} \quad (3.31)$$

Based on the coherence condition, each response pulse correspond to a coherent state. The condition states the existence of situations where the set of

components propagates with a constant speed and fixed concentrations [71]. Hence for each characteristic retention time, the following holds true :

$$t_{r,i}^j = t_{r,k}^j \quad \text{with} \quad i, j, k = 1, \dots, N_c \quad (3.32)$$

For a competitive isotherm model chosen apriori, the partial derivatives of the isotherm with respect to each component ($\frac{\partial q_i}{\partial C_i}$) can be substituted into equation 3.31. This along with the coherence condition (equation 3.32) can then be solved for the directional derivatives $\frac{dC_k}{dC_i}$. However, for an N_c component system, this would mean finding roots a polynomial of the same order [66]. Hence this method has been predominantly used for simpler systems (N_c upto 2).

Figure 3.4 illustrates a perturbation experiment with three components. The perturbation is achieved using a concentration smaller than the plateau value. The resulting response gives three response pulses. The perturbation concentration could also be higher than the equilibrium concentration and should be sufficiently large enough to get a distinguishable response. Besides, care should be taken that perturbing the system do not change the equilibrium. The main advantage of perturbation method is that detector calibration could be avoided altogether. Again analogous to FA, large amount of substances are needed to evaluate a full branch of isotherm.

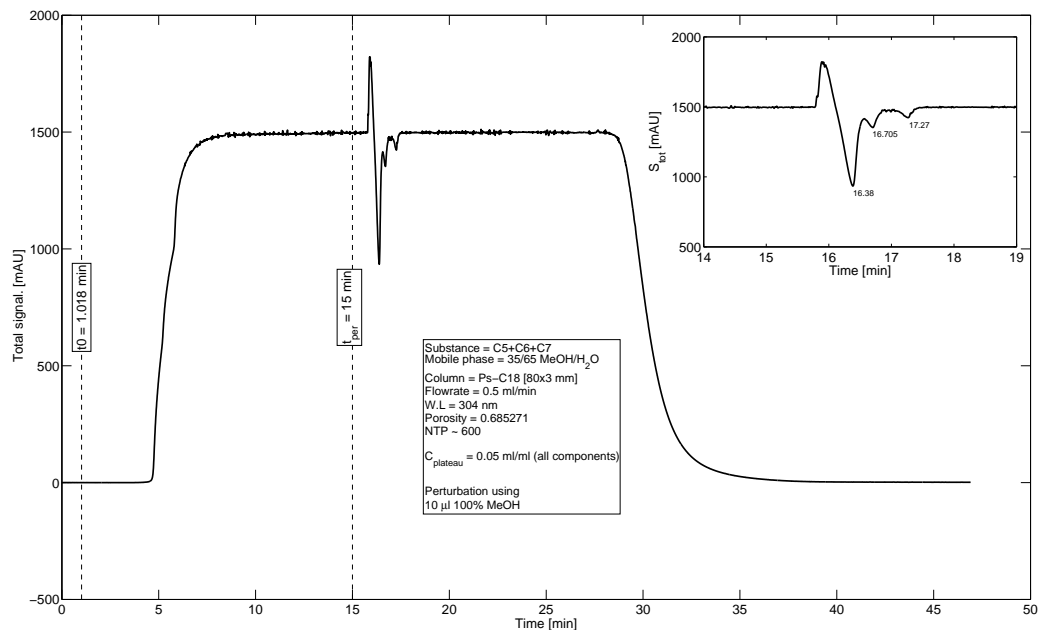


Figure 3.4: An example of perturbation method with a ternary mixture

3.2.3.3 Elution by characteristic point

This method is again based on equilibrium theory, given a column with high efficiency, the dispersed part of the chromatogram alone is sufficient to deduce the local slopes of the isotherm. For an experimental chromatogram, equation 3.8 could be re-arranged and integrated with respect to C_i to get corresponding values of q_i . The major drawback however is that this method is applicable only for single components [54]. On the other hand, only a very small amount the component is needed to generate a full branch of non-linear chromatogram.

3.2.3.4 Inverse method

Inverse method relies on fitting the numerical solution of a column and an adsorption isotherm model with experimentally obtained data. Starting from an initial value, the isotherm parameters can be iteratively changed using a suitable optimization algorithm to minimize differences between the two profiles. Any accurate column model with suitable boundary conditions could be used to generate the numerical solution. However, care should be taken also to incorporate any extra column effects present. The minimization problem using ED model and competitive Langmuir isotherms for example can be formulated as :

$$\min_{a_i, b_i} \sum_i \left\| \frac{C_i^{sim} - C_i^{exp}}{C_i^{exp, max}} \right\| \quad \text{for } i = 1, \dots, N_c \quad (3.33)$$

subject to the model equations 3.10, the inlet condition 3.5 and the equilibrium relationship 3.27.

The greatest drawback of the method is that any inaccuracy resulting from the column chosen model reflects in the fitted parameters [5]. On the other hand, given sufficiently accurate models and the calibration data, any number of components could be fitted with low sample amount required for experiments. More about solving optimization problems of the type given by equation 3.33 is explained in section 3.5. Next section illustrates few techniques used to solve underlying mass balance equations.

3.3 Numerical solution of model equations

Due to the overloaded nature of preparative chromatography, the adsorption isotherms considered are often non-linear. This in conjunction with the mathematical models described in section 3.1 almost always results in a system of equations which are very hard to solve analytically. Thus leading to numerical solutions of the underlying equations.

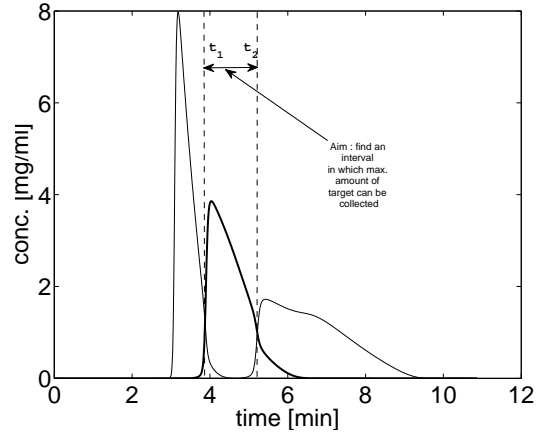
The Craig model (equation 3.1) introduced in section 3.1.1 in combination with competitive Langmuir isotherm (equation 3.27) results in a set of non-linear equations at each step k . These equations for each component are implicit (in terms of C_i) in nature and require iterative solution at each step [61]. Suitably re-arranged, the equations can be solved very quickly using the fixed point iteration method [72], with initial values of C_i for the k^{th} step taken from the preceding step. This numerical solution strategy was applied in this thesis wherever Craig model was used.

Unlike the Craig model, which by nature itself is a difference equation, the equilibrium dispersive model (equation 3.10) introduced in section 3.1.2 represents a system of PDEs. A standard approach is to solve such equations using a finite difference scheme (FDS) [73]. One such stable and fast scheme is based on the first order forward in space and backward in time FDS. The basic principle used by Rouchon et al. [62] involves choosing (constant) space and time discretization step such that the resulting stable solution exhibits a numerical dispersion that matches actual dispersion, given by $D_{app,i}$ in equation 3.10. By doing so, the second order PDE can be reduced to a first order one (equation 3.3). A detailed explanation can be found for example in [61]. The numerical stability of the FDS is mandated by the Courant-Friedrichs-Lewy condition, which is characterized by the Courant number (a_{cou}). For the stability of forward in space and backward in time scheme, this number can take any arbitrary value above 1 [54]. For a single component, based on its dispersion coefficient and an arbitrary but stable Courant number, the space step length (Δz) of the FDS can be easily calculated. The time step length Δt is then derived based on the Δz , a_{cou} chosen and the velocity associated with an infinitesimal concentration of the component (equation 3.7 with $\left. \frac{dC_i}{dt} \right|_{C_i \rightarrow 0} = a_i$). An a_{cou} value of 2 was found to be most suitable so that the corresponding space step length matched the HETP of the column [74].

Although the Rouchon's solution method described above was developed focusing a single component under linear conditions, the method can also be used for multi-component preparative elutions. Over the years, numerous theoretical studies has been carried out based on this fast solution scheme. In multi-component cases, the dispersive term $D_{app,i}$ is replaced by an average value to represent all components. Similarly, an effective wave velocity u_c (equation 3.7) is used to determine Δt by averaging the Henry coefficients of the components. With high column efficiency and adequate non-linear effects, the ED model could be solved using Rouchon's method with sufficient accuracy to predict the migration of components [54].

3.4 Performance parameters

In general, the function of performance parameters for a chromatographic process is to facilitate an evaluation of efficiency and quality of separation. In analytical chromatography, these parameters are usually the peak capacities and resolution. However, in preparative chromatography, the typical performance parameters are strongly bound to the amounts of one or more substances isolated, e.g. in our case the target component.



From a given chromatogram, the amount of target i collected is given by :

$$m_i = \dot{V}_f \int_{t_1}^{t_2} C_i dt \quad (3.34)$$

where t_1 and t_2 are the cut-times for collecting the target component (figure 3.5). Determining accurate cut-times is a difficult task and significantly influences any subsequent performance parameters calculated based on m_i .

The cut-times are usually calculated by maximizing m_i with either a purity or yield constraint. The purity of a substance collected in the interval t_1 - t_2 can be defined as [5]:

$$Pu_i = \frac{m_i}{\sum_{i=1}^{N_c} m_i} \quad (3.35)$$

with the recovery yield given by

$$Y_i = \frac{m_i}{C_{inj,i} v_{inj}} \quad (3.36)$$

where $C_{inj,i}$ and v_{inj} are the injected concentration and volume of the component. Given a purity, the recovery yield could be calculated or vice versa.

Another important performance parameter evaluated from m_2 is the production rate, which is defined as the amount of substance collected per unit time scaled to an entity. The scaling entity could be the amount of adsorbent, volume of the column or its cross sectional area [5]. Time scale on the other

hand is often the cycle time (t_{cyc}), which is the time period between two subsequent injections. Depending on the operation mode, this t_{cyc} could have many definitions. For example in batch isocratic elution, the time between the appearance of the first component and the end of the component train is used to specify t_{cyc} . When the cross sectional area (A_{col}) of the column is used as the scaling entity, the production rate of component i is written as :

$$Pr_i = \frac{m_i}{A_{col}t_{cyc}} \quad (3.37)$$

In addition to the objective functions listed above, a number of indices including specific production and the solvent consumption rate are also used as performance indices. More details can be found for example in [75, 54]. Production rate and yield in this study are used as performance parameters to compare various chromatographic operation modes. Occasionally hybrid objective functionals are also employed, for example Felinger and Guiochon [76] found that when production rate and yield are simultaneously maximized, the optimum conditions usually results in a configuration with high yields, with a small sacrifice in productivity. The product of production rate and yield is used later in this thesis as performance index. Challenges involved in finding accurate cutting time will be discussed in chapter 4.

3.5 Optimization of parameters

Optimization can be used as a tool to design an ideally operating preparative system. Additionally, by optimizing one or more performance indices mentioned in the previous section, performance of different chromatographic operating modes can be analyzed and compared. Mathematical models representing preparative separations are generally non-linear in nature. Thus, the objective functions evaluated by solving such a system usually depends also in a non-linear manner on the design variables. The theory of classical non-linear programming is very well established. Within this framework, a general non-linear optimization (maximization or minimization) problem can be represented as [77]:

$$\max_{X \in \mathbb{R}^n} f(X) \quad (3.38)$$

such that

$$g(X) = 0 \quad (3.39)$$

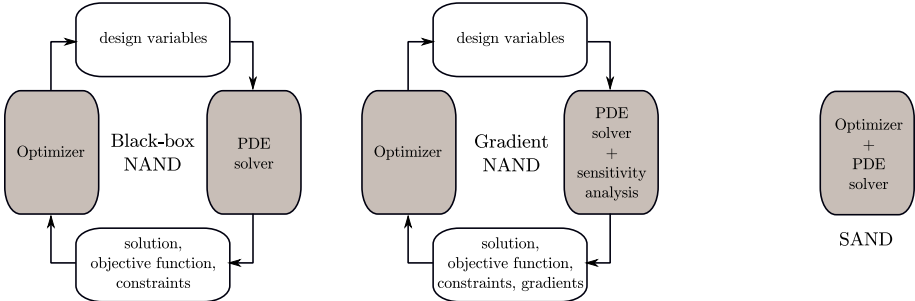
$$h(X) \leq 0 \quad (3.40)$$

where X represents the set of design variables or degrees of freedom. For example in designing preparative separations, variables could be the column dimension (length, internal diameter etc.), particle diameter, flowrate, modifier concentration etc. The objective function ($f(X)$) could be one or a combination of many performance indices described in the previous section.

A set of equality constraints is given by $g(X)$, most of which arise due to conservation laws involving the design variables if applicable. On the other hand, the inequality constraints ($h(X)$) usually are off-shoots of the bounds placed on the variables.

The formulation given above (equations (3.38)-(3.40)) can only be used if $f(X)$ is explicitly defined. But preparative separation in almost all cases described by a set of partial differential equations (PDE)[52, 54]. Hence the objective functions are evaluated from the solution of these PDEs (e.g. equations 3.3 and 3.10). Thus we come across an implicit dependency in terms of the design variables. The formulations given in the form above (equations 3.38-3.40) are thus insufficient to describe such optimization problem.

In this context, the optimization encountered can be formulated as a PDE constrained problem with any of the objective functions introduced in the previous section (3.4). The equality and inequality constraints may be added based on the design parameters chosen. The important addition however is the set of PDEs itself as constraints. For example, to a formulation like the one above (3.38-3.40), the underlying mass balance equations given by 3.3 or 3.10 and the corresponding inlet conditions (equation 3.5) are added for completeness. This sort of a formulation can be seen as the most generalized version and the actual path in finding the optimal values of X can take many routes depending on the complexity of the problem.



(a) Nested analysis and design (NAND) with black-box (b) Nested analysis and design with gradients (c) Simultaneous analysis and design (SAND)

Figure 3.6: Different optimization approaches for a PDE constrained problem [78, 79]

PDE constrained optimization is an actively researched field today [80, 81]. Figure 3.6 shows the schematic representation of different approaches involved in solving such problems [78, 79]. The core part in all approaches involves a PDE solver in addition to an optimizer. The solutions generated are passed on to the optimizer along with other results based on the category in consideration. The solution of PDEs itself is an immensely large area, more

details on numerical solution of PDEs can be found for example in [82]. The role of the optimizer is to analyze the outputs generated by the PDE solver and perturb the design variables, minimizing / maximizing the objective function. Based on this concept two main different approaches are practiced today, namely the nested analysis and design (NAND) and the simultaneous analysis and design (SAND). The former can be again distinguished into black-box based and gradient based NAND.

The easiest to implement and the most widely practiced variant is the black-box NAND type optimization (figure 3.6a). The solver could take any form including commercial solvers to user programmed routines. The characteristic however is that in this approach, the solver takes design variables as inputs and generates the solution, a scalar objective function value and the constraint information. The greatest advantage of this set-up is that a wide variety of optimizers could be employed in this configuration. More details on optimizers are explained in the next section. The gradient based NAND implementation uses a PDE solver with an additional functionality doing a sensitivity analysis of the problem. This has an advantage that along with the solutions, the gradients of the objective functions and constraints are also generated, which can be used efficiently by a suitable gradient based optimizer. The NAND implementations can suffer from repeated and time consuming solution of the PDEs and intermediate convergence of the PDE solver [83].

The most efficient way of solving a PDE constrained problem is by using the SAND approach. Where, the PDEs are fully discretized and the corresponding algebraic equations are posed as equality constraints along with the main optimization problem. Thus the solution of the PDEs now become a part of the massive non-linear programming problem [80]. This formulation is by far the most efficient, albeit its relatively difficult implementation.

3.5.1 Optimizers

Most of the preparative chromatographic optimizations in this thesis have been carried out using the Black-box NAND approach because of its simplicity in implementation and non-smooth objective function handling capacity. The most basic form of optimizer is a grid search. Given a limited number of design variables (usually two to three), the easiest way is to finely divide the variables between its upper and lower bounds and call the PDE solver at each of these points. Besides its simplicity in implementation, the mutually independent function evaluations could be easily parallelized. Additionally, grid search can handle discontinuities in the objective function and allows the use of multiple objective functions. The main disadvantage however is the exponential dependency of the execution time on the number of design

variables [84]. This strategy has been widely employed in finding the optimal values of many preparative objective functions[85, 86].

The time consuming exhaustive search could be avoided by using heuristic optimizers. Examples in this category include random search and Nelder-Mead optimization algorithms [87]. A class of these algorithms can be further distinguished into meta-heuristics. These algorithms combine different concepts derived from classical heuristics, artificial intelligence, biological evolution, neural systems and statistical mechanics to minimize one or more objective functions. Examples in this category include genetic algorithm, simulated annealing etc [88]. The main advantage again is that it is gradient free, allowing discontinuous objective functions. Compared to grid search, heuristic algorithms scan the domain much faster and can handle much more degrees of freedom. These algorithms too have been extensively implemented in chromatographic optimizations [89, 90, 91, 92, 93].

All of the heuristic search methods mentioned above use a gradient free search method. However, the feasible solution reached using these method do not certify the optimal solution [88]. But, given a convex domain and a smooth objective function, gradient based optimizers can find local optimal solution with very fast convergence rates [77]. Especially the gradient based NAND strategy can be employed very efficiently in this case. The results of the sensitivity analysis could be used by a suitable gradient based optimizer, e.g a sequential quadratic programming (SQP) routine. The simultaneous approach can be used even more efficiently to find local minimum of the objective function. The greatest disadvantage of these two approaches is that their applicability is greatly dependent on the smoothness of the objective function. Kawajiri and Biegler [94] used both gradient based nested and simultaneous design approaches to optimize simulated moving bed and power feed processes.

A set of much more simpler but important optimization problems concerning the estimation of cut-times from a chromatogram are discussed in the next chapter.

Chapter 4

Optimization of cut-times in preparative chromatography

While evaluating the preparative isolation of a target component from a mixture of multi-components, the performance parameters (Pr_i and Y_i) introduced in section 3.4 play a central role. The amount of the target substance collected (m_i) significantly influences any objective function calculated based on it. The m_i itself is related to the cut-times involved as given in equation (3.34).

This chapter provides some insights into various approaches involved in finding the cut-times for a ternary preparative chromatogram with the intermediate component as the target. These individual methods are then analyzed in the next section with the help of two case studies. In the end, few conclusions concerning their efficiency, accuracy and robustness that can be drawn are highlighted.

4.1 Approaches to find cut-times

The general task of finding cut-times for an intermediately eluting target component i in a multi-component chromatogram can be formulated as a maximization problem, constructed as :

$$\max_{t_1, t_2} m_i \quad (4.1)$$

s.t.

$$Pu_i \geq Pu_{lim} \quad \text{with} \quad Pu_{lim} \in [0, 1] \quad (4.2)$$

Hereby, the maximization of the amount of target collected (equation 4.1) is applicable to any intermediately eluting component. The m_i and Pu_i for the target are calculated using equations (3.34) and (3.35). It is worth noting that in case of separation of binary mixtures, either t_1 or t_2 is fixed depending on the choice of the target (trailing or leading component), consequently reducing the problem. Although the purity limit given by Pu_{lim} can take

any arbitrary real value in the interval 0 to 1, it is usually chosen relatively close to unity, so as to yield a high purity product.

The maximization problem given by equations (4.1) and (4.2) is illustrated in figure 4.1 for the target component ($i=2$, $N_c=3$) in the $t_1 - t_2$ space. The lower right half of the figure is empty because, the second cut-time is always greater than or equal to the first cut-time. In the figure, the isolines generated by the target amount collected increases with decreasing t_1 and increasing t_2 to a maximum possible value of $m_{inj,i}$, which is the injected mass of the component. On the other hand, widening the $t_1 - t_2$ interval causes a drop in the purity (thin lines) of the collected fraction. The optimum for the given purity limit is at the point where the isoline representing required purity (thin lines) meet the m_2 isolines (thick lines) tangentially. This holds true as long as the cut-times are continuous in nature.

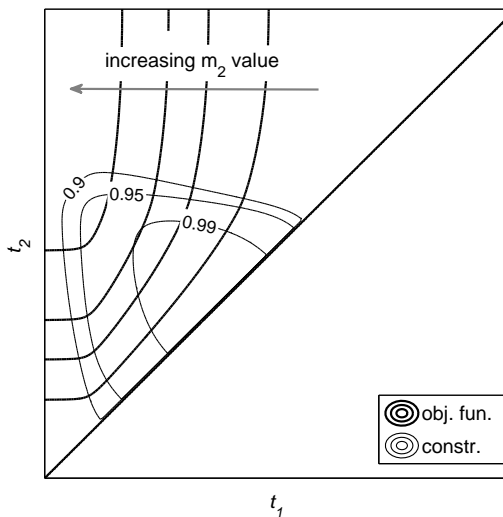


Figure 4.1: Contours of the objective function (thick lines) and the purity constraint (thin line), corresponding to the chromatogram in figure 3.5

This has the advantage that the maximization of the form given by equations (4.1) and (4.2) can be readily applied to get optimal t_1 and t_2 . However in reality, chromatograms generated by detectors or by numerical solutions of mathematical models usually results in discrete data. These elution profiles at the end of a column are generally represented by an $N_t \times N_c$ matrix, with N_t being the number of time steps and N_c the number of components. For such a discrete system, the integral term in equation (3.34) can be replaced with a summation as :

$$m_i = \dot{V}_f \Delta t \sum_{k=k_1}^{k=k_2} C_i^k \quad (4.3)$$

where Δt represents the constant time step, k the index of each of these time steps, k_1 and k_2 being the corresponding indices for t_1 and t_2 respectively.

Based on the nature of the data in hand, cut-times optimizations can be classified into discrete and continuous variants.

4.1.1 Discrete cut-time optimization

Given a data set consisting of multi-component concentrations over discrete time points, the optimal $t_1 - t_2$ interval can be found using two approaches. The first one is based on evaluating local purities and was first suggested by Shan and Seidel-Morgenstern [95]. The second approach developed in this work involves the introduction of binary variables to describe the selection of data points in order to formulate and solve the task as a mixed integer non-linear problem.

4.1.1.1 By evaluating local purities

For a multi-component discrete chromatogram, the local purity of a component i at a time step k can be written as:

$$Pu_{loc,i}^k = \frac{C_i^k}{\sum_{i=1}^{N_c} C_i^k} \quad (4.4)$$

The first step in maximizing the amount of target collected involves choosing an initial cut-time interval $t_1^0 - t_2^0$. Figure 4.2 shows a plot of local purity of the target ($i=2$) against the time for the chromatogram shown in figure 3.5. The interval $t_1^0 - t_2^0$ represents a period inside which $Pu_{loc,i}^k$ always remains above the purity limit, which in this case is 0.99. Thus, any integral purity (equation (3.35)) calculated within this interval provides a value above 0.99. This interval becomes the starting point for the algorithm proposed by Shan and Seidel-Morgenstern [95]. Once the $t_1^0 - t_2^0$ is calculated, the interval could be widened in either of the directions (towards lower or higher retention times) or in both directions to increase the value of m_2 as long as the purity criterion (equation (4.2)) is satisfied. The study found out that, expanding the interval in both directions results in larger amount of the target collected than expanding the interval in either of the directions [95].

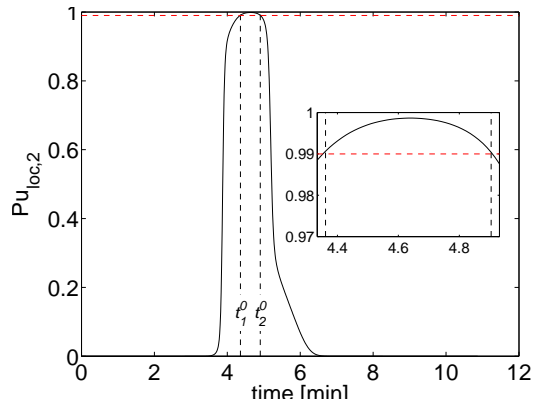


Figure 4.2: Local purity (Pu_{loc}) of the target component against time. $t_1^0 - t_2^0$: interval in which $Pu_{loc} \geq Pu_{lim}(0.99)$

Figure 4.3 shows an example of the trajectory taken by the algorithm expanding in both directions. Starting from $t_1^0 - t_2^0$, the algorithm expands the interval in a direction giving maximal increase in m_2 , until the purity reduces to the chosen Pu_{lim} value. The last set of time points ($t_1^* - t_2^*$ in the figure) satisfying the purity constraint is taken as the optimal values. Owing

to the discrete nature, the resulting purity lies typically slightly above the Pu_{lim} unless the isoline representing Pu_{lim} passes through $t_1^* - t_2^*$. However, given very fine concentration data, i.e for very small Δt s, this difference tends to zero.

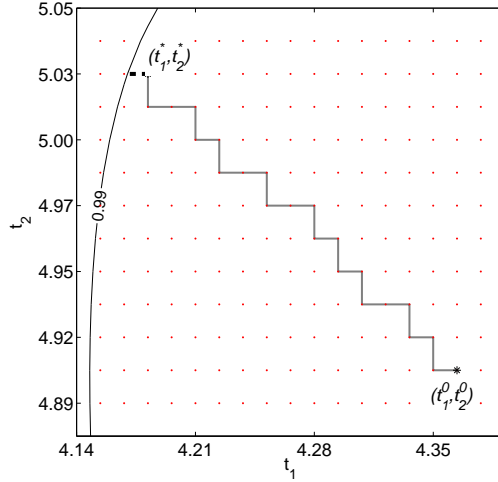


Figure 4.3: Trajectory taken by the algorithm when expanding in both directions (thick gray line). Dashed segment : terminal step when $Pu_{des,2} < Pu_{lim} = 0.99$

The algorithm thus finds a good approximation for the cut-times. The main advantages are its simplicity and fast convergence.

4.1.1.2 Optimization using binary variables

The maximization problem given by equations (4.1), (4.2), (4.3) and (3.35) can be solved using more sophisticated mathematical tools. The idea is to introduce an additional integer binary variable x^k for each time point k . The variable can take either a value of 1 if the point is selected or a value of 0 when not selected. On a uniform time grid ($\Delta t = \text{constant}$), the maximization of the objective function constructed using the new binary variable can be written as:

$$\max m_i = \dot{V}_f \Delta t \sum_{k=1}^{N_t} x^k C_i^k \quad \text{with } x^k \in \{0, 1\} \quad (4.5)$$

It is worth noting that unlike in equation 4.3, here the summation limits consider the full length vector C_i^k running from $k = 1$ to N_t . And by fixing the value of $x^k = 1$ for $k = k_1 \dots k_2$ and 0 otherwise, the same effect is achieved. It is this $k_1 - k_2$ interval that needs to be found by the optimization routine.

The purity constraint again can be reformulated by similar means.

$$Pu_i = \frac{\sum_{k=1}^{N_t} x^k C_i^k}{\sum_{i=1}^{N_c} \sum_{k=1}^{N_t} x^k C_i^k} \geq Pu_{lim} \quad (4.6)$$

With the additional variables introduced, however, come new constraints. The formulation given above does not say anything about the sequence of the time points to be selected. In order to ensure continuity between the points k_1 and k_2 , the addition of two new constraints is necessary. These are :

$$x^k = \begin{cases} 1 & \text{if } (x^{k-1} = 1 \text{ AND } x^{k+1} = 1) \\ 0 & \text{if } (x^{k-1} = 0 \text{ AND } x^{k+1} = 0) \end{cases} \quad \forall k \in [2, N_t - 1] \quad (4.7)$$

The constraints given by the equation above simply forces the nodes chosen to be in one single sequence. i.e. by avoiding any single x^k with value 1 in between two nodes with zero values or vice versa.

The linear objective function (equation (4.5)) together with the non-linear constraints (4.6) and (4.7) form the optimization problem which can be categorized as a mixed integer non-linear problem (MINLP). Although the purity constraint could be formulated as a linear constraint (by shifting the denominator of equation (4.6) to the R.H.S), the problem would still be non-linear as long as the continuity constraints are enforced.

The discussion so far has been with the consideration of the whole time domain containing data. Given any chromatogram, the insignificant parts of the chromatogram could be disregarded, taking into account only a certain area of interest. This interval could be fixed or evaluated based on chromatogram specific criteria like threshold concentrations or areas. For instance, in the chromatogram illustrated in figure 3.5, concentration of the target component is negligible before 3.5 min and after 6.5 min. Thus, the chromatogram could be cut short to this interval based on a suitable threshold concentration (C_{thr}). The best option that favors higher performance parameters, is to set C_{thr} as a fraction of the maximum concentration of the chromatogram [95]. Reducing data is particularly helpful in applying this MINLP formulation as there are as many binary variables as the number of data points considered.

4.1.2 Continuous cut-time optimization

Based on the fact that continuous optimizations are easier to carry out than discrete ones [77], it is desirable to use concentration profiles which are smooth functions of time. From the modeling point of view, these profiles can be provided by solving the underlying mass balance equations (given in the last chapter). In linear chromatography, such functions are more easily derived. Most of the multi-component analytical chromatograms can be described by near gaussian functions, e.g. [96]. In contrast to linear systems, analytical solutions for preparative multi-component cases are hard to conceive. Only in few simple cases, there are analytical solutions of the equilibrium dispersive model to describe single component overloaded chromatograms [97, 98, 99].

On the other hand, prediction of multi-component preparative chromatograms can be done using a set of analytical expressions derived from the solution of the ideal model. This method which involves neglecting any sort of mass transfer effect generates solutions with shock fronts, that are discontinuous in time [54]. More details on the analytical solution of simplified mass balance equations can be found for example in [54, 53].

In reality however, the discontinuous shock fronts of overloaded chromatograms are smoothed out by non-ideal dispersive effects. These individual peaks can therefore be effectively described by empirical but continuous functions. Over the years many research groups have proposed a multitude of such functions with varying complexities. A review with over 90 such function can be found in [100]. Many sets of the functions can be used for describing a variety of chromatograms including those characterized by peak asymmetry and tailing.

Given an over loaded multi-component discrete chromatogram, a suitable multi-parameter continuous empirical function could be parameterized for each component. A great advantage of using empirical functions is that they require only few parameters to describe the profiles. However, these functions are rather limited to chromatograms with known characteristics including peak asymmetries, shock and tailing fronts. In contrast, on the basis of various underlying factors, a multi-component preparative chromatogram could exhibit very complex non-standard shapes including multiple maxima. In such cases, empirical functions are often inaccurate to describe the actual chromatogram. In this context, interpolating functions could be effectively used. Among all such functions, a cubic spline interpolation is a suitable candidate, due to the fact that the resulting function is double differentiable (sufficiently smooth)[101, 102] and can be readily used with a gradient based optimizers.

Smooth functions ($C_i = f_i(t)$) could thus be generated by fitting any suitable empirical function or by interpolation of the discrete data. These function could then be used in equations (4.1) and (4.2) to maximize the interval $t_1 - t_2$ in a continuous manner.

4.2 Comparison of methods

As discussed in the previous sections, there are two discrete and a continuous approach available to maximize the cut-time interval. In order to compare the accuracy and efficiency of the three methods, two test cases were considered. The first case was for a ternary chromatogram consisting of symmetric peaks with an analytical expression for the amount of target collected. In the second test case, an overloaded non-linear chromatogram was considered, generated for three components using the equilibrium dispersive model.

4.2.1 Symmetric case

The symmetric linear ternary chromatogram for this case was generated using the Lorentzian (Cauchy) function given by [103, 104]:

$$C_i = \frac{h_i}{1 + 4 \left(\frac{t - t_{r,i}}{\sigma_i} \right)^2} \quad (4.8)$$

where $h_i, t_{r,i}$ and σ_i are the three parameters of the empirical function. Here, h_i represents the height of the peak, $t_{r,i}$ the retention time and the peak broadening characterized by σ_i .

The continuous concentration profiles generated using parameters given in table 4.1 is plotted in figure 4.4. The main advantage of using a Lorentzian function is that, it has an analytical expression for its definite integral [105]. On the contrary, most of the empirical functions tabulated by Marco and Bombi [100] does not have a definite integral and have to be determined numerically.

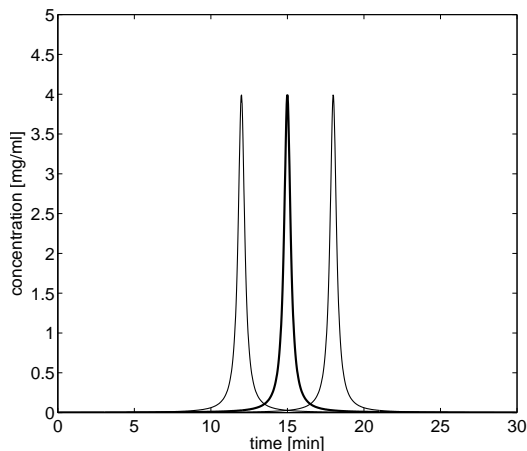


Figure 4.4: Symmetric chromatograms with middle component as target (thick line) generated by the Lorentzian function 4.8. Parameters from table 4.1

Assuming a constant flowrate (\dot{V}_f) of 1 ml/min, the mass of component

i collected (as per equation (3.34)) was derived as :

$$m_i = \frac{h_i}{2\sigma_i} \left[\tan^{-1} \left(2 \frac{t_2 - t_{r,i}}{\sigma_i} \right) - \tan^{-1} \left(2 \frac{t_1 - t_{r,i}}{\sigma_i} \right) \right] \quad (4.9)$$

with $h_i, \sigma_i, t_{r,i}, t_1, t_2 \geq 0$

For the chromatogram in figure 4.4, the amount of target ($i = 2$) collected was maximized with a purity constraint of $Pu_2 \geq 0.90$. The optimal value was found to be $m_2 = 2.8706$ mg, with $t_2 = 13.1663$ and $t_1 = 16.8337$ min. The continuous optimizations including this one were carried out in MATLAB with 'fmincon' as the optimizer. The optimal values above were used to compare the efficacy of the three different more widely applicable optimization approaches describe in the previous section.

Table 4.1: Parameters used for the chromatograms given in figure 4.4

Parameters	$i=1$	$i=2$	$i=3$
	(target)		
h_i [mg/ml]	4	4	4
$t_{r,i}$ [min]	12	15	18
σ_i [min]	0.5	0.5	0.5

The data needed for generating the discrete chromatogram was generated again using equation (4.8), however using different discrete time sets (time data with various Δt). The algorithm based on local purity (LocPur) was applied with 'expansion in both directions'. For the mixed integer (MINLP) optimization, the freely usable online NEOS server for optimization [106] was employed in AMPL[107] programming environment. In case of continuous optimization (ContOpt), for each data set, cubic spline interpolation within the time intervals was used to describe the concentrations. The areas under the chromatogram were determined using the MATLAB function based on trapezoidal rule for numerical integration. For the example considered in figure 4.4, the time span covered was 0 to 30 min. This interval was uniformly discretized using different Δt to generate as many sets of time data with N_t number of points ($N_t = 30/\Delta t$).

Figure 4.5 shows the influence of the degree of discreteness (N_t) on the performance evaluated using different optimization approaches. The amounts of target collected with corresponding purity and the CPU times* required are compared. In figure 4.5d, m_2 values obtained using the three different algorithms are compared to the available analytical value (solid black line in

*Evaluated on a PC with the following configuration:
Processor, Intel Pentium D CPU @ 3.00GHz with 2 GB RAM running on SUSE LINUX 10.1

the figure, $m_2 = 2.8706$ mg). All the three methods deviate from actual value for chromatogram on coarse time data ($N_t \leq 200$). The largest difference is seen with LocPur algorithm, however the maximum difference seen at $N_t = 180$ is only around 0.42 %. In all cases, the differences diminish with increasing number of grid points (increasing N_t). The results of the MINLP optimization are same as that of the local purity based algorithm. The continuous optimization on the other hand yields m_2 values that coincide well with the actual m_2 value. By virtue of the domain considered, trends of MINLP and LocPur are discrete in nature, whereas ContOpt does not exhibit any visible discontinuities. A sum of these effects is reflected in the calculated purities (figure 4.5b). Purities by LocPur and MINLP always remain slightly above 0.9 (Pu_{lim}), whereas ContOpt respects the constraint more tightly. Both these results are a consequence of the $t_1 - t_2$ interval found by the different algorithms. This is shown in figure 4.5c. The results of MINLP are excluded from the figure because they are the same as those for LocPur. Once again, a smoother and larger $t_1 - t_2$ interval is found by ContOpt in comparison with a fluctuating and slightly smaller interval reached by MINLP and LocPur. The last figure shows an example of the time required to execute each of these optimization routines as a function of the time nodes N_t . It took only a couple of milli seconds to execute LocPur irrespective of the size of the problem. This behavior is same for ContOpt, however it takes in this case close to a second for execution. Online NEOS server was used because of the non availability of a local solver. Eventhough contemporary MINLP solvers can solve large scale problems in a very small amount of time [108], solution of the MINLP implementation in this study took few seconds of CPU time. A large part of this time included the time taken for data transfer to and from the NEOS server, in addition to the queue waiting time.

An overall analysis of figure 4.5 suggests that very good estimates of m_2 can be achieved even on a coarse grid with the LocPur algorithm. The greatest advantage of using local purity based algorithm is its speed. Besides, implementing the algorithm does not require access to special optimization packages or use of advanced modeling languages. The correctness of this algorithm in this simple case was confirmed by MINLP optimization, which gives exactly the same result for the symmetric chromatograms considered in this test example. A small drawback of using this fast algorithm is the discontinuity of m_2 with respect to the number of grid points. Any objective function based on m_2 (e.g. Productivity and Yield) would be equally discontinuous. ContOpt on the other hand is the most accurate algorithm and is fairly fast. It's solution however requires interpolation functions and the application of a constrained non-linear optimizer. Solving MINLP would require further advanced solvers and use of special modeling languages (e.g. AMPL).

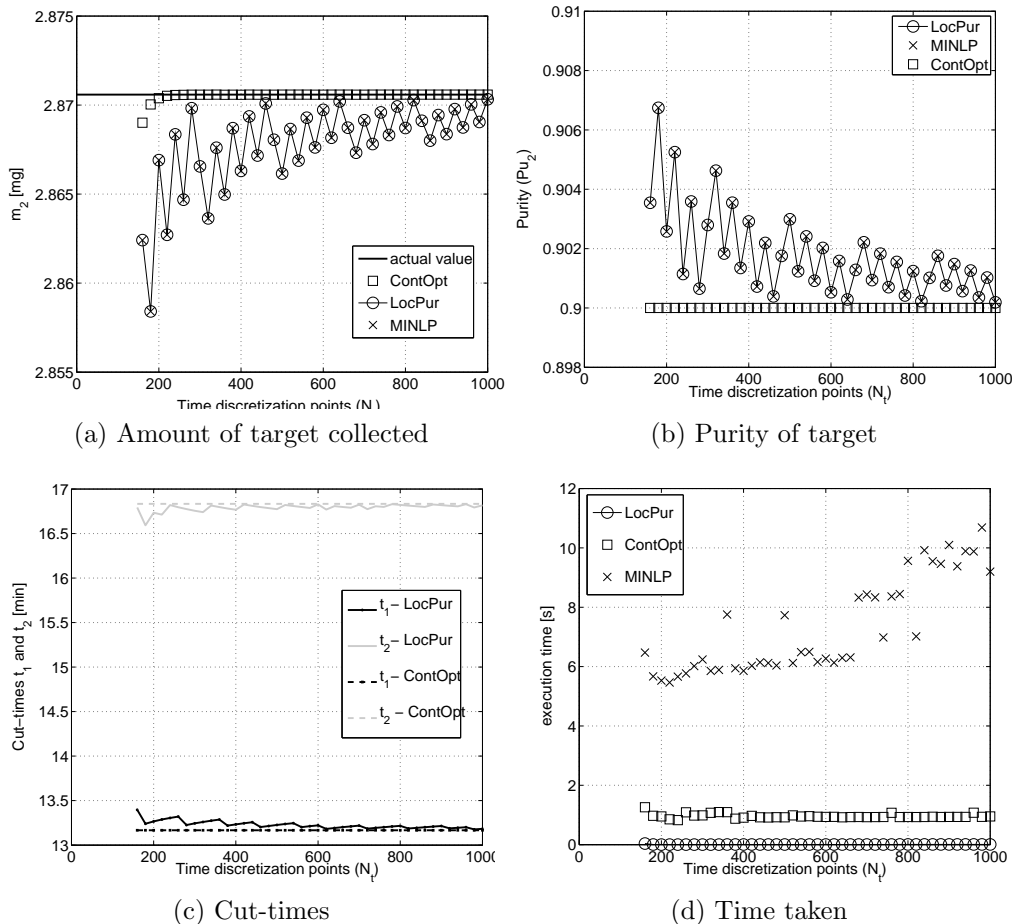


Figure 4.5: Influence of the degree of discreteness on the performance of different optimization approaches

4.2.2 Non-linear case

In this case, the equilibrium dispersive (ED) model introduced in section 3.1.2 was used to generate a ternary non-linear chromatogram using competitive Langmuir adsorption isotherms (equation 3.27). The model was solved numerically using Rouchon's method explained in section 3.3. Parameters tabulated in table 4.2 were used for the numerical solution. Chromatograms with different Δt (subsequently different N_t) were obtained by varying the Courant number (a_{cou}) between 1.5 and 2.5. The resulting chromatograms for these two limits are illustrated in figure 4.6. Minor discrepancies in the two profiles with different Courant numbers arise due to the inaccuracies associated with the numerical solution of the ED model, explained in section 3.3. As expected, the differences are more pronounced for the low retaining component and less prominent towards higher retention times.

As in the previous case, the three optimization approaches were again

used to maximize the interval $t_1 - t_2$ for the intermediately eluting target. The resulting values of m_2 , Pu_2 , t_1 and t_2 are plotted in figure 4.7.

As shown in figure 4.7a, the m_2 values estimated using all three methods increase with increasing degree of discretization (N_t). This is a direct result of the profile discrepancies associated with changing Courant number. The m_2 values obtained as a function of N_t using LocPur method is again very discrete in nature. An important observation in this case however is that there are many occurrences where the MINLP formulation gives slightly better m_2 estimates than LocPur method, which otherwise are no different. This was not seen in the symmetric case. Results predicted by the MINLP method are thus the same or slightly better than those predicted by LocPur method, suggesting that in the non-linear case, the latter could generate sub optimal solutions. The second key observation is that unlike in the previous case, the m_2 values estimated using ContOpt are not entirely continuous with respect to the grid size. They nevertheless give the slightly more reliable estimates for m_2 in comparison with the other two methods.

The discontinuities in m_2 arise from the t_1 and t_2 values predicted by the optimization algorithms. The dependencies of these two cut-times are illustrated in figures 4.7b and 4.7c. Due to a greater change in the profiles towards lower retention and as a result of the peak asymmetry, estimated t_1 varies considerably with grid size (from around 36 to 34.5 min). In contrast, t_2 being on the more retained tailing side, does not show a large variation. In case of t_1 , ContOpt yields the lowest estimates (lower t_2 implies larger m_2) among all algorithms. MINLP likewise gives the same or better result as the LocPur method. For the relatively insensitive variable t_2 , MINLP shows large fluctuations in the optimal values and in some instances results in values higher than that obtained by ContOpt.

Figure 4.7d shows the resulting purity of the target component estimated by the three methods. Given the continuous nature of variables in ContOpt, the generated Pu_2 values are exactly at the limit set ($Pu_{lim} = 0.95$). This however is no longer true in the other two discrete cases with the resulting purity always above the constrained limit.

In general, presence of non-linearities could impart discontinuities in the m_2 estimated using the continuous optimization method implemented. Additionally, based on the nature of the isotherms, the sensitivities of t_1 and t_2 can increase or decrease. The LocPur algorithm on the other hand can lead to suboptimal solutions in complex cases.

Table 4.2: Parameters used to simulate the preparative chromatogram in figure 4.6

Parameter	Value
Column length (L)	20 [cm]
Inner dia. (d_c)	0.8745 [cm]
Porosity (ϵ_j)	0.775
Theoretical plates (N)	700
Flowrate (\dot{V}_f)	1 [ml/min]
Injected concentration ($C_{inj,i}$)	20 [g/l]
Purity limit (Pu_{lim})	95%
Threshold concentration (C_{thr})	10^{-4} [g/l]
Saturation capacity ($q_{sat,i}$)	50 [g/l]

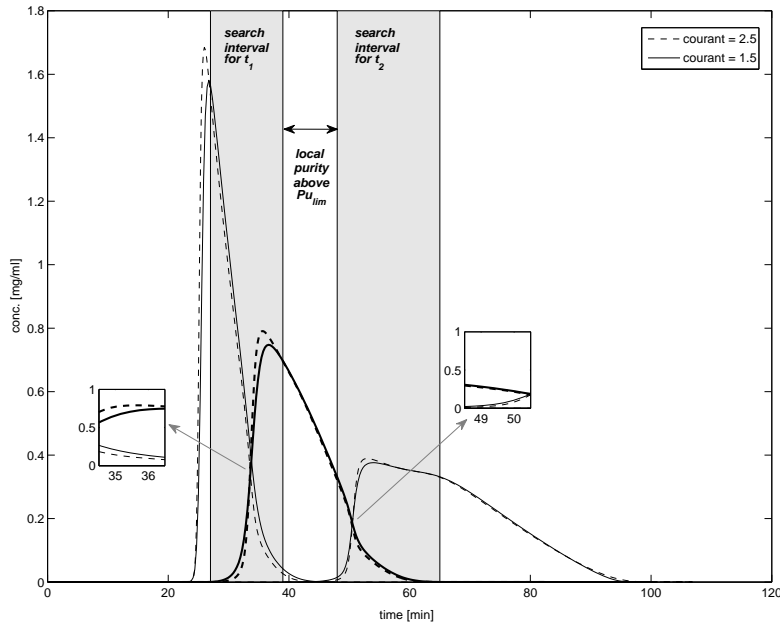


Figure 4.6: Sample preparative chromatograms simulated with $a_1 = 13.33$, $a_2 = 20.00$, $a_3 = 30.00$. Other parameters from table 4.2. Time discretization points of the chromatogram (numerical solution of ED model, see section 3.3) changed by varying the Courant number between 1.5 and 2.5

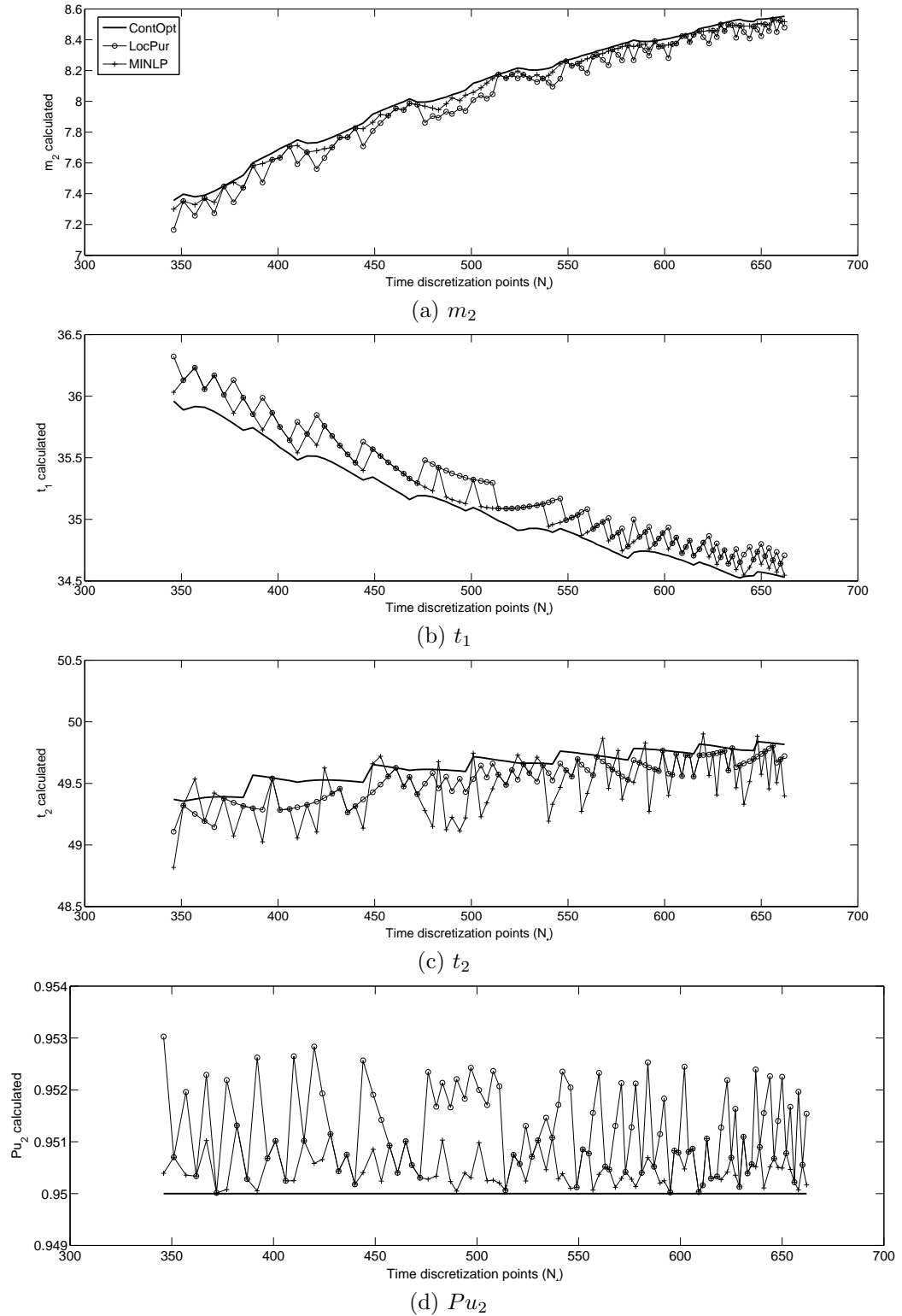


Figure 4.7: Influence of the degree of discreteness (N_t) on the performance of different optimization approaches, using an asymmetric overloaded chromatogram (figure 4.6)

4.3 Conclusions

Using a symmetric linear and an overloaded non-linear chromatogram, three different approaches to find optimal cut-times for the intermediately eluting component were studied. A discrete optimization strategy based on binary variables (MINLP) and a continuous method based on interpolating functions (ContOpt) were developed and compared with an established strategy based on the evaluation of local purities (LocPur). The MINLP formulation generated exactly the same results as obtained by LocPur for symmetric chromatograms. Whereas in the non-linear case, many instances were found where the solutions given by LocPur were slightly suboptimal. Even though the method based on local purity gives results that are discontinuously dependent on the grid size used to produce the chromatogram, they are sufficiently accurate and the results are obtained extremely fast. The discontinuity factor is of paramount relevance when an objective function derived from the mass of the target is used later in a continuous optimization problem. Presence of discontinuities would lead to unrealistic Jacobians, which might adversely effect convergence. The question of imparting continuity to the LocPur method is still open. One way to get around this problem is to fit the discrete data to an interpolating function, and to use continuous optimization. Another advantage of addressing the cut-time finding process as an optimization problem is that, additional purity constraints with regard to other fractions (e.g. $Pu_1 \leq 0.05$ or $Pu_3 \geq 0.01$) could be easily implemented.

In order to eliminate the discontinuous dependence of the amount of target collected on the grid size, the local purity algorithm could be further improved to impart continuity. Finally it should be mentioned that, the problem discussed here was considering a single maxima for the local purity of the target in time as illustrated in figure 4.4. In reality however, the occurrence of multiple maxima cannot be ruled out. Hence the cut-time finding algorithms should be validated considering such possible situations and should be further improved.

In the next chapter, the optimized cut-times found using the LocPur method for the intermediately eluting component of a ternary mixture are used to compare the separation performances of different chromatographic operation modes.

Chapter 5

Theoretical study using closed-loop recycling with an initial gradient

Results of this chapter were published earlier by the author in *Journal of Chromatography A* [93].

5.1 Introduction

Preparative chromatography is an important process for the isolation and purification of value added components from complex mixtures. The first important step in solving a specific separation problem is to find a suitable combination of stationary and mobile phases. This selection is usually performed based on the results of screening experiments at an analytical scale. Once the chromatographic system is fixed, there are several degrees of freedom which should be exploited in an optimal manner. In classical isocratic elution, in the first row these degrees of freedom are; the column dimensions, the injected amounts and the flow rates [54]. It has been demonstrated frequently, that classical elution is not always the most attractive mode of operation [52]. Often production rates and yields achievable using this mode are not sufficient. For this reason several alternative operation highlighted in the first chapter can be implemented.

The closed-loop recycling concept, introduced in section 1.3, can be effectively used to increase the number of theoretical plates without increasing the actual length of the chromatographic column. The strategy involves repeated recycling of certain parts of the elution profile containing the target component until the required separation is reached. As simulated for a model ternary system in figure 5.1, the fraction containing the target component can be collected in the example case considered at the end of the fourth cycle with high purity and yield.

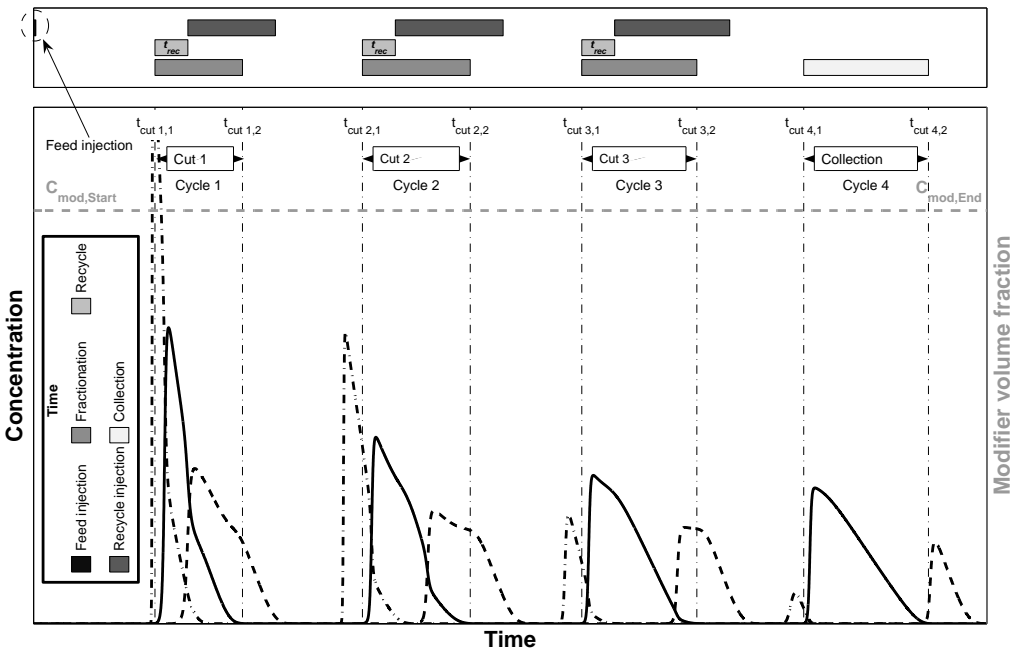


Figure 5.1: Simulated concentration profiles for a closed-loop recycling configuration (see figure 1.2). The intermediate part of the profiles containing the second (target) component is recycled until the required purity and yield are achieved

Another promising alternative to improve production rates are the use of solvent gradients. As mentioned in section 1.4.1, by increasing the elution strength of the mobile phase, the slowly eluting components could be speeded up, reducing the cycle time. A concept of linear solvent gradient was illustrated in figure 1.3.

It should be emphasized that the better separation performance achievable by employing alternative operation modes is due to additional specific degrees of freedom compared to classical elution. For example, in the closed-loop recycling mode, variables like the number of cycles and concentration thresholds for fractionation could be additionally optimized. In linear gradient elution, the variables $C_{mod,start}$, $C_{mod,end}$, $t_{g,end}$ and $t_{g,start}$ (figure 1.3) could be selected to improve the performance of the process.

The objective of the work presented in this chapter was to evaluate theoretically the potential of combining the advantages of both solvent gradient and recycling modes. More specifically, an attempt was made to investigate if an innovative process scheme which exploits closed-loop recycling combined with an "initial" gradient (CLR-G) could be advantageous with respect to

typical objective functions compared to conventional isocratic batch elution (B-ISO), batch gradient elution (B-G) and conventional isocratic closed-loop recycling (CLR-ISO). The evaluation was carried out theoretically using a simulation study considering a ternary feed mixture in which the intermediately eluting component as the target component.

5.2 Closed-loop recycling with an initial gradient

The recycling strategy of the CLR-G scheme resembles that of the conventional closed-loop recycling process, illustrated in figures 1.3 and 5.1. However, the first cycle is exposed to a linear gradient (varying the content of the modifier in solvent between $C_{mod,start}$ and $C_{mod,end}$). A part of this linear gradient might be recycled back together with the part of the elution profile containing unresolved components. Figure 5.2 illustrates concentration profiles at the outlet of the column (simulated with the model considered in section 5.4) for 4 cycles applied to separate component 2.

The amount of modifier in the mobile phase was changed in the simulation immediately after the injection of the sample was completed. Hence, the gradient profile appears at the end of the column after a period equivalent to the sum of the retention time of the solvent (which is assumed here to have no interaction with the solid phase) and the injection time of the samples. The whole part of the profile of effluent containing the intermediate component is, recycled along with parts of the overlapping neighboring components 1 and 3. This part of the profile, including a solvent composition profile is recycled directly back to the column inlet forming the second (recycled) injection. Hereby, the re-injection of the recycled part of the profile occurs at the inlet of the column after an additional dead time due to a finite volume of the recycle path (t_{rec}). Thus, the elution profile part injected for the second cycle (cut 1) could also still contain a modifier profile that will be recycled along with the components. Again, the modifier in the reinjected part is not retained and continues to propagate through the column with the mobile phase velocity, which in turn might influence the elution profile of the most retained component from the first injection (depending also on the volume of the sample injected). In the example used for illustration, soon after the re-injection of the part of the profile in the second cycle, the modifier volume fraction reaches its final value ($C_{mod,end}$) and subsequent cycles behaves like an isocratic closed-loop recycle scheme exploiting exclusively this final modifier concentration. The recycling procedure can be stopped after a fixed number of cycles or as soon as required purity and yield criteria are met. In the case illustrated in figure 5.2, the target component 2 is harvested in the fourth cycle. Finally for periodic operation, a regeneration step is needed to re-equilibrate the column back to the mobile phase concentration $C_{mod,start}$.

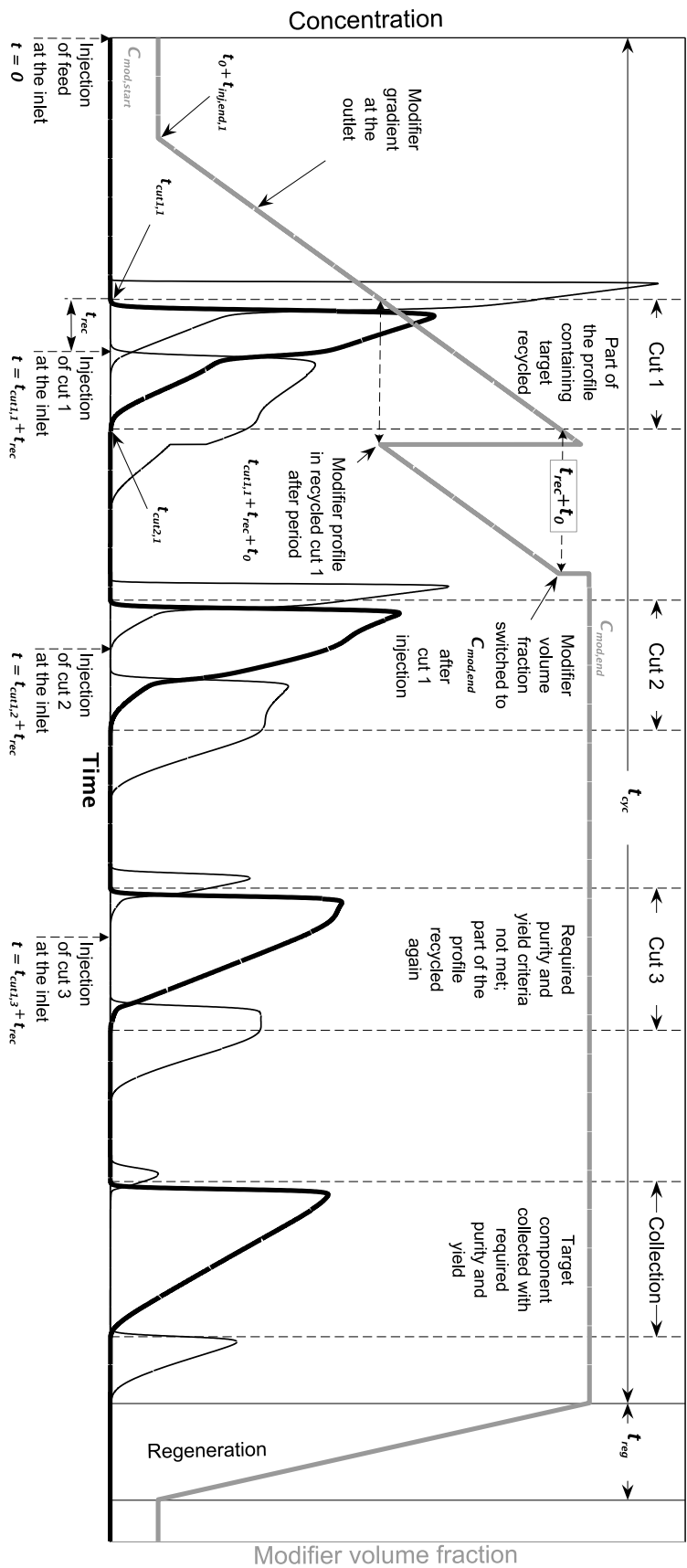


Figure 5.2: Simulated concentration profiles at the outlet of the column for closed loop recycling with initial gradient (CLR-G) using 4 cycles (Conditions : $L_{f,tot} = 18$, $G=3\%$ /min, other parameters from Table 5.2).

5.3 Adsorption equilibria

In order to compare the different chromatographic operation modes mentioned above, competitive Langmuir adsorption isotherms were used (introduced in section 3.2.2, equation 3.27). The effects of changing mobile phase concentration were incorporated into the adsorption isotherm parameters a_i and b_i as a function of C_{mod} (see equations 3.28 and 3.29). When the Henry coefficients of two closely eluting peaks vary with C_{mod} , their separation factors ($\alpha_{i,j}=a_j/a_i$ with $a_j > a_i$) also vary. With an increase in modifier volume fraction, the separation factor between two neighboring components could remain *constant*, decrease (*converging* case) or increase (*diverging* case). Since we consider here a set of two separation factors associated with a ternary mixture ($\alpha_{1,2}$ and $\alpha_{2,3}$), each with three possible dependencies on C_{mod} , 9 different cases are possible in principle (*constant-constant*, *divergent-convergent*, *divergent-divergent* etc.). Combinations involving *constant* and the case *divergent-divergent* have been omitted in this study. Thus, the proposed CLR-G scheme was analyzed below and compared with the conventional operational modes for the following three $\alpha_{1,2}$ and $\alpha_{2,3}$ cases :

- *convergent-convergent*
- *convergent-divergent*
- *divergent-convergent*

The *convergent-convergent* type is often exhibited in the reversed phase separation of small molecules in a homologous series, for example [109]. The types of adsorption isotherm behaviors mentioned above were investigated considering typical retention time and selectivity dependences of small molecules with change in solvent strength. As in [35], the values of $a_{1,i}$ and $a_{2,i}$ (equation 3.28) given in table 5.1 were generated in such a way that the Henry coefficient a_2 is reduced from 39 to 6 with increasing modifier volume fraction between 5 and 50 %, along with an increase in selectivities ($\alpha_{1,2}$ and $\alpha_{2,3}$) from 1.2 to 1.3 (*divergent*) or a decrease in selectivities from 1.3 to 1.2 (*convergent*). The gradient start and end values of the modifier volume fractions were fixed at the values mentioned, i.e. 5 and 50%. Additionally, the saturation capacities of the stationary phase ($q_{sat,i}$) were assumed to be 50 [mg/ml] for all components. Based on this assumption and the calculated $a_{1,i}$ and $a_{2,i}$ values, isotherm parameters $b_{1,i}$ and $b_{2,i}$ could be derived from equation 3.29 and the relation $b_i = a_i/q_{sat,i}$. All parameters applied below are summarized in table 5.1. As an example, the dependencies of a_i and $\alpha_{i,j}$ on C_{mod} for the *convergent-divergent* case are illustrated in figure 5.3.

Table 5.1: Adsorption isotherm parameters of equations 3.28 and 3.29, for three different cases (see Figure 5.3 for illustration)

Isotherm parameters	First component $i = 1$	Second component $i = 2$ (target)	Third component $i = 3$
convergent - convergent			
$a_{1,i}$	0.0025	0.0022	0.0019
$a_{2,i}$	-0.7782	-0.8129	-0.8477
$b_{1,i}$	0.3856	0.2715	0.1967
$b_{2,i}$	-0.7782	-0.8129	-0.8477
for $C_{mod} = 5.0$			
a_i	30.0000	39.0000	50.7000
b_i	0.6000	0.7800	1.0140
$\alpha_{i,i+1}$	1.3000	1.3000	-
for $C_{mod} = 50.0$			
a_i	5.0000	6.0000	7.2000
b_i	0.1000	0.1200	0.1440
$\alpha_{i,i+1}$	1.2000	1.2000	-
convergent - divergent			
$a_{1,i}$	0.0025	0.0022	0.0014
$a_{2,i}$	-0.7782	-0.8129	-0.7782
$b_{1,i}$	0.3856	0.2715	0.2177
$b_{2,i}$	-0.7782	-0.8129	-0.7782
for $C_{mod} = 5.0$			
a_i	30.0000	39.0000	46.8000
b_i	0.6000	0.7800	0.9360
$\alpha_{i,i+1}$	1.3000	1.2000	-
for $C_{mod} = 50.0$			
a_i	5.0000	6.0000	7.8000
b_i	0.1000	0.1200	0.1560
$\alpha_{i,i+1}$	1.2000	1.3000	-
divergent - convergent			
$a_{1,i}$	0.0033	0.0022	0.0019
$a_{2,i}$	-0.8477	-0.8129	-0.8477
$b_{1,i}$	0.3325	0.2715	0.1967
$b_{2,i}$	-0.8477	-0.8129	-0.8477
for $C_{mod} = 5.0$			
a_i	32.5000	39.0000	50.7000
b_i	0.6500	0.7800	1.0140
$\alpha_{i,i+1}$	1.2000	1.3000	-
for $C_{mod} = 50.0$			
a_i	4.6154	6.0000	7.2000
b_i	0.0923	0.1200	0.1440
$\alpha_{i,i+1}$	1.3000	1.2000	-

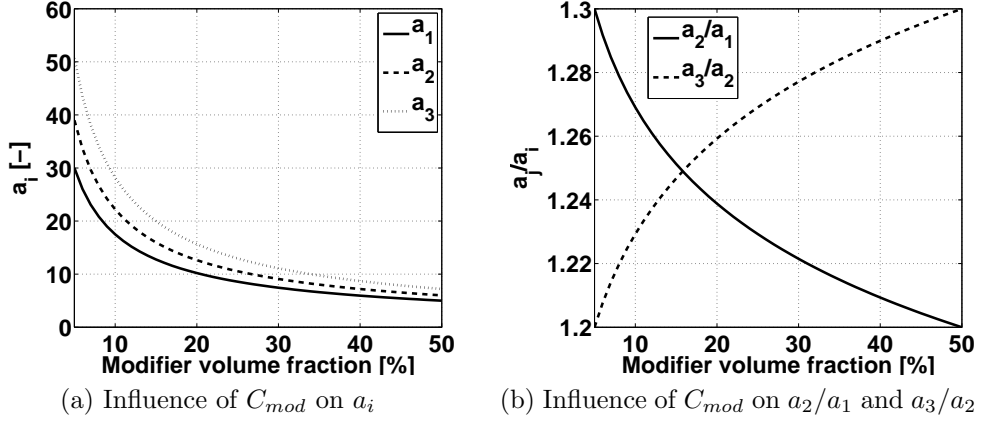


Figure 5.3: Dependencies of adsorption isotherm parameter a_i (equations 3.28 and 3.29) on modifier volume fraction C_{mod} ; *convergent-divergent* case, (parameters from Table 5.1)

Table 5.2: Parameters of the chromatographic system analyzed

System parameters	Value
Length of the column (L)	10 [cm]
Cross sectional area of the column (A_{col})	0.6 [cm ²]
Total column porosity (ϵ)	0.775
Number of theoretical plates (N)	1000
Linear velocity of mobile phase (u)	2.1505 [cm/min]
Initial injected sample concentration ($C_{inj,i}$) ($C_{inj,1}=C_{inj,2}=C_{inj,3}$)	20 [g/l]
Desired purity of component 2 ($P_{u_{lim}}$)	99%
Threshold concentration for fractionation (C_{thr})	10^{-3} [g/l]

5.4 Column model and numerical solution

The Craig model introduced in section 3.1.1 was used to simulate the elution profiles for all the modes studied. It is particularly suited for modeling separation processes involving solvent gradients [54]. The corresponding equation 3.1 was used to simulate the propagation of components in the column. In the equation, the equilibrium loadings

$$q_{i,p} = q_{i,p}(C_{1,p}, C_{2,p}, \dots, C_{N,p}, C_{mod}) \quad (5.1)$$

are also dependent on C_{mod} as described by equations 3.27, 3.28 and 3.29. To adjust the predictions of this discrete stage model to the real continuous

process, each shift (from k to $k + 1$) corresponds to a real time step given by

$$\Delta t = \frac{t_0}{N} \quad (5.2)$$

$$\text{with } t_0 = \frac{\epsilon A_{col} L}{\dot{V}_f} \quad (5.3)$$

where t_0 is the elution time of a non-retained compound or the column hold up time. To complete the mathematical model, proper inlet and boundary conditions are needed. The following conditions were used:

$$C_{i,j}^0 = 0 \quad i = 1, N_c \quad j = 1, N \quad (5.4)$$

$$C_{i,0}^k = \begin{cases} C_{i,inj} & \text{for } 0 \leq k\Delta t \leq t_{inj,end,1} & [\text{r}=1, \text{ feed injection}] \\ C_{i,P,k\Delta t-t_{rec}} & \text{for } t_{inj,start,r} \leq k\Delta t \leq t_{inj,end,r} & [\text{r}>1, \text{ recycle}] \\ 0 & \text{for } k\Delta t \geq t_{inj,end,r} & [\text{r}=1, N_{cyc}, \text{ elution}] \end{cases} \quad (5.5)$$

In the above equation, $t_{inj,start,r}$ and $t_{inj,end,r}$ represent the starting and ending time of injection in the r^{th} cycle out of N_{cyc} , with $t_{inj,start,1} = 0$.

The inlet conditions for the non retained modifier with a first cycle linear gradient can be written as:

$$C_{mod,z}^0 = C_{mod,start} \quad (5.6)$$

$$C_{mod,0}^k = \begin{cases} C_{mod,start} + (k\Delta t - t_{g,start})G & \text{for } C_{mod} \leq C_{mod,end} \\ C_{mod,end} & \text{for } C_{mod} > C_{mod,end} \\ C_{mod,P,k\Delta t-t_{rec}} & \text{for } t_{inj,start,r} \leq t \leq t_{inj,end,r} \\ & r = 2, N_{cyc} \end{cases} \quad (5.7)$$

where G represents the slope of the gradient, and $t_{g,start}$ the start time of the gradient (in most of the cases after the injection of sample, i.e after $t_{inj,end,1}$). Figure 5.4 illustrates some profiles of the modifier volume fractions for different gradient slopes G . The implicit set of equations resulting from the Craig model (equations 3.1, 3.27, 3.28 and 3.29) were solved using the strategy explained in section 3.3.

5.5 Operating parameters and objective functions

Since a good part of this study is devoted in comparing the chromatographic operating modes introduced before, focus was set on the effect of parameters specific to these modes. To evaluate the specific amounts injected, a dimensionless total loading factor was considered, which incorporates the column geometry, saturation capacity, volume and concentration of the injected

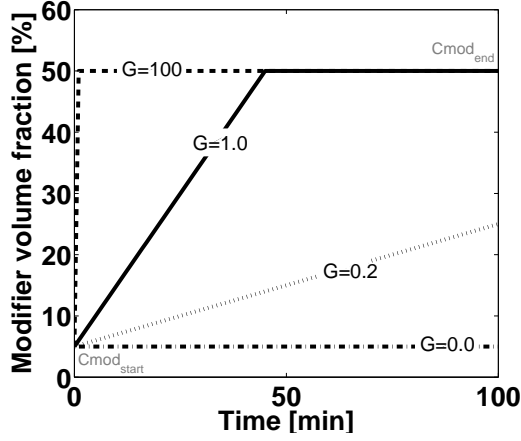


Figure 5.4: Illustration of linear modifier gradients with different slopes (G in $\%/min$)

sample [54]:

$$L_{f,tot} = \sum_{i=1}^{N_c} L_{f,i} \quad (5.8)$$

$$\text{with } L_{f,i} = \frac{(t_{inj,end,1} \dot{V}_f) C_{inj,i}}{(1 - \epsilon) A_{col} L q_{sat}} 100 \quad (5.9)$$

The objective functions considered were the production rate (Pr_2) and the recovery yield (Y_2) of the second eluting component (target), introduced in section 3.4 (see equations 3.36 and 3.37). The Y_2 calculated were determined for a purity ($Pu_{2,des}$) constraint of 99%. When estimating the production rate, of significant importance is the cycle time. When gradient elution is used, the column needs to be periodically regenerated before a new injection can be performed. Hence, an additional time t_{reg} was added to the conventional cycle time, i.e:

$$t_{cyc,reg} = t_{cyc} + t_{reg} \quad (5.10)$$

$$t_{reg} = t_0 r_f \quad (5.11)$$

Although this is a very optimistic assumption, below the regeneration time was assumed to be the mobile phase retention time ($t_{reg} = t_0$; i.e. $r_f=1$ which implies that just one column volume is invested for regeneration). The productivity evaluation carried out in this study assumed initially the same regeneration time for all operational modes considered. To which extent this assumption favors the gradient techniques is discussed later together with a more thorough analysis of the effect of regeneration on the performance parameters.

5.6 Optimization

Mathematical optimization is an excellent tool for comparing the performance indices of various operation modes. Optimization approaches involved in preparative chromatography were briefly explained in section 3.5. In our case, the presence of the integer variable N_{cyc} (number of cycles) influences the objective function Pr_2 via equations 5.4 to 5.7. Each increment in N_{cyc} leads to a sharp change in Pr_2 . Thus, the objective function in consideration is discontinuous in nature giving rise to difficulties when using gradient based optimization algorithms. Hence the simple grid search strategy was implemented by generating the values of the objective functions on each point of a uniform grid formed by the decision variables. The independent function evaluations representing each point in the search space were carried out in a grid computing environment. The search space was split into a number of sub search spaces corresponding to the number of computers available on the grid. Each sub search space was explored independently at the same time by each available computer, thus saving considerable amounts of time. This sort of a parallel grid search approach gives sets of optimal solutions (optimal fronts) rather than a unique single solution. In this study, such optimal fronts were generated and compared for the three adsorption isotherm cases introduced above (*convergent-convergent*, *convergent-divergent* and *divergent-convergent*) and the four different operational modes (B-ISO,B-G,CLR-ISO and CLR-G) considered.

In the optimization of preparative separations, the primary degrees of freedom are column dimensions, flow rate and concentrations of the injected feed. The column dimensions in general are scaled very easily with production rate. The optimal value of linear velocity is dictated by equations that relate it to the column HETP, for example the Van Deemter equation (equation 3.20). On the other hand upper limits of flow rates are constrained by the maximum pressure drop of the column that could be handled. The influence of these primary degrees of freedom mentioned above are rather well understood [54]. Thus, the focus in this study was to study the effect of those parameters specific to the operational modes considered. The general PDE constrained optimization problem in this study can be formulated as :

$$\max_{t_{inj,end,1}, C_{mod}, G} Pr_2, Y_2 \quad (5.12)$$

subject to constraints arising from the system dynamics (equations 3.1, 3.27, 3.28, 3.29, 5.4-5.7), the purity (equation 3.35) and the bounds on the design variables as given in Table 5.3. For all modes, the search was carried out with two decision variables. The total loading factor ($L_{f,tot}$ related to $t_{inj,end,1}$ through equations (5.8) and (5.9)) was included in all cases along with the variable specific to the operational modes, namely the modifier volume fraction (C_{mod}) for isocratic cases and the gradient slope (G) for gradient cases,

as shown in Table 5.3. The calculation was based on fixing the feed concentration as $C_{inj,i} = 20$ mg/ml for $i = 1, 3$. Thus the loading factor is a measure of the injected volume V_{inj} . The number of cycles (N_{cyc}) performed can also be framed as a decision variable, however the recycling model was implemented in such a way that N_{cyc} was incremented (or recycling was carried out) until a specified yield was achieved or the peaks from subsequent cycles started to overlap.

Also this output value of N_{cyc} is considered for comparison later in this study. Additional degrees of freedom like the linear mobile phase velocity and starting and ending values of the modifier gradients were kept constant (Tables 5.2 and 5.3). Thus, the aim of the study was to identify general trends regarding a comparison of the operational modes considered, and not to perform a complete optimization of all possible degrees of freedom.

5.7 Results and discussion

5.7.1 *Convergent-convergent case*

Initially, the *convergent-convergent* case (both $\alpha_{i,j}$ decreases with increasing C_{mod}) was implemented to compare the conventional operation modes (B-ISO, B-G and CLR-ISO) with the CLR-G mode. The parameters given in Tables 5.1 and 5.2 were used in the simulations. Thus, in this case, both $\alpha_{1,2}$ and $\alpha_{2,3}$ values varied between 1.2 and 1.3 in the modifier volume fraction range from 5 to 50 %. Figure 5.5 shows the optimal fronts in the $Pr_2 - Y_2$ domain for all the four operational modes considered, with the corresponding values of decision variables and required number of cycles depicted in figure 5.6.

It can be seen that the production rates (Pr_2) corresponding to recovery yields above 80% for the closed-loop recycle with gradient (CLR-G) scheme are considerably higher than any other three schemes. The differences in Pr_2 are rather small in comparison with the closed-loop isocratic recycling (CLR-ISO) case for yields below 80 %. Additionally the production rates for batch isocratic and gradient elution (B-ISO and B-G) remain much lower compared to both schemes involving recycling. This is due to the fact that in the latter

Table 5.3: Degrees of freedom considered for the four operational modes (fixed: $C_{mod,start}, C_{mod,end}, t_{g,start}$)

Operational mode	Decision variables
B-ISO	$L_{f,tot}^*, C_{mod}^\dagger$
B-G	$L_{f,tot}^*, G^\ddagger$
CLR-ISO	$L_{f,tot}^*, C_{mod}^\dagger$
CLR-G	$L_{f,tot}^*, G^\ddagger$

* search range: 0.5-25 % with increment 0.5

† search range: 5-50 % with increment 1

‡ search range: 0.1-5 %/min with increment 0.1 for convergent-convergent case, 1 - 50 %/min with increment 1 for other two cases

cases, the column could be loaded to a larger extent. This is evident from the corresponding decision variable $L_{f,tot}$ (figure 5.6a). The optimal total loading factors for the batch modes are below 10 % whereas those corresponding to CLR-ISO and CLR-G schemes reaches 20 %. Comparing the optimal fronts for the B-ISO and B-G cases, it can be seen that the gradient elution outperforms the isocratic case. The differences in production rate however are not very significant for yields above 99 % where both B-ISO and B-G schemes give almost identical results. Figure 5.6b shows the number of cycles (N_{cyc}) that was needed to reach maximum production rates for a given yield. The values of N_{cyc} varied between 2 and 5 for the schemes involving recycling and was obviously 1 for classical batch elution. It is evident that higher recovery yields require more cycles for a given purity. Considering the gradient slope it has to be kept in mind that for the *convergent-convergent* case, a less steeper gradient ($0 < G < 1$ %/min) implies that the modifier volume fraction remains close to the starting value ($C_{mod,start}$) longer, leading to better separation but slower elution. Whereas at very steep gradient slopes ($G > 10$ %/min), elution is much faster with reduced separation. It is clear from figure 5.6c that at least for the B-G case, higher recovery yields correspond to lower G values. A similar trend is seen for the B-ISO in figure 5.6d, where higher yields are obtained at lower modifier volume fractions, again as a result of better separation. However in the case of the CLR-ISO, the optimal C_{mod} values remain close to 50% ($\alpha_{1,2}$ and $\alpha_{2,3}$ values are at the lower limit of 1.2) suggesting that the maximum production rate achieved is due to faster elution with multiple cycles rather than better separation in any single cycle.

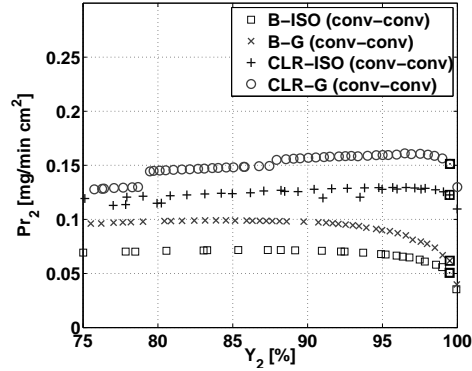
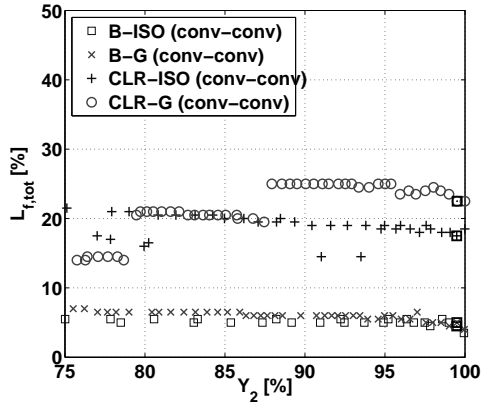
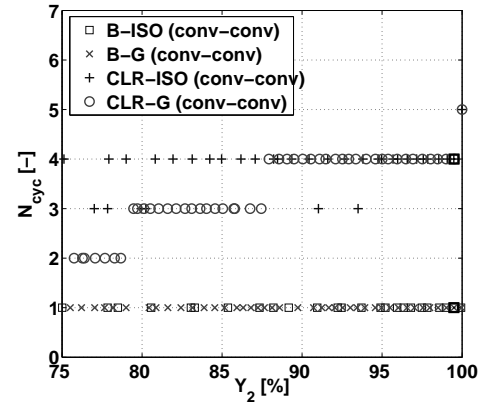


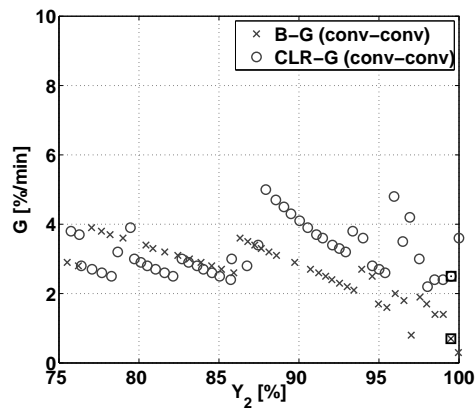
Figure 5.5: Optimal front plot: Pr_2 v/s Y_2 ; Convergent - convergent case



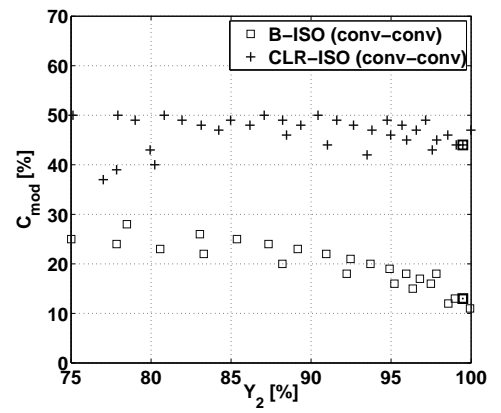
(a) Loading factors, $L_{f,tot}$



(b) Number of cycles, N_{cyc}



(c) Gradient slope, G

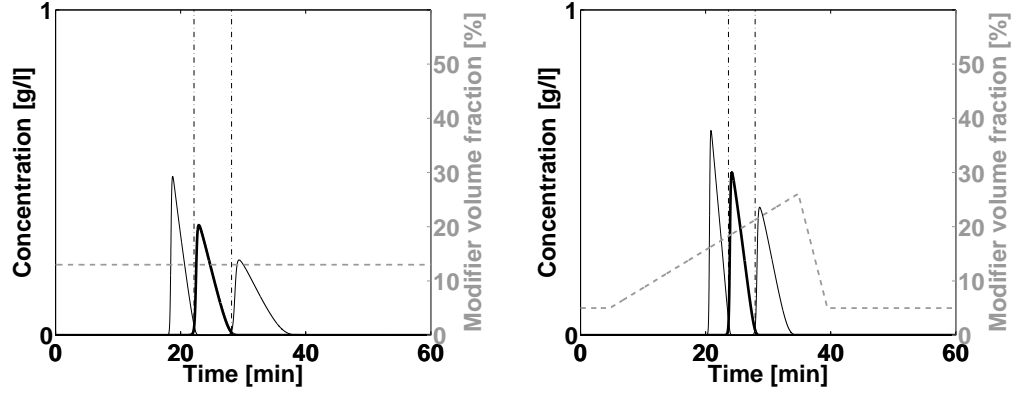


(d) Modifier volume fraction, C_{mod}

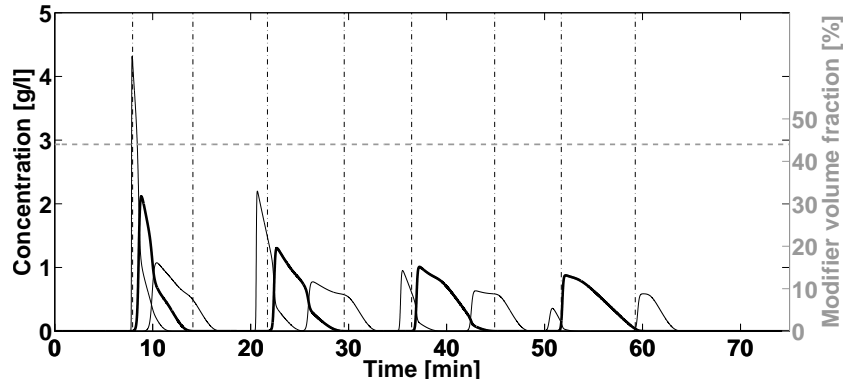
Figure 5.6: Decision variables corresponding to the optimal front plot (figure 5.5) for the *convergent-convergent* case

Summarizing the comparisons made using *convergent-convergent* adsorption isotherm case, it can be noted that the CLR-G scheme certainly outperforms the other three conventional techniques. The improvement in the separation performance of CLR-G scheme over the isocratic scheme is a result of the improved separation in the first cycle using a gradient which is combined with fast resolution of the components using the subsequent isocratic recycling mode.

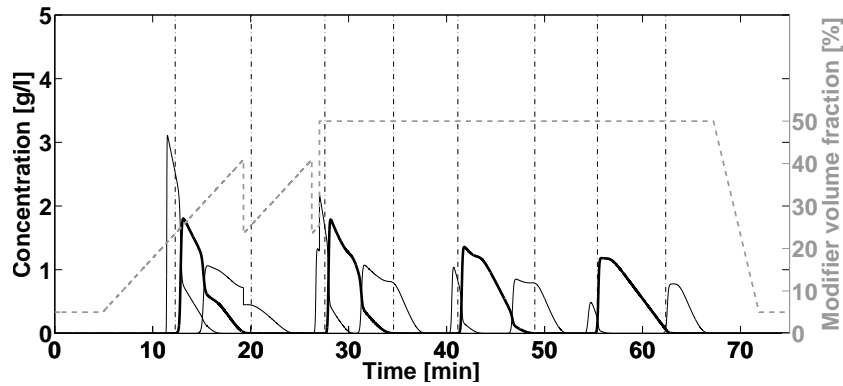
For the sake of illustration, the simulated elution profiles for all the four operational modes with parameters corresponding to the maximum production rate at a recovery yield of $Y_2 = 99.5\%$ (enlarged squares in figures 5.5 and 5.6) are plotted in figure 5.7.



(a) B-ISO, with, $N_{cyc} = 1$, $C_{mod} = 13\%$ and $L_{f,tot} = 4.5\%$ $\rightarrow Pr_2 = 0.0505$ mg/min cm² and $Y_2 = 99.48\%$
 (b) B-G, with, $N_{cyc} = 1$, $G = 0.7$ %/min and $L_{f,tot} = 5\%$ $\rightarrow Pr_2 = 0.0618$ mg/min cm² and $Y_2 = 99.49\%$



(c) CLR-ISO, with $N_{cyc} = 4$, $C_{mod} = 44\%$ and $L_{f,tot} = 17.5\%$ $\rightarrow Pr_2 = 0.1226$ mg/min cm² and $Y_2 = 99.48\%$



(d) CLR-G, with $N_{cyc} = 4$, $G = 2.5$ %/min and $L_{f,tot} = 22.5\%$ $\rightarrow Pr_2 = 0.15132$ mg/min cm² and $Y_2 = 99.50\%$

Figure 5.7: Elution profiles at the column outlet for the four operation modes considering the *Convergent-convergent* case with optimized parameters corresponding to a yield around 99.5%; enlarged squares in figures 5.5 and 5.6 (other standard parameters from table 5.2)

5.7.2 Comparison in a wider parameter range

From the optimal front plots (figure 5.5) presented above, it can be seen that the CLR-G scheme outperforms the others in certain cases, however the performance of the scheme needs to be compared over a larger range of loading factors to identify correctly the domains of outperformance. Lower modifier volume fraction in the first cycle of a CLR-G mode compared to the subsequent ones supports better peak resolution initially, and the required separation at the specified purity and yield is achieved by recycling actions at higher volume fraction of the modifier. The combination of the two chromatographic techniques (gradient, recycling) helps in achieving the desired result faster with improved production rates. Additionally the presence of recycling steps results in less solvent consumption compared to batch operations. In order to compare the production rates of the CLR-G scheme to its closest competitor, the conventional CLR-ISO scheme, the two configurations were studied more systematically by varying the total loading factor up to 25%, above the value at which the elution profiles from two consecutive cycles start to overlap. Other parameters, namely the C_{mod} and G , were taken from the optimum values corresponding to the *convergent-convergent* case (enlarged squares in figures 5.6c and 5.6d).

The discrete nature of the objective function (Pr_2) can be noted from figure 5.8. The drop in Pr_2 values corresponds to the prolongation of the cycle time as a result of an extra cycle that is required to reach the specified separation criteria. The production rate of the CLR-G scheme often falls below that given by the isocratic case for a given loading factor when the number of cycles required by the two schemes are equal. It can also be seen that the column for the CLR-G scheme could be loaded to a larger extent than for the CLR-ISO scheme. CLR-G needs only one cycle to reach the required target component separation for total loading factors below 3, whereas the optimal CLR-ISO case with $C_{mod} = 44$ requires at least two cycles in any case. The CLR-G scheme in consideration would facilitate separation for $L_{f,tot}$ values up to 24.5 as against 19.25 for the optimal isocratic case. It can also be noticed that the performance of CLR-G

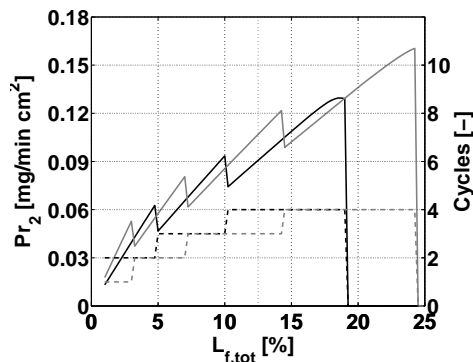


Figure 5.8: Comparison of CLR-ISO and CLR-G schemes; production rates (solid lines) and number of cycles required (dashed lines) for the *convergent-convergent* case: CLR-ISO with $C_{mod} = 44$ (black) and CLR-G with $G = 2.5$ (gray), other parameters from Table 5.2

drops below that of CLR-ISO when the number of cycles required is the same for both schemes, for a given sample loading factor. This under-performance of the CLR-G scheme occurs as a result of relatively longer retention times of the components in the first cycle of CLR-G scheme (with an initial gradient) compared to that of the CLR-ISO scheme, resulting in a longer overall cycle and thus diminished production rates. Hence under such circumstances when cycle times are likely to be higher than that for CLR-ISO scheme, the proposed scheme would be less attractive in terms of production rates. However, both modes of operations involving recycling can be operated at higher loading conditions to improve production rates significantly compared to conventional single cycle batch elutions.

The results discussed above were attained using identical regeneration times. Hence in order to evaluate more specifically the effect of regeneration, the r_f value in equation (5.11) was varied over a wide range to elucidate its effect on the objective functions.

5.7.2.1 Role of regeneration time

The regeneration time for the production rate evaluation is incorporated into the cycle time (equation (5.10)), and was taken as t_0 ($r_f=1$) for all the calculations presented above. Often regeneration is not required in case of isocratic operations. However occasionally it is carried out due to the presence of strongly retained impurities [32]. In contrast, it is a necessary step in the case of an operation involving gradient elution. The production rates for the four operational modes were compared at optimal conditions corresponding to $Y_2 \simeq 99.5\%$ (enlarged squares in figures 5.5 and 5.6 characterized by parameters in Fig. 5.7) by varying the regeneration factor between 0 and 6 as shown in Fig. 5.9.

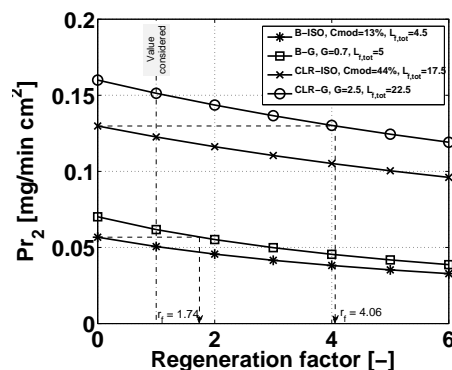


Figure 5.9: Dependence of production rate on the regeneration factor (r_f); in accordance with equations 3.37, 5.10 and 5.11

The production rates of batch elutions estimated at lower loading factors are lower than those for closed-loop operations throughout the range of r_f considered, with Pr_2 decreasing for increasing r_f for all the four cases in accordance with equations 3.37 and 5.10. In the case of isocratic closed-loop recycling without any regeneration ($r_f=0$), it could be seen that under the given conditions, the production rates achievable by the CLR-G scheme are

still higher for r_f up to 4.06. Similarly in the case of batch elution, the gradient case with regeneration outperforms the isocratic case for regeneration factors up to 1.74.

The performance of operational modes involving gradient elution were compared with those of the isocratic case in a more realistic manner: the regeneration factor r_f in case of the former was set to 5 and those for the latter at 0, i.e without regeneration during isocratic operation. figure 5.10 shows the resulting optimal fronts plot. Clearly with no regeneration time the CLR-ISO scheme yields marginally better production rates at higher yields than the CLR-G scheme. This is also true for the simple batch case, where the B-ISO schemes outperform the B-G scheme significantly at high recovery yields. Thus, the influence of the regeneration time is a critical factor when comparing operational modes involving gradient elution to that of isocratic ones. In order to see any appreciable degree of outperformance; even in case of simple batch elutions, the time devoted for regeneration needs to be as low as possible.

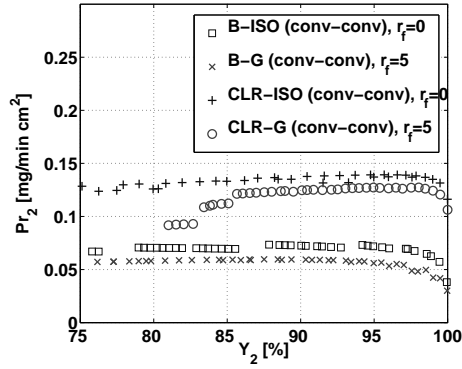


Figure 5.10: Optimal fronts plot: Pr_2 v/s Y_2 ; Convergent - convergent case; isocratic modes without regeneration ($r_f=0$) and gradient modes with longer regeneration time ($r_f=5$)

5.7.3 Convergent-divergent case

In the convergent-divergent case, the separation factor $\alpha_{1,2}$ decreases from 1.3 to 1.2 for a change in C_{mod} from 5 to 50%, whereas $\alpha_{2,3}$ increases from 1.2 to 1.3 for the same C_{mod} change. This implies that with increasing modifier volume fraction, the first component moves towards the second (target) component and the third component away from the second. Figure 5.11 shows the optimal fronts for all four operational modes for $r_f=1$, with the corresponding values of decision variables and the required number of cycles depicted in figure 5.12.

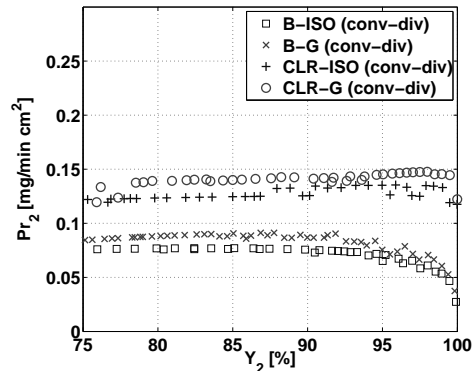
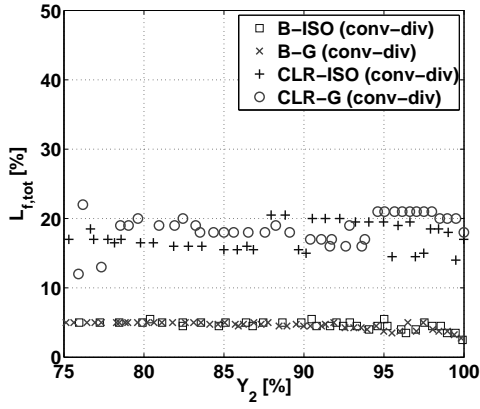


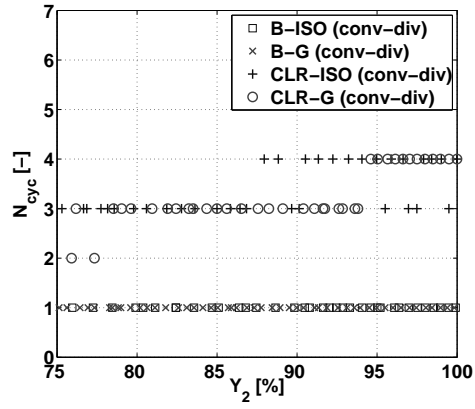
Figure 5.11: Optimal fronts plot: Pr_2 v/s Y_2 ; Convergent - divergent case

The difference in the performance of the CLR-G mode in this case is

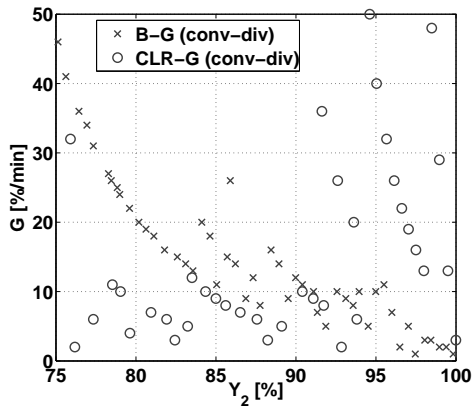
not significantly different from that of CLR-ISO. Their optimal fronts are very close to each other, with the one corresponding to CLR-G being slightly higher (figure 5.11). Similarly the performance of the batch elutions (B-ISO and B-G) are nearly identical. This marginal difference in performance arises from the fact that there is no special advantage of CLR-G over CLR-ISO in terms of loadability and number of cycles required. It is evident from figures 5.12a and 5.12b that the decision variables $L_{f,tot}$ and N_{cyc} obtained for both schemes lie very close to each other. Unlike in *convergent-convergent* case where the G values corresponding to the optimal front fall below 10%, in this case they are seen in a wider range up to 50 %. However the trend seen in B-G scheme with respect to the optimal G values are similar to that of the *convergent-convergent* one, i.e higher recovery yields correspond to lower G values. Likewise, the C_{mod} values corresponding to the optimal front of B-ISO also shows a decreasing trend for increasing Y_2 . Compared to the *convergent-convergent* case, optimal values of Pr_2 are found at relatively higher values of G and C_{mod} . This is because of the fact that an increase in G or C_{mod} increases the separation factor between the target and the most retained component (i.e $\alpha_{2,3}$) and favors improved production rates.



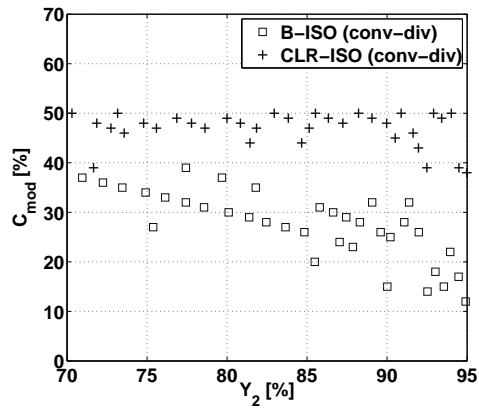
(a) Loading factors, $L_{f,tot}$



(b) Number of cycles, N_{cyc}



(c) Gradient slope, G



(d) Modifier volume fraction, C_{mod}

Figure 5.12: Decision variables corresponding to the optimal fronts plot (Figure 5.11) for the *convergent-divergent* case

5.7.4 Divergent-convergent case

In the third case of possible adsorption isotherm behavior considered, $\alpha_{1,2}$ increases from a value 1.2 to 1.3 for increasing values of C_{mod} , while $\alpha_{2,3}$ decrease from 1.3 to 1.2. Thus with increasing modifier volume fraction, the first component moves away from the target and the third one moves towards it. Figure 5.13 shows the optimal fronts for all four operational modes considered, with the corresponding values of decision variables and the required number of cycles depicted in figure 5.14.

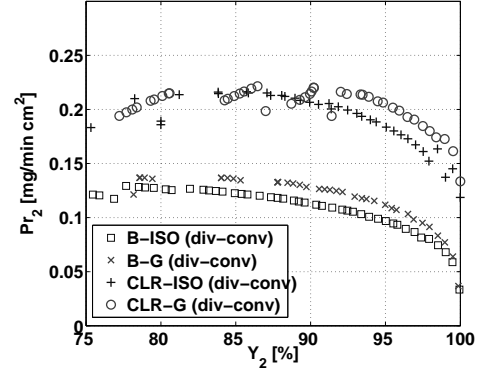


Figure 5.13: Optimal fronts plot: Pr_2 v/s Y_2 ; Divergent - convergent case

It can be noticed that in this case, the production rates for all operational modes considered are much higher than that of those obtained for the *convergent-convergent* and *convergent-divergent* cases (figures 5.5 and 5.11). A higher separation factor between the first and the second (target) component ($\alpha_{1,2}$) has a more pronounced influence on the production rate of the target component than a similar separation factor between the second and third component ($\alpha_{2,3}$) [95]. This fact is confirmed by the obtained results.

Compared to the CLR-ISO scheme, the performance of CLR-G is not significantly higher. Similarly, the optimal fronts plot for the batch gradient elution lies very close to the batch isocratic case. The total loading factors and number of cycles that corresponds to the optimum lie in a range similar to the previous cases. In comparison with the previous two cases, the optimal values of G shows similar trend (figure 5.14c), i.e yields close to 100% are achieved at lower values of the gradient slopes, both in B-G and CLR-G schemes for reasons explained before. However since an increase in G increases $\alpha_{1,2}$ and thereby favoring much larger Pr_2 compared to the *convergent-divergent* case, even higher optimal G values are seen for both batch and closed-loop gradient schemes. Similarly for optimal C_{mod} values as shown in figure 5.14d, optimal Pr_2 at very high yields are achieved at lower values of C_{mod} compared to those for lower yields. As a result of the increased production rates with increased $\alpha_{1,2}$ values, C_{mod} remains close to 50%/min for lower yields in both isocratic schemes.

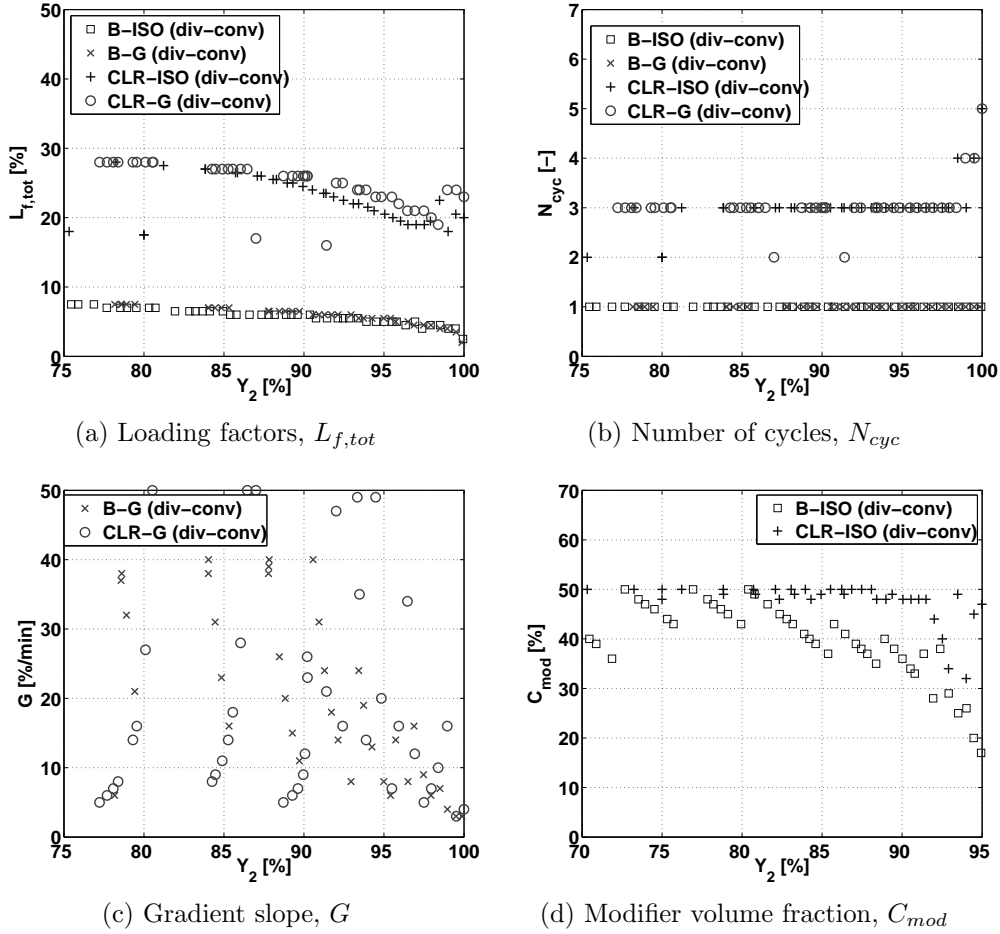


Figure 5.14: Decision variables corresponding to the optimal fronts plot (Fig. 5.13) for the *divergent-convergent* case

5.8 Conclusions

In this chapter, a new preparative chromatographic operation mode with characteristics of conventional closed-loop isocratic recycling and gradient elution (CLR-G) was evaluated theoretically for the separation of a ternary mixture considering the intermediately eluting component as the target. The resulting production rates (Pr_2) over a range of recovery yields of the target component (Y_2) were compared for different adsorption isotherm behaviors (*convergent-convergent*, *convergent-divergent* and *divergent-convergent*) with those of the conventional batch (B-ISO and B-G) and recycling (CLR-ISO) operational modes.

Applying recycling, larger amounts of substance can be separated per unit time. Hence the CLR-ISO and CLR-G operational modes yields higher production rates compared to the batch modes. As shown in figure 5.8, for

the *convergent-convergent* case, the initial gradient often allows the CLR-G scheme to achieve the desired degree of separation at a given loading in fewer cycles than the CLR-ISO process. Under such circumstances, applying the CLR-G scheme would result in a higher production rate than the CLR-ISO scheme.

The CLR-G scheme shows a distinct degree of outperformance when the separation factors between the target component and its two neighbors decrease with decreasing Henry coefficients. The improvements however are not significant and the performance closely matches that of the conventional CLR-ISO scheme when either of the two separation factors increase with decreasing Henry coefficients (*convergent-divergent* and *divergent-convergent* cases).

The improvement in performance achieved by the CLR-G scheme comes however with a drawback, i.e the requirement for regeneration at the end of the cycles. Hence to apply the CLR-G scheme involving regeneration of the column, it has to be kept in mind that this regeneration time needs to be as short as possible. Another factor to be considered in large scale chromatographic process is the recycling of solvents, which in fact becomes more difficult in the presence of solvent gradients.

The conclusions made above outline the potential of using CLR-G scheme in the preparative isolation of a target component. For a comprehensive picture on the application of CLR-G scheme, further rigorous theoretical and experimental work is needed. The experimental realization could be easily done by adding the valves needed to implement the conventional closed-loop recycling along with a gradient system to the conventional equipment. One of the potential problems of efficient and reliable recycling implementations will be the need for component specific detectors to facilitate precise fractionation. In addition, for successful practical applications, dispersion caused in the recycle loop by the pump must be carefully minimized.

The preparative separation concepts considered in this chapter relied on exploiting the benefits of changes in solvent strength and recycling concepts. Another possibility to improve the performance parameters of separating an intermediate target compound is to optimally use different stationary phases. A theoretical study that was carried out is explained in the next chapter.

Chapter 6

Theoretical study of ternary separations using multiple stationary phases

Excerpts of results in this chapter were published earlier by the author in *Journal of Chromatography A* [86].

6.1 Introduction to the separation problem

As reviewed in section 1.4.2, the application of multiple stationary phases in analytical chromatography are widespread. By using intermediate capture and injection mechanisms, chromatographic columns with multiple stationary phases could be used in the 2D mode to improve peak capacities and resolution (analytical). In addition to the mixed mode operation, another faster and easier method is to directly couple multiple stationary phases without any storage in between.

In this chapter, the objective was to extend the concept of directly coupling and the concept of mixing several stationary phases to preparative chromatography. To get some insight, the potential of using a two stationary phase configuration was investigated theoretically, studying the preparative separation of multi-component mixtures, where intermediately eluting components were treated as the targets. For assumed (typical) adsorption isotherm parameters, the influence of relative segment lengths, injected volumes and the segment order on the production rates and yields of the target components was investigated for the serially coupled case. The key parameter considered for mixed mode was the mix ratio.

6.2 Theory

A serial connection of two chromatographic segments A and B filled with different stationary phases is illustrated in Fig. 6.1. In addition to the individual segment lengths (l_A and l_B), each segment is characterized by a specific equilibrium between the fluid and stationary phase concentrations. In liquid

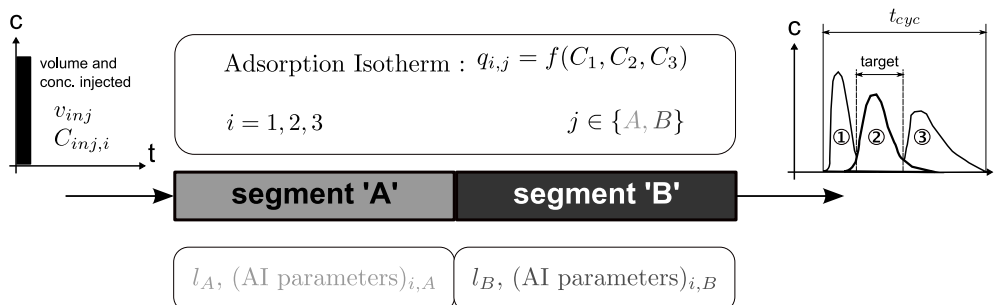


Figure 6.1: Preparative isolation of a target component by serially coupling two chromatographic segments.

chromatography, the separation factors and retention times differ slightly in similar stationary phases when exactly the same mobile phase is used, e.g [110, 111]. In certain cases however, the variations can be significant. For example in [112, 113], embedding polar groups in RP and HILIC gives rise to variations in selectivities including reversals in addition to influences on retention times. Thus, it can happen that for different stationary phases and the same mobile phase, a) specific separation factors of a target component with respect to its immediate neighbors can differ and b) all components elute slower or faster with constant or varying degrees of separation.

In order to illustrate the influence of discrete changes in stationary phase on the separation of an intermediately eluting component, the following possible scenarios were investigated in a case study :

- *Case I*: Selectivity differences
- *Case II*: Retention time differences

Case I contemplates a scenario where a segment in which the target component nearly co-elutes with its less retained neighbor is coupled to another one where the target nearly co-elutes with its more retained neighbor or vice versa. This case is illustrated in Fig. 6.2a. *Case II* is illustrated in Fig. 6.2b, where a chromatographic segment characterized by faster elution but relative poor separation is coupled with one characterized by better separation but slower elution. In reality, feed mixtures consists often of much more than three components. Hence in *Case III*, a separation problem with seven components [50] was analyzed using again two stationary phases possessing different properties.

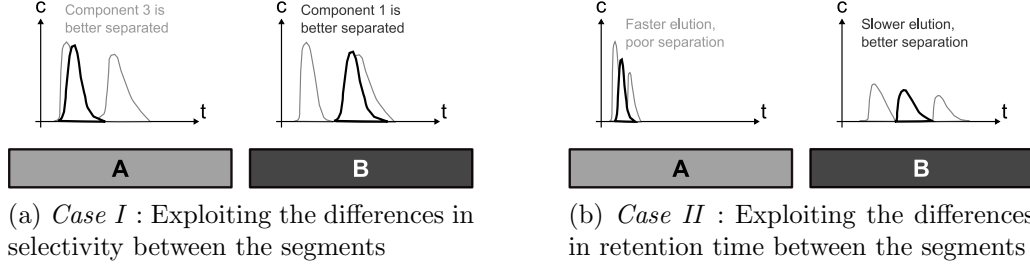


Figure 6.2: Scheme representing preparative separation of a ternary mixture for two cases of different adsorption isotherm sets (a and b).

6.2.1 Column model and isotherm parameters

To model the ternary system, the equilibrium dispersive model introduced in section 3.1.2 was used because of its speed and accuracy. The mass balance equations given in equation 3.10 were integrated numerically using the Rouchon's finite difference method [62] along with the following boundary conditions :

$$C_i|_{l_j=0} = \begin{cases} C_{inj,i} & \text{for } 0 \leq t \leq t_{inj,end,j} \text{ and } j = j^1 \text{ (first segment)} \\ C_i|_{x=l_{j^*}} & \text{for } t_{inj,start,j} \leq t \leq t_{inj,end,j} \text{ and } j \neq j^1 \\ & (j^* \rightarrow \text{preceding segment}) \end{cases} \quad (6.1)$$

In the conditions above, the first segment inlet condition were taken as a pulse injection. The second segment then used the elution profile of the preceding (first) segment as the input profile.

In case of the isotherm model, the competitive Langmuir relationship introduced in section 3.2.2 were used. The equilibrium dependancy given by equation 3.27 can be extended for multiple stationary phases as:

$$q_{i,j} = \frac{a_{i,j}C_i}{1 + \sum_{k=1}^{N_c} b_{k,j}C_k} \quad \text{with } i = 1, N_c \text{ and } j \in \{A, B\} \quad (6.2)$$

In the above equation, the parameters $a_{i,j}$ and $b_{i,j}$ represents the isotherm parameters for each component i in stationary phase j . The separation factor between two neighboring components were calculated according to the equation 3.26. The parameters used in this study to describe the adsorption isotherm behaviors of *Case I* and *Case II* are shown in Table 6.1.

To demonstrate the effect of competition between neighbors in *Case I*, the separation factors were specified to be 1.1 and 2.0 for the two segments

in changing order. Identical Henry constants ($a_{2,j}=5$) were assumed for the second eluting component in both segments. The corresponding Henry coefficient for the neighbors were then calculated using the $\alpha_{i,k,j}$. To take into account non linear behavior, a constant saturation capacity (q_{sat}) of 50 [g/l] was assumed for all the components in each of the stationary phases. This allowed to specify parameters $b_{i,j}$ from the relation $b_{i,j} = a_{i,j}/q_{sat}$. For *Case II*, to the target component in the 'fast elution poor separation' segment was given an $a_{2,A}$ value of 1.0. To mimic a poor separation, the separation factors ($\alpha_{2,1,A}$ and $\alpha_{3,2,A}$) were set to 1.1. On the other hand, for the 'slow elution good separation' segment B, an $a_{2,B}$ value of 12 was used and separation factors $\alpha_{2,1,B} = \alpha_{3,2,B} = 2.0$. The Henry coefficients $a_{1,A}$, $a_{3,A}$, $a_{1,B}$ and $a_{3,B}$ of the neighbors were then calculated. To specify the $b_{i,j}$ values, again $a_{i,j}/q_{sat}$ with $q_{sat} = 50$ g/l was used.

Table 6.1: Adsorption isotherm parameters of equation (6.2), for ternary mixtures of *case I* and *case II*, see Fig. 6.14 for illustration

Isotherm parameters	First component $i = 1$	Second component $i = 2$ (target)	Third component $i = 3$	Separation factors
<i>Case I</i>				
$a_{i,A}$	4.5455	5.0000	10.0000	$\alpha_{1,2,A}=1.1$, $\alpha_{2,3,A}=2.0$
$b_{i,A}$	0.0909	0.1000	0.2000	for segment A
$a_{i,B}$	2.5000	5.0000	5.5000	$\alpha_{1,2,B}=2.0$, $\alpha_{2,3,B}=1.1$
$b_{i,B}$	0.0500	0.1000	0.1100	for segment B
<i>Case II</i>				
$a_{i,A}$	0.9091	1.0000	1.1000	$\alpha_{1,2,A}=1.1$, $\alpha_{2,3,A}=1.1$
$b_{i,A}$	0.0182	0.0200	0.0220	for segment A
$a_{i,B}$	6.0000	12.0000	24.0000	$\alpha_{1,2,B}=2.0$, $\alpha_{2,3,B}=2.0$
$b_{i,B}$	0.1200	0.2400	0.4800	for segment B

For *Case III* a 7 component mixture was considered. The $a_{i,j}$ values were taken from Nyiredy et al. [50] for two segments (denoted as 'CN' and 'PH' in their work), as tabulated in Table 6.2.

From the $a_{i,A}$ values and calculated separation factors between each components, it can be seen that segment A yields a poor separation with a faster elution. On the other hand, the components remain longer in segment B (higher $a_{i,B}$ values) with good separation between components 1-2 and 3-4. Non-linear behavior was introduced in the same manner as described above for *Case I* and *Case II*.

Table 6.2: Adsorption isotherm parameters of equation (6.2), a 7 component mixture *case III*, $a_{i,j}$ values from Nyiredy et al. [50] and calculated $b_{i,j}$ values for $q_{sat} = 50$ [g/l]

Component i	Segment A			Segment B		
	$a_{i,A}$	$\alpha_{i,i+1,A}$	$b_{i,A}$	$a_{i,B}$	$\alpha_{i,i+1,B}$	$b_{i,B}$
1	4.6823	1.0952	0.0936	13.2370	1.4047	0.2647
2 (target 1)	5.1282	1.0870	0.1026	18.5940	1.1017	0.3719
3 (target 2)	5.5741	1.0400	0.1115	20.4850	1.2462	0.4097
4	5.7971	1.0769	0.1159	25.5280	1.0123	0.5106
5	6.2430	1.0357	0.1249	25.8430	1.1342	0.5169
6	6.4660	1.0345	0.1293	29.3100	1.0753	0.5862
7	6.6890	—	0.1338	31.5160	—	0.6303

6.2.2 Objective functions and operating parameters

Since the main part of this study was to compare the performance of different chromatographic segments coupled in series, suitable objective functions had to be formulated. The product of production rate (Pr_i , equation 3.37) and recovery yield (Y_i , equation 3.36) was chosen as the one to be maximized. In a multi component mixture, the fastest and slowest eluting components are much more easy to isolate than the intermediate ones, hence below only optimized $Pr_i Y_i$ values of intermediate components were considered (i.e. $Pr_2 Y_2$ for *Cases I* and *II*, $Pr_i Y_i$ with $i = 2, 3$ for *case III*).

In the optimization of a preparative separation, the importance of primary degrees of freedoms such as the flowrate, column dimensions and the concentrations of feed are rather well understood [54]. Hence only those parameters relevant to the multiple segment arrangement (relative segment lengths, orders and injected sample sizes) were studied below. The relative segment length can be defined as $x_j = l_j/L$. With L being the overall length, which is for two segments $l_A + l_B$, where l_j represents the length of segment j . The total length of the two segments was taken as 20 cm, with internal column diameter of 3 mm to resemble an available segment assembly [51]. Additionally, the porosity (ϵ_j) of the two segments were assumed to be 0.6 with an identical HETP of 0.01 cm. The volumetric flowrate considered was 0.6 ml/min (i.e. $u = 14.14$ cm/min), analogous to the one used in [50]. Yield and purity were estimated from the elution profiles using a threshold concentration to fix the cycle times (t_{cyc}). The fractionation of the elution profiles were based on a desired purity of 99 % with a threshold concentration of 10^{-3} g/l. The feed concentrations were set to 20 g/l for all the components in order to operate in the non linear range of the adsorption isotherms. The standard parameters used in the study are summarized in Table 6.3.

Table 6.3: Parameters of the chromatographic system analyzed

Parameter	Value
Total length of the coupled segments (L)	20 [cm]
Inner diameter of each segment (d_c)	0.3 [cm]
Total segment porosity (ϵ_j) ($\epsilon_A = \epsilon_B$)	0.6 [-]
Height Equivalent to Theoretical Plates (HETP) (Number of theoretical plates = 2000)	0.01 [cm]
Volumetric flow rate (\dot{V}_f)	0.6 [ml/min]
Initial injected sample concentration ($C_{inj,i}$) ($C_{inj,1}=\dots=C_{inj,N_c}$)	20 [g/l]
Desired purity of component i (Pu_{lim})	99%
Threshold concentration for fractionation (C_{thr})	10^{-3} [g/l]

6.2.3 Parametric study and optimization

To study the influence of coupling two chromatographic segments on the separation performance, the relative length x_A was varied between 0 and 1. A value of $x_A = 1$ implies the use of segment A alone and $x_A = 0$ implies that only segment B is used. Additionally to elucidate the influence of segment order, performance differences in the two possible configurations A-B and B-A were analyzed. In addition, the injected volume (V_{inj}) was changed systematically in a wide range in order to study its influence.

As discussed in section 3.5.1, a popular meta-heuristic optimization approach is the genetic algorithm (GA) [114]. The concept of the GA is based on the principles of genetics and the Darwinian principle of natural selection, i.e., the survival of the fittest. Such principles are embodied in the GA by employing a series of probabilistic operators such as reproduction, crossover and mutation all of which are inspired by natural genetics. The GA has been successful in solving engineering optimization problems in many previous studies [115, 116].

Thus optima of $Pr_i Y_i$ were searched in the two parameter space $x_A - V_{inj}$ for both segment orders (A-B and B-A) using MATLAB GA Toolbox. Parameter x_A was varied in the feasible range between 0 and 1. Whereas V_{inj} was varied in a sensitive region, where the productivity increases from zero to reach a maximum and decreases to zero with increase in V_{inj} . Hence only this range was considered for the optimization of each scenario. The set of solver configurations summarized in Table 4 was used for the search.

Table 6.4: Solver settings used for MATLAB Genetic Algorithm Toolbox

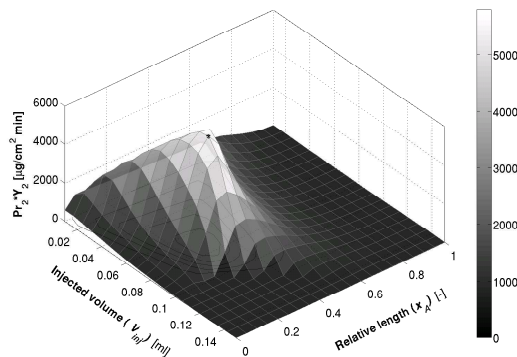
Parameter	Value
Population size	20
Number of generations	100
Fitness scaling	Top fitness scaling
Selection	Tournament selection
Crossover	Scattered crossover
Crossover fraction	0.8
Mutation	Random mutation
Elite count	10% of population

6.3 Results and discussions

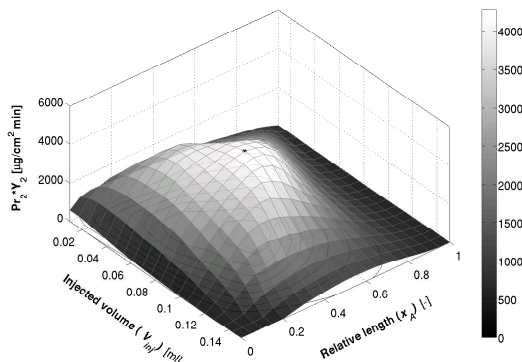
6.3.1 Case I

In this configuration, the target to be isolated nearly co-elutes with its more retained (segment A) or less retained (segment B) neighbor. As mentioned before, the quest was to investigate the influence of the relative length of each of these segments and the order of arrangement on the separation performance.

Initially, the performances of the individual segments alone were analyzed. The optimal values of V_{inj} were estimated for $x_A = 1$ (A alone) and $x_A = 0$ (B alone). The results are given in Table 6.5. It can be observed that segment B in which components 2 and 3 are well separated from component 1 ($\alpha_{2,3,B} > \alpha_{1,2,B}$) performs much better ($Pr_2Y_2 = 604.1$ against $14.1 \mu\text{g}/\text{cm}^2 \text{ min}$). Component 2 eluting very close to component 3 results in a peak overlap between the two. As a result of the non linear peak shapes, the tailing part of component 2 (with pro-



(a) Case I ; order A-B



(b) Case I ; order B-A

Figure 6.3: Case I : Pr_2Y_2 plot in V_{inj} - x_A space for the two segment orders, other parameters from Tables 6.1 and 6.3

gressively lower concentrations) overlaps with the third component. On the other hand, the shock front of the target component remains well separated from the first component, thus the high concentrated, non overlapping part of the target component at a higher concentration can be collected with the required purity. Hence segment B facilitates the isolation of the target with a high yield.

However, component 2 elutes very close to the component 1 in segment A. Therefore the trailing part of the component 1 overlaps with the shock front and the high concentrated part of the target peak, resulting in a lower recovery yield. Besides, higher values of $a_{3,A}$ ($a_{3,A} = 10$ compared to $a_{3,B} = 5.5$) contribute to a longer cycle time, decreasing the production rate.

To analyze the influence of order in a coupled column, a parametric study was carried by varying x_A in the range between 0 to 1 and V_{inj} in the range between 0.01 and 0.15 ml. The resulting objective function values (Pr_2Y_2) are plotted in the $V_{inj} - x_A$ parameter space as shown in Fig. 6.3 for both segment orders (A-B and B-A). The Pr_2Y_2 value increases with increasing volume injected initially until they reach a maximum and then decreases due to overlapping peaks. Similar trend is also seen along varying relative length. For any given value of V_{inj} there is an optimal value of x_j providing a maximum value of Pr_2Y_2 .

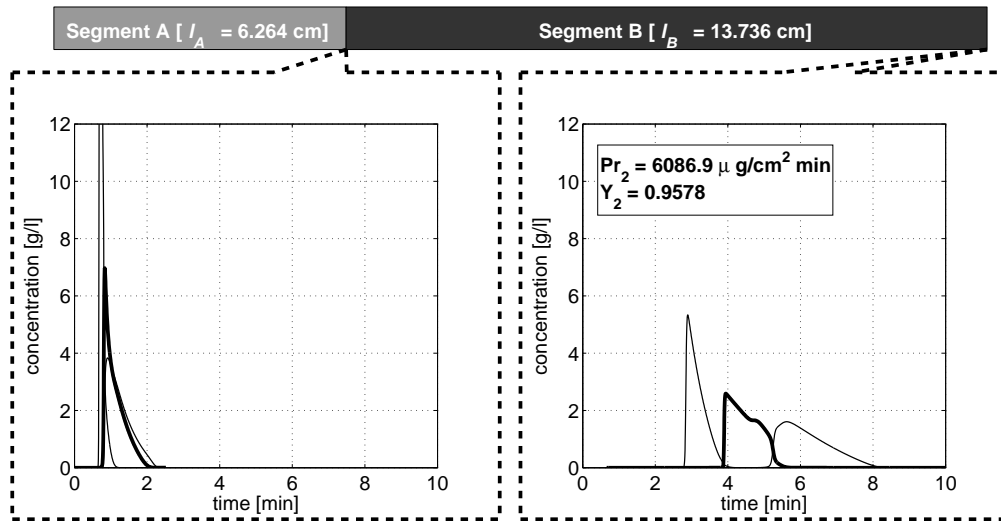
In order to find an optimum value for comparison, the search space as shown in Fig. 6.3 was scanned using MATLAB Genetic Algorithm (GA) Toolbox for both segment arrangements. The resulting optimum values are tabulated in Table 6.5. The two segments when coupled in both arrangement with optimal relative lengths, perform better than the individual segments with the same total length. Additionally, the assembly with segment order A-B clearly outperforms the one with B-A order (5829.8 against 4336.0 $\mu\text{g}/\text{cm}^2$ min). The resulting elution profiles of the optimal case (Table 6.5) along

Table 6.5: *Case I* : Optimal values of Pr_2Y_2 for the combination and individual segments ($x_A \in \{0, 1\}$), along with the resulting parameters. Optimized using GA Toolbox (settings from Table 6.4)

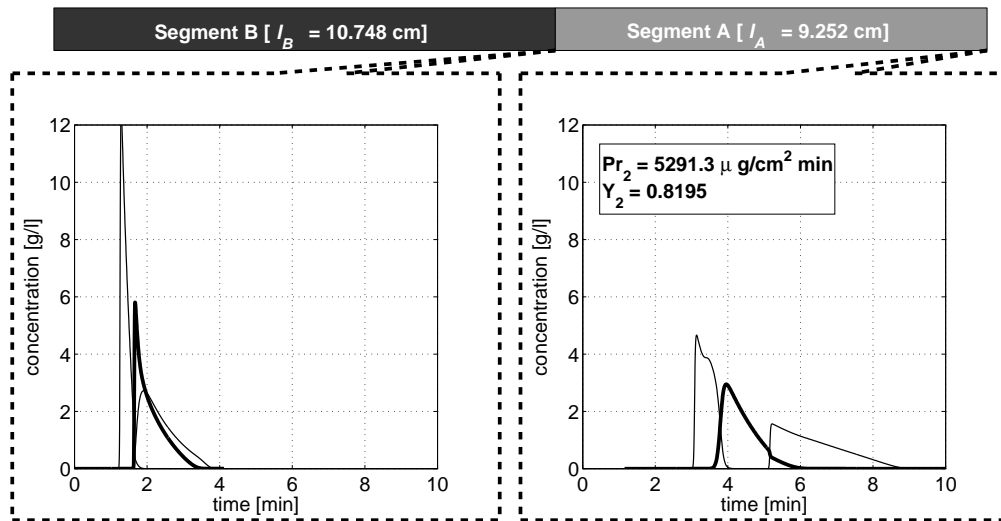
Segment order	Pr_2Y_2 [$\mu\text{g}/\text{cm}^2$ min]	V_{inj} [ml]	x_A [-]	Pr_2 [$\mu\text{g}/\text{cm}^2$ min]	Y_2 [-]
A	14.1	0.0109	1	104.5	0.1352
B	604.1	0.0131	0	1016.2	0.6114
A-B	5829.8	0.0744	0.3132	6086.9	0.9578
B-A	4336.0	0.0814	0.4626	5291.3	0.8195

with the profiles in between the two segments are plotted in Figures 6.4a and 6.4b. Even though segment A is inferior in separating the target compared

to segment B, the optimization results suggest that separation performance can be improved by serially connecting segments A and B. This observation is specific to *Case I* and is related to the fact that the target component has identical retention times in both segments ($a_{2,A} = a_{2,B}$). However, the approach described above should also be able to identify optimum conditions for other thermodynamic constellations.



(a) Order A-B : $V_{inj} = 0.0744$ ml, $x_A = 0.3132$ with $Pr_2 Y_2 = 5829.8 \mu\text{g}/\text{cm}^2 \text{ min}$. Co-elution of target component with least retained component in the first segment aids better separation. Parameters from Tables 6.1 and 6.3



(b) Order B-A : $V_{inj} = 0.0814$ ml, $x_A = 0.4626$ with $Pr_2 Y_2 = 4336.0 \mu\text{g}/\text{cm}^2 \text{ min}$. Target component eluting with the most retained component in the first segment yields relatively lower separation. Parameters from Tables 6.1 and 6.3

Figure 6.4: *Case I* : Elution profiles for the optimal parameters (see Table 6.5)

Unlike in preparative separations, one of the objectives in analytical (linear) separations is to find an optimal separation factor between the target and its neighbors. In a column assembly with the *Case I* type adsorption isotherm parameters, an optimal analytical separation can be achieved also by simply varying the relative segment lengths. The resulting effective separations factors ($\alpha_{i,k,eff}$) are related to x_A in the following way [49]:

$$\alpha_{i,k,eff} = \frac{a_{k,eff}}{a_{i,eff}} \quad \text{with } a_{k,eff} > a_{i,eff} \quad \text{and} \quad (6.3)$$

$$a_{i,eff} = a_{i,A}x_A + a_{i,B}(1 - x_A) \quad (6.4)$$

The effective separation factors for x_A in the range 0 to 1 is plotted in Fig. 6.5. The optimal analytical separation occurs when the target is equally separated from both of its neighbors ($\alpha_{1,2,eff} = \alpha_{2,3,eff}$). In this case it is found to be at $x_A = 0.4260$. On the other hand the preparative separation predicts optimal Pr_2Y2 values at $x_A = 0.3132$ (A-B) and $x_A = 0.4626$ (B-A). In the configuration A-B, where the initial separation occurs in segment A (target nearly co-elutes with first component), the optimal preparative separation seems to happen when the effective separation factor between first and second (target) component is high (i.e. $\alpha_{1,2,eff} > \alpha_{2,3,eff}$, for $x_A = 0.3132$). Similarly for B-A configuration in which initially the target nearly co-elutes with the component 3, the optimal preparative separation occurs when $\alpha_{1,2,eff} < \alpha_{2,3,eff}$, at $x_A = 0.4626$. Thus, it can be summarized that unlike in analytical separations, as a result of the underlying non-linearities of adsorption isotherms, for preparative separation the performance is significantly influenced by the order of the chromatographic segments.

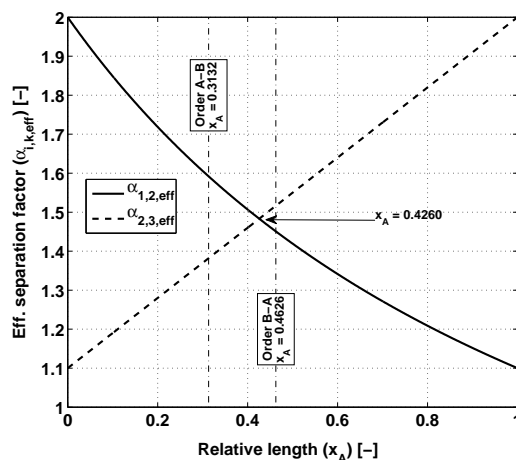


Figure 6.5: Effective separation factors of the serial assembly as a function of relative segment lengths, equation (6.3). Optimal values of $\alpha_{i,k,eff}$ for preparative case ($x_A = 0.3132$ for A-B and $x_A = 0.4626$ for B-A) different from that of analytical case ($x_A = 0.4260$)

6.3.2 Case II

In the second case studied, the focus was to exploit essentially retention time differences, where a chromatographic segment which is characterized by fast elution but poor separation is coupled to a segment which yields better

separation at the cost of slow elution. For the applied adsorption isotherm parameters (Table 6.1), the optimum values of Pr_2Y_2 were searched again in the $V_{inj} - x_A$ space, within the sensitive ranges ($V_{inj} : 0.05 - 0.25$ ml and $x_A : 0 - 1$). The resulting optimum values for individual segments A and B and their assemblies in the orders A-B and B-A are tabulated in Table 6.6.

Table 6.6: *Case II* : Optimal values of Pr_2Y_2 for the combination and individual segments ($x_A \in \{0, 1\}$), along with the resulting parameters. Optimized using GA Toolbox (settings from Table 6.4)

Segment order	Pr_2Y_2 [$\mu\text{g}/\text{cm}^2 \text{ min}$]	V_{inj} [ml]	x_A [-]	Pr_2 [$\mu\text{g}/\text{cm}^2 \text{ min}$]	Y_2 [-]
A	0	-	1	0	0
B	4337.7	0.2034	0	4376.2	0.9912
A-B	4382.3	0.1868	0.0898	4410.7	0.9936
B-A	4337.7	0.2034	0	4376.2	0.9912

Since the components migrate very fast with very poor separation in segment A, the given length of A alone does not lead to any successful separation in the range of volumes of sample injected. However with sufficient retention time and good separation, there exists an optimal value ($Pr_2Y_2 = 4337.7 \mu\text{g}/\text{cm}^2 \text{ min}$) for an injected volume of 0.2034 ml when segment B alone is used. At this optimum there is nearly complete separation ($Y_2 = 0.9912$).

Subsequently, coupling of both segments was studied. The order A-B results in an optimum with x_A value of 0.0898 and slightly improved performance ($Pr_2Y_2 = 4382.3 \mu\text{g}/\text{cm}^2 \text{ min}$). With the other order B-A however, the optimization results in a x_A value of 0, suggesting that no improvement in performance is possible by connecting segment A after segment B. The Pr_2Y_2 value of segment order A-B is marginally higher than that for the single segment B, suggesting that a segment with fast elution but poor resolution placed before a more retaining but better separating segment has a potential to further improve separation performance.

Comparing the segment B and the A-B combination, Y_2 shows only a negligible improvement from B to A-B ($Y_2 = 0.9912$ against 0.9936). The observed improvement in Pr_2Y_2 values arises due to the increased production rate Pr_2 as a result of decreased

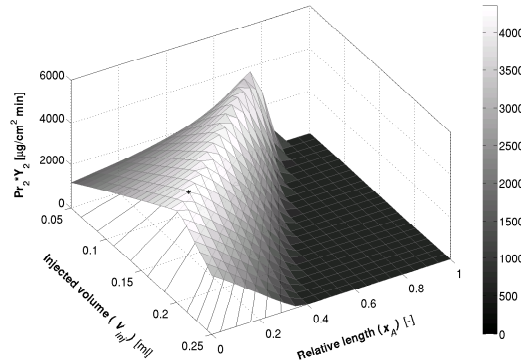


Figure 6.6: *Case II* : Pr_2Y_2 plot in $V_{inj} - x_A$ space for the segment order A-B, other parameters from Tables 6.1 and 6.3

cycle time rendered by adding a slice of segment A. Fig. 6.6 shows the plot of Pr_2Y_2 in the 2 parameter space. It can be seen that the optimal values of objective function for x_A in the range 0 - 0.7 are very similar. The change seen in objective function by adding segment A to the assembly seems insignificant in this case, however its influence in combination with differences in selectivities are much more prominent and is analyzed in *Case III*.

6.3.3 Case III

For the 7 component mixture, initially the influence of order was tested in the linear range. With the parameters from Table 6.2, simulations were carried out equating all $b_{i,j} = 0$ (equation (6.2)) for both segment orders. The x_A and V_{inj} used were fixed to be 0.5 and 0.01 ml respectively. The resulting elution profiles for both orders are plotted in Fig. 6.7. Clearly the chromatograms for both segment orders closely coincide, thus any objective function based on them would result in equivalent values. It has to be noted that taking any other value of x_A would also give a coinciding chromatograms under linear conditions for both orders.

In order to evaluate the influence of order in the overloaded regime, non linearities were incorporated as described above. Closely examining the isotherm parameters and separation factors for the two column segments ($\alpha_{i,i+1,A}$ and $\alpha_{i,i+1,B}$), it can be seen that, as in *Case II*, segment A facilitates fast elution at the cost of poor separation. Whereas segment B is characterized by relatively high Henry coefficients, resulting in slower elution but with appreciable separation of most of the components. It can also be seen that $\alpha_{1,2,B}$, $\alpha_{2,3,B}$ and $\alpha_{3,4,B}$ are sufficiently large compared to the separation factors of the rest of the pairs, implying a better separation of components 1, 2 and 3 from its neighbors. The fact that component 1 is the least retained component makes it easier to separate. Hence only the separation performance of components 2 and 3 were considered in our study (target components).

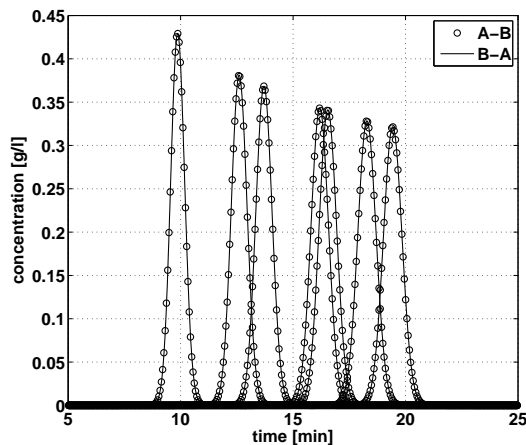


Figure 6.7: Linear case: elution profile of the 7 components in the linear range for both segment orders, with $b_{i,j} = 0$ l/g, $V_{inj} = 0.01$ ml and $x_a = 0.5$. Other parameters from Tables 6.2 and 6.3

The objective function plots for component 2 in the two parameter space

$x_A - V_{inj}$ are shown in Fig. 6.8. The highest values of Pr_2Y_2 are seen at very low injection volumes for both orders. This is because of the low separation factors of both segments (compared to *Cases I and II*). Similarly, due to the very low separation factors for segment A ($\alpha_{i,i+1,A} < 1.1$), its role in the overall separation using the assembly reduces, hence maximum values of the objective function were found to lie around very low values of x_A . In addition to that, complete elution of all 7 component takes longer time (higher t_{cyc}), thus reducing the production rates. The optimized values of the Pr_2Y_2 as identified are tabulated in Table 6.7

Analogous to *Case II*, the poor selectivities in segment A result in no separation when used alone ($x_A = 1$). However, using segment B alone does separate component 2, but with relatively low recovery yield ($Y_2 = 0.6333$) as a result of the close proximity with component 3 ($\alpha_{2,3,B} = 1.1017$). Coupling the two segments serially results in a minor improvement when segment A with a small length ($x_A = 0.0686$) is placed before segment B. Similar to *Case II*, the improvement in Pr_2 by using initially a slice of segment A is reflected in Pr_2Y_2 . In the other order however, the optimal value of x_A turned out to be 0, reiterating the fact that order B-A does not help improve the separation performance. The elution profiles at the end of both segments for the optimal case A-B given in Table 6.7 are shown in Fig 6.9

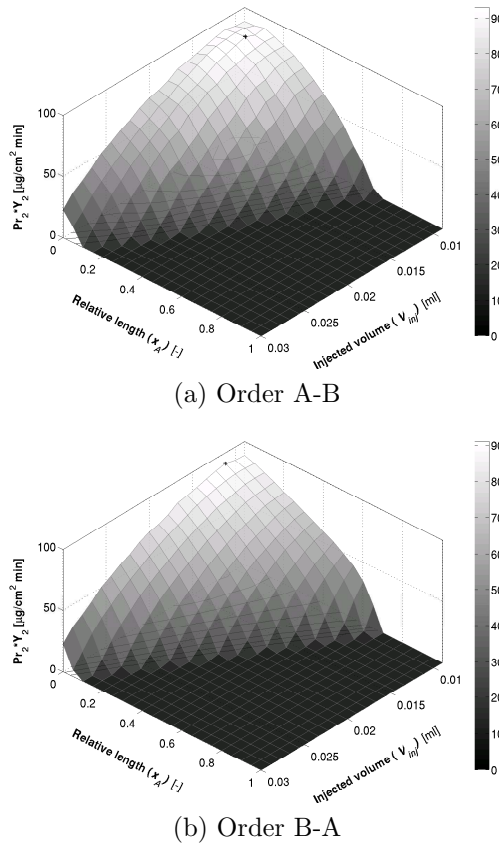


Figure 6.8: *Case III* : Pr_2Y_2 plot in $V_{inj} - x_A$ space for both segment orders, other parameters from Tables 6.2 and 6.3

Table 6.7: *Case III*, component 2 : Optimal values of Pr_2Y_2 for the combination and individual segments ($x_A \in \{0,1\}$), along with the resulting parameters. Optimized using GA Toolbox (settings from Table 6.4)

Segment order	Pr_2Y_2 [$\mu\text{g}/\text{cm}^2 \text{ min}$]	V_{inj} [ml]	x_A [-]	Pr_2 [$\mu\text{g}/\text{cm}^2 \text{ min}$]	Y_2 [-]
A	0	-	1	0	0
B	90.7383	0.0112	0	143.2845	0.6333
A-B	93.6668	0.0105	0.0686	149.5221	0.6264
B-A	90.7383	0.0112	0	143.2845	0.6333

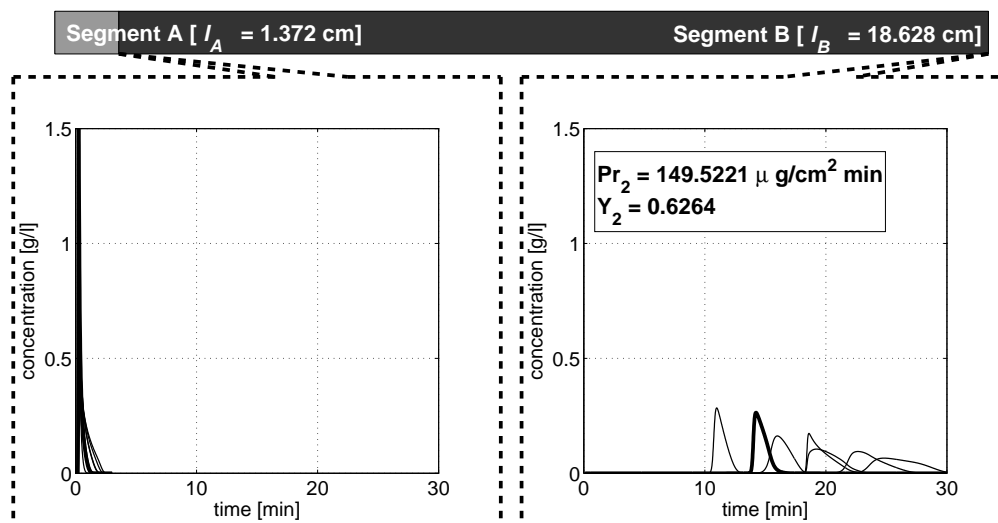


Figure 6.9: *Case III*: Elution profiles of order A-B for the optimal case (component 2) in Table 6.7, $V_{inj} = 0.0090$ ml, $x_A = 0.0686$ with $Pr_2Y_2 = 93.6668 \mu\text{g}/\text{cm}^2 \text{ min}$. Parameters from Tables 6.2 and 6.3

The objective function plots for component 3 are shown in Fig. 6.10. Similarly the highest values of Pr_3Y_3 are observed at the lowest bound of V_{inj} considered. However, the segment order A-B shows a maxima around a relative length $x_A = 0.2$, suggesting that such an arrangement would result in a better separation of component 3. The optimal values of Pr_3Y_3 are tabulated in Table 6.7.

Compared to component 2, the separation factors between component 3 and its less retained neighbor are much lower ($\alpha_{2,3,B} < \alpha_{1,2,B}$, Table 6.2), thus the resulting yield and production rate are reduced. It can be seen that the Pr_3Y_3 values for the segment order A-B are in this case again higher than that of segment B alone. Similarly, the optimal values of x_A for separation of component 3 too turned out to be 0 for the segment order B-A. In comparison with Pr_2Y_2 , it can be seen that change in Pr_3Y_3 is significant by placing a

small segment of A before B in the assembly. The minor change in Pr_2Y_2 is because of the fact that, component 2 is not very well separated from component 3 in segment B alone ($\alpha_{2,3,B} = 1.1017$). Adding segment A to the assembly further reduces the separation between 2 and 3 ($\alpha_{2,3,A} = 1.0870$), increasing peak overlap and reducing yield. Additionally, because of the relatively better separation between components 2 and 1 in segment B ($\alpha_{1,2,B} = 1.4047$), the influence of component 1 is not significant. Thus, a serial coupling with $x_A = 0.0686$ (Table 6.8) results in increased production rate (faster elution) with diminished yield. The improvement achieved in Pr_2 is compensated with the loss in yield, resulting in a net non-significant change in Pr_2Y_2 . In case of component 3, again it is relatively well separated from component 4 in segment B ($\alpha_{3,4,B} = 1.2462$). Besides, in an assembly with $x_A = 0.1599$, the change in selectivity between 2 and 3 is small, resulting in a small change in Y_3 . But because of the faster elution achieved, Pr_3 is significantly

Thus it can be summarized that an initial fast pre-separation using segment A helps the slower but better separation occurring in segment B. For the sake of illustration, the elution profiles at the end of each segments are shown in Fig 6.11 for the optimal case A-B in Table 6.8. improved, which results in a better Pr_3Y_3 .

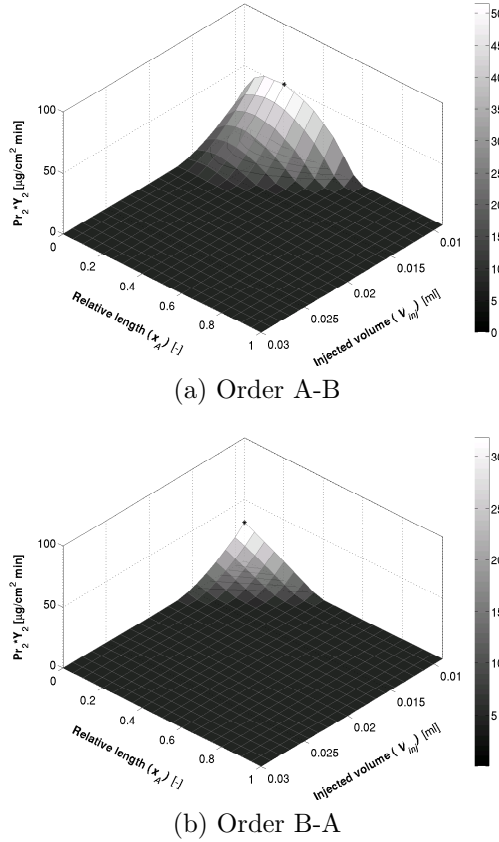


Figure 6.10: *Case III* : Pr_3Y_3 plot in $V_{inj} - x_A$ space for both segment orders, other parameters from Tables 6.2 and 6.3

Table 6.8: *Case III* , component 3 : Optimal values of Pr_3Y_3 for the two segment orders and the resulting parameters, using GA Toolbox (settings from Table 6.4)

Segment order	Pr_3Y_3 [$\mu\text{g}/\text{cm}^2 \text{ min}$]	V_{inj} [ml]	x_A [-]	Pr_3 [$\mu\text{g}/\text{cm}^2 \text{ min}$]	Y_3 [-]
A	0	-	1	0	0
B	31.7768	0.0090	0	78.8840	0.4028
A-B	51.9097	0.0090	0.1599	107.8390	0.4814
B-A	31.7768	0.0090	0	78.8840	0.4028

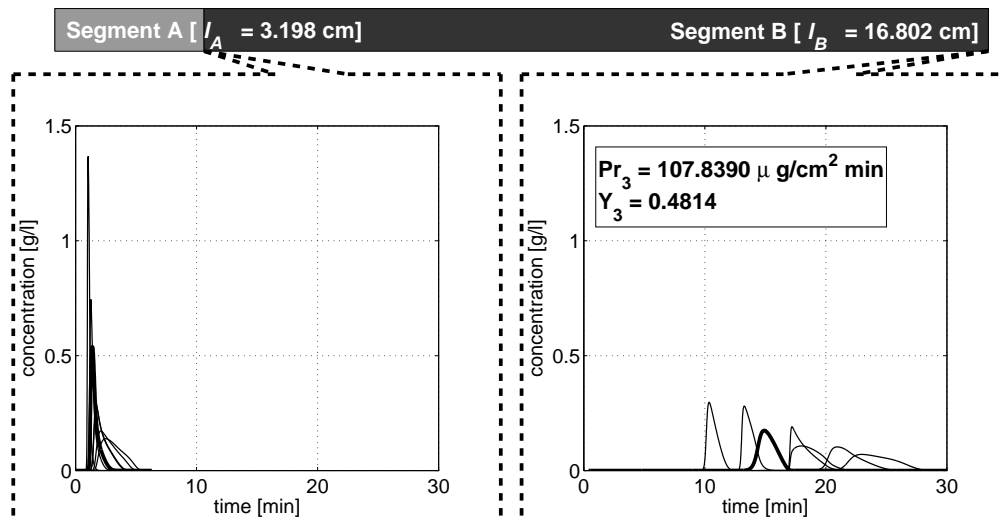


Figure 6.11: *Case III*: Elution profiles of order A-B for the optimal case (component 3) in Table 6.8, $V_{inj} = 0.0090$ ml, $x_A = 0.1599$ with $Pr_3 Y_3 = 51.9097 \mu\text{g}/\text{cm}^2 \text{ min}$. Parameters from Tables 6.2 and 6.3

6.4 Mixed mode operation

So far in this study, the two different stationary phases were coupled directly to isolate the target component. Another possibility is to use them in a mixed manner, i.e by mechanically mixing the stationary phases with a fixed mixing ratio in a single segment. Again, there have been some efforts to realize such a concept in the analytical separation of enantiomers using chiral stationary phases (CSP). For instance, Zhang and Francotte [117] used mixed cellulose based CSPs (coated on silica gel) to separate an array of racemates. They also found that in such a configuration, the effective Henry coefficients of a component on mixed stationary phases was as a linear relationship between the mix ratio and the Henry coefficients corresponding to individual stationary phases. Provided the same relationship hold in non-linear regime, the effective solidphase loading ($q_{eff,i}$) for such a mixed configuration with two stationary phases (A and B) can be written as :

$$q_{eff,i} = y_A q_{i,A} + (1 - y_A) q_{i,B} \quad (6.5)$$

with y_A representing the mix ratio of the reference stationary phase A. When y_A tends to zero, the stationary phase is almost entirely composed of stationary phase B and for a $y_A = 1$, the mixed configuration is entirely A.

With this relationship in hand, the most promising case exhibiting selectivity differences (*Case I*) was used to find a maximum value for $Pr_2 Y_2$. For calculating individual stationary phase loadings ($q_{i,j}$), the $a_{i,j}$ and $b_{i,j}$ values for *Case I* were taken from table 6.1. Analogous to the serially coupled

configuration, the mix ratios y_A and the injected volume V_{inj} were varied to optimize Pr_2Y_2 using Genetic Algorithm (with other parameters from tables 6.3 and 6.4 respectively).

Figure 6.12 shows the plot of Pr_2Y_2 in the $V_{inj} - y_A$ space. Similar to the serial coupling case, using stationary phase A ($y_A=1$) or B ($y_A=0$) alone leads to insufficient separation. The maximum value of Pr_2Y_2 (6140.5 $\mu\text{g}/\text{cm}^2\text{min}$) was found for $y_A = 0.4008$ and $V_{inj} = 0.0856$ ml. This optimal objective function value for mixed mode is slightly more (above 5%) than that obtained for the A-B serial coupling configuration (given in table 6.5), demonstrating that a mixed configuration has a potential to outperform the serial coupling mode in terms of the performance parameters considered. This observation holds as long as the effective equilibrium relationship given by equation 6.5 holds. In case of the serial coupling configuration, the first segment isolates first or the last component to a great extent initially, this separation is then compromised to a certain extent in the second segment. By using the above mentioned mixed configuration, such a scenario can be avoided, improving the production rate. Thus, an integrated approach to the problem has a potential to facilitate better separation performance.

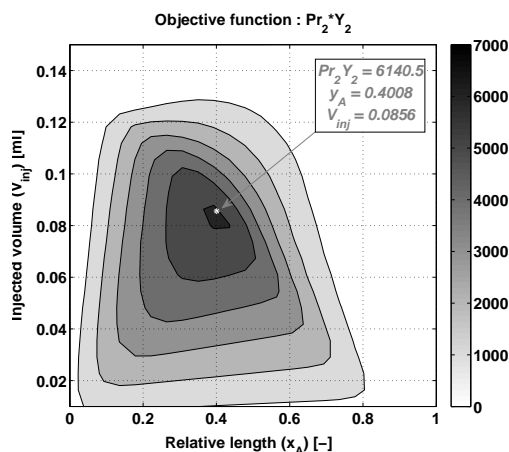


Figure 6.12: Mixed mode with *Case I*: Pr_2Y_2 plot in the $V_{inj} - y_A$ space with maximum $Pr_2 = 6506.58 \mu\text{g}/\text{cm}^2\text{min}$ and $Y_2 = 0.9437$. Other parameters from tables 6.3 and 6.4).

6.5 Role of selectivity reversals

The isotherm parameters considered so far exhibited no selectivity reversals, i.e. in both segments considered, the elution order remains unchanged. However in reality, a drastic change in elution order with the change of stationary phase is not entirely uncommon. A lot of examples can be found in the analytical separations [118, 119, 50]. To envisage the influence of selectivity reversals, two sub cases (of *Case I*) were considered.

- *Case I-A* : Minor selectivity reversal towards lower retention in segment A
- *Case I-B* : Minor selectivity reversal towards higher retention in segment B

In *Case I-A*, the target component elutes slightly before the first component in segment A. Whereas in segment B, the third component elutes slightly ahead of the target component. The isotherm parameters perturbed in this fashion are tabulated in table 6.9.

Table 6.9: Isotherm parameters for minor selectivity reversals

Isotherm parameters	First component	Second component	Third component	Separation factors
	$i = 1$	$i = 2$ (target)	$i = 3$	
<i>Case I-A</i> : Minor selectivity reversal towards lower retention in segment A				
$a_{i,A}$	5.5555	5.0000	10.0000	$\alpha_{1,2,A}=\mathbf{0.9}$, $\alpha_{2,3,A}=2.0$
$a_{i,B}$	2.5000	5.0000	5.5000	$\alpha_{1,2,B}=2.0$, $\alpha_{2,3,B}=1.1$
<i>Case I-B</i> : Minor selectivity reversal towards higher retention in segment B				
$a_{i,A}$	4.5454	5.0000	10.0000	$\alpha_{1,2,A}=1.1$, $\alpha_{2,3,A}=2.0$
$a_{i,B}$	2.5000	5.0000	4.5000	$\alpha_{1,2,B}=2.0$, $\alpha_{2,3,B}=\mathbf{0.9}$

For the two scenarios considered, the Pr_2Y_2 values were calculated for serial coupling (A-B) and mixed mode configurations in the two dimensional space, this is illustrated in figure 6.13. As a result of change in elution orders, the maximum values of Pr_2Y_2 exhibited a marked reduction in comparison to those obtained for the original data set (given in table 6.5 and figure 6.12). The maxima for *Case I-A* seems to appear around an x_A value of 0.23 in case of serial coupling (figure 6.13a) and y_A value of 0.33 for the mixed mode (figure 6.13b). This illustrates that in this case, due to the selectivity reversal of the target component towards lesser retention in segment A, the use of segment A is favored to a lower extent. Similarly for *Case I-B*, the reversal occurs in segment B, resulting in a decreased use of segment B for optimal separation of the target ($x_A = 0.41$ in figure 6.13c against 0.31 in table 6.5 and $y_A = 0.476$ in figure 6.13d against 0.4 in figure 6.12). It is also worth noting that, the separation performance would further be diminished if both segments exhibit selectivity reversals of the form described above.

In extreme cases of reversals, i.e. when the target in either of the segments is well separated and appears as the first or last component in the elution, then clearly, that single segment alone could be used for the best separation performance. For the sake of illustration, a version of this extreme but plausible case is depicted in figure 6.14. The elution order is drastically changed in segment A alone ($\alpha_{1,2,A}=0.7$). As a result, the target component elutes first and is well separated from its more retaining neighbor. Irrespective of the configuration used, this extreme reversal obviously results in a maximum Pr_2Y_2 value using segment A alone ($x_A = 1$ and $y_A = 1$ in figures 6.14a and 6.14b). However in both modes, there exist a sub optimal local Pr_2Y_2 maximum for very low x_A or y_A values.

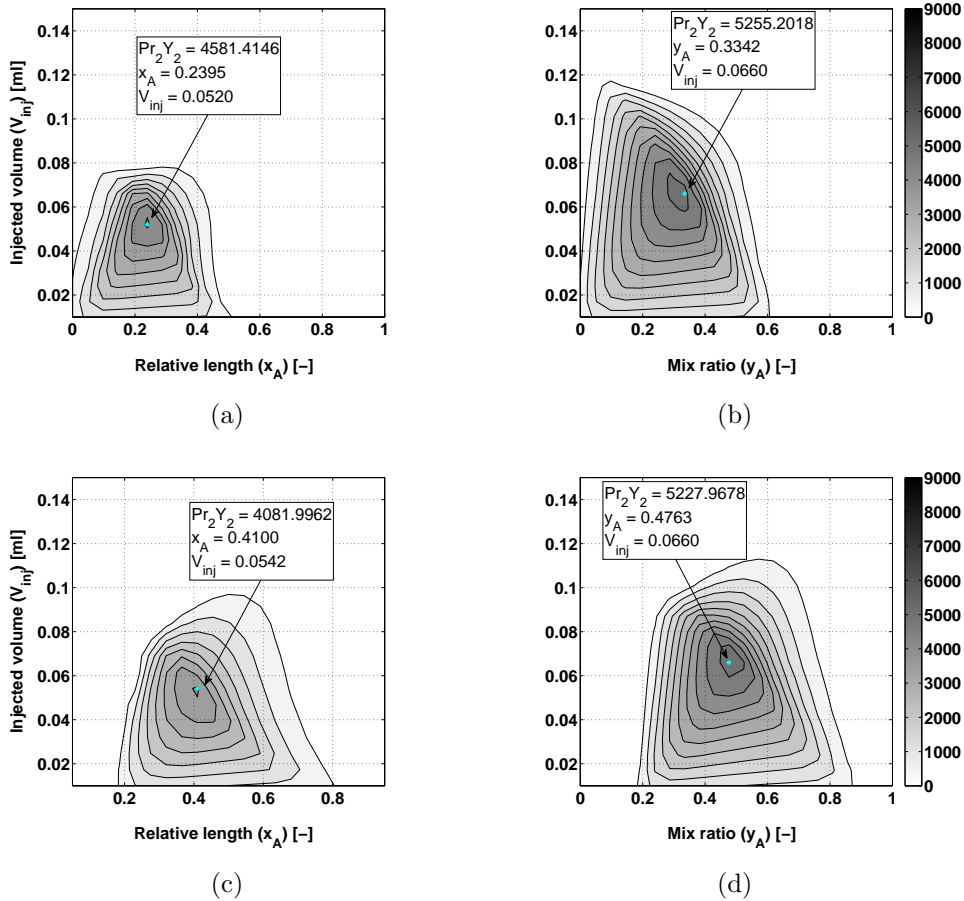


Figure 6.13: Influence of selectivity reversals: (a) *Case I-A* : serial coupling A-B (b) *Case I-A* : mixed mode (c) *Case I-B* : serial coupling A-B (d) *Case I-B* : mixed mode

In short, presence of selectivity reversals can adversely effect the use of multiple stationary phases in serially coupled or mixed mode configurations to isolate an intermediately eluting target component. This however depends on the degree of selectivity reversals, in extreme cases that aid separation (resulting in target eluting as first or last component), the single segment separation alone could be used.

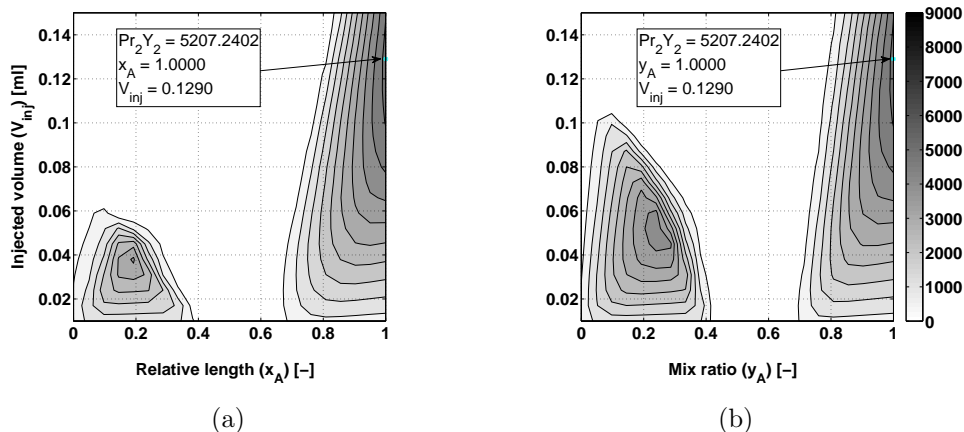


Figure 6.14: Example of extreme selectivity reversal: (a) serial coupling A-B (b) mixed mode. For $a_{2,A}$, $a_{2,B} = 5$, $\alpha_{1,2,A} = \mathbf{0.7}$, $\alpha_{2,3,A} = 2.0$, $\alpha_{1,2,B} = 2.0$ and $\alpha_{2,3,B} = 1.1$

6.6 Conclusions

In this chapter, two different configurations involving multiple stationary phases were evaluated for preparative separation of an intermediately eluting component from a multi-component mixture. Using the two segments in series to separate a ternary and a seven component mixture, the influences of segment lengths, their order of arrangement and the volume of sample injected were analyzed. Similarly, the influences of mix ratio were analyzed for a mixed mode configuration. An objective function incorporating both production rates and recovery yield was used to compare separations belonging to two typical scenarios characterized by retention time and separation factor differences in the two stationary phases considered.

Serial coupling of segments with different stationary phases was found to be beneficial when the target nearly co-elute with different neighbors in different segments. Owing to the underlying non-linearities of the adsorption isotherms, the order of coupling was seen to have a significant impact on the preparative separation performance. In addition, the optimal relative lengths of segments differed from that for an analytical separation. The segment where the target co-elutes with the less retained neighboring component, when placed before the segment with opposite behavior, yielded noticeably higher separation performance. Besides, exploiting the retention time differences, a segment which facilitates fast separation when placed before a segment characterized by slow elution but better separation, showed potential improvement in separation. The improvement in separation by using combination of the two concepts was demonstrated also for the isolation of the second and third eluting components of a model mixture of seven substances

studied earlier under linear (analytical) conditions. The integrated approach by mechanically mixing the stationary phases showed promising improvements in the separation performance. These observations with respect to a preparative separation can be applied to any multicolumn chromatographic system reflecting the specific adsorption isotherm behaviors discussed, irrespective of the underlying retention mechanisms. However, their application makes sense as long as any selectivity reversals if at all present are marginal.

In the two scenarios studied exploiting the retention time and selectivity differences, it was found that an easy separation step carried out before a more difficult one helps to improve the overall separation performance. Unlike in conventional solvent gradient operation, using multiple stationary phases with a unique mobile phase reduces the additional time required for column regeneration.

In the next chapter, the general trends observed from the theoretical investigation of the serial coupling concept are demonstrated experimentally using a test system.

Chapter 7

Experimental demonstration and illustration of theoretical tools

7.1 Introduction

A concept of serially coupling multiple stationary phases for chromatographic separations was analyzed theoretically for preparative applications in the last chapter. The influence of the order and the relative length of each segments on the separation performance was studied theoretically for a system exhibiting selectivity differences.

The main aim of this chapter was to experimentally illustrate and quantify the theoretical results obtained in the previous chapter. Using a test system with two stationary phases and three components, general trends involved in such serial couplings were validated. Using fundamental adsorption isotherm parameters, an optimization study was carried out to elucidate the influences on key performance parameters introduced in the last chapter.

7.2 Experimental system

A brief summary of the samples, equipment, stationary and mobile phases used is given in this section.

The ternary system used consisted of two cycloketones, Cyclohexanone (C6) and Cycloheptanone (C7) and Phenol (Ph). All the three components were of synthesis grade purity, purchased from Merck, Darmstadt, Germany. The mobile phase was composed of 30% HPLC grade Methanol (Fisher, Loughborough, UK) and 70% de-ionized water purified using a Milli-Q system (Millipore, Bedford, MA, USA).

Two sets of chromatographic columns were used for the experiments. The first set consisted of a Zorbax Eclipse XDB-C18 column and a Zorbax Bonus-

RP column. Both columns (dimensions 250x4.6 mm with 5 μm particles) were purchased from Agilent technologies, Pao Alto, CA, USA. The former consists of a stationary phase entirely made of octadecyl silica (C18). On the other hand, the alkyl group in Bonus-RP column is made of a C14 chain with an embedded amide linkage. Further in this thesis, such alkyl-silica bonded phases with a polar amide group are referred to as EPS (enhanced polar stationary phase). These long columns were used to measure the adsorption isotherm parameters.

The second set of segments were taken from the so called POPLC kit (Bischoff Chromatography, Leonberg, Germany). The kit consisted of five different stationary phases, each with different segments with varying lengths (1,2,4,6 and 8 cm respectively with 3mm internal diameter). The main advantage of these segments is that they could be coupled together serially with minimal dead volume in between [51]. Only the C18 phase (ProntoSIL 100-5-C18 SH 2) and the EPS phase (ProntoSIL 100-5-C18 EPS 2) were used for the validation. Unlike the Zorbax columns, the EPS phase in the POPLC kit was based on octadecyl silica.

The chromatographic equipment consisted of a Dionex P580 A low pressure gradient pump, a Dionex ASI-100 autosampler and a Dionex UVD 170S/340S UV diode array detector along with Chromeleon Chromatography Data System (Dionex Softron, Idstein, Germany). By injecting a tracer component without any column in between the automatic injector and the UV detector, the plant dead volume was determined in preliminary tracer experiments to be 0.1232 ml.

7.3 Demonstration of trends

In order to quantify the impact of coupling segments serially, the ternary mixture separation was tried on individual segments. The longest available segments (8cm) of C18 and EPS were used to separate the C6, Ph and C7 mixture. Feed mixtures with nearly same concentrations for all components ($C_{inj,C6} = 20.07$, $C_{inj,Ph} = 19.75$ and $C_{inj,C7} = 20.42$ mg/ml respectively) were injected at a set flow rate of 0.5 ml/min. Figure 7.1 shows the resulting chromatograms of two injections (linear and overloaded) carried out on C18 and EPS segments. It can be seen that the C18-EPS system closely resembles the ternary mixture exhibiting selectivity differences introduced in the previous chapter (figure 6.2a). In the analytical separation ($V_{inj}=2 \mu\text{l}$), C18 fails to resolve the first and second eluting component. On the contrary, all three components can be resolved using the EPS segment alone. The scenario changes when the columns are overloaded ($V_{inj}=30 \mu\text{l}$) and result in insufficient separation with both segments.

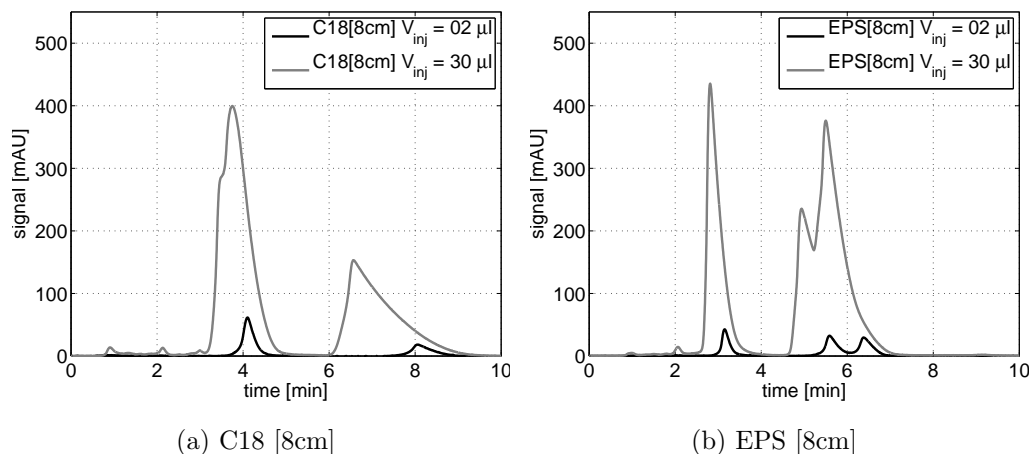
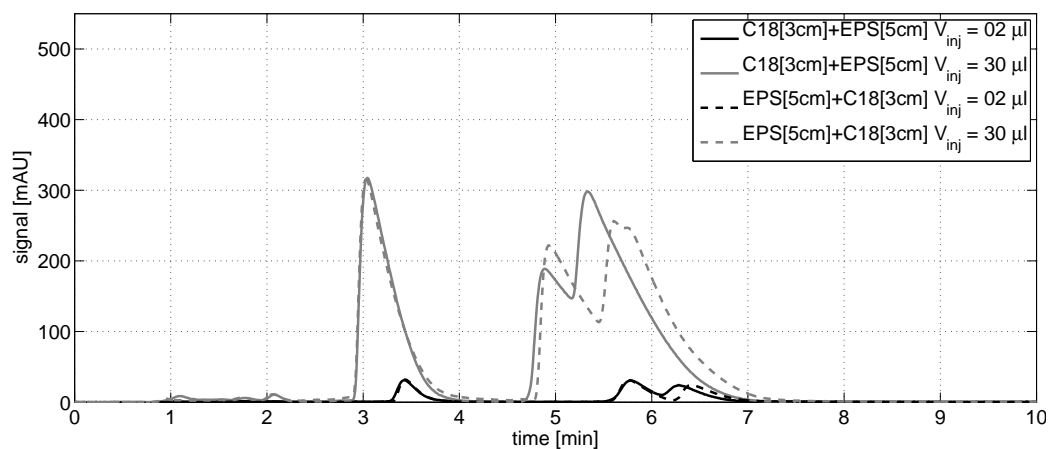


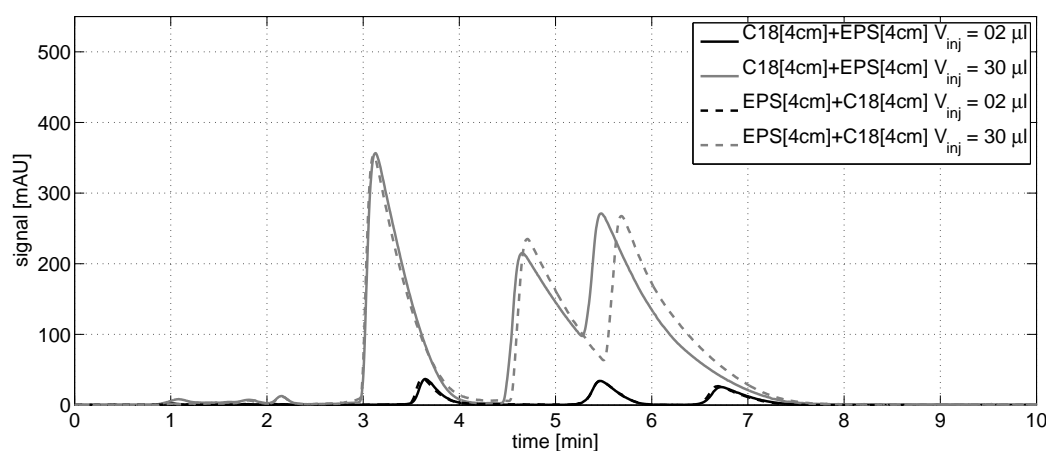
Figure 7.1: Separation of a small ($V_{inj}=2\mu\text{l}$, black lines) and overloaded ($V_{inj}=30\mu\text{l}$, gray lines) injection sample using C18 and EPS segments

Based on the result above, the two segments were coupled serially in 3 different combinations. The lengths of each segments considered were 3,4 and 5 cm with total length always adding up to 8 cm. Both linear and overloaded separation were carried out with all these combinations along with changing orders (C18-EPS and EPS-C18). Corresponding results are shown in figure 7.2.

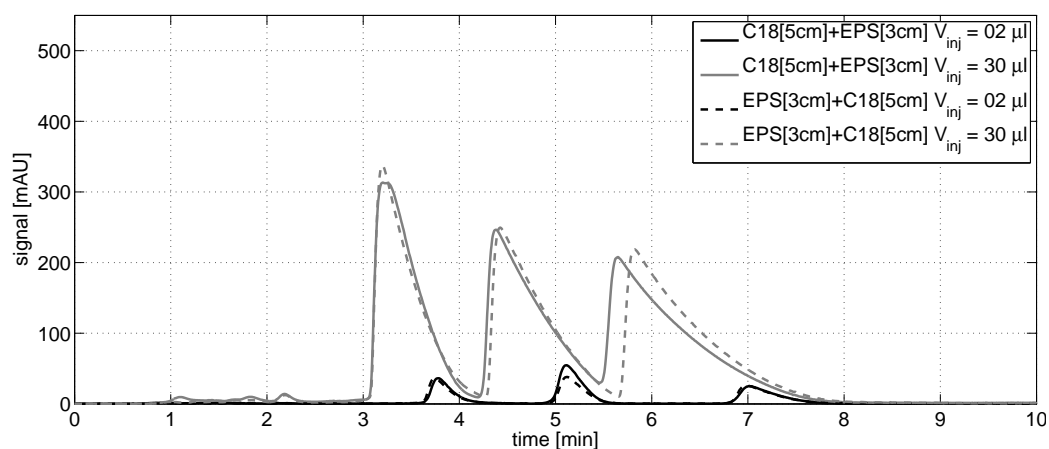
Starting with a C18 segment of 3cm (figure 7.2a), increasing the relative length of C18 shifts the intermediately eluting component towards lower retention times. This is evident in both injection cases. A good separation of the components is achieved for the combination with 5 cm C18 and 3 cm EPS segments (figure 7.2c). It can also be noted that there are significant changes in the preparative elution profiles ($V_{inj}=30\mu\text{l}$) with change in the segment order. Such differences in the overloaded profiles can be seen for all the three combinations. On the other hand, segment order seems to hardly influence the linear profiles ($V_{inj}=2\mu\text{l}$), confirming similar results found in the previous chapter theoretically.



(a) C18 [3cm] + EPS [5cm]



(b) C18 [4cm] + EPS [4cm]



(c) C18 [5cm] + EPS [3cm]

Figure 7.2: Separation of a small ($V_{inj}=2 \mu\text{l}$, black lines) and overloaded ($V_{inj}=30 \mu\text{l}$, gray lines) injection sample using C18 and EPS segments. Solid lines: segment order C18-EPS, dashed lines: segment order EPS-C18. Total segment length = 8 cm.

7.4 Quantitative analysis

The trends seen in the described experiments were quantified by measuring adsorption isotherms for the ternary system and optimizing subsequently the injection volume and the relative lengths were optimized for maximum productivity-yield of Phenol.

7.4.1 Adsorption isotherms

In order to measure the adsorption isotherms of the components, the longer Zorbax columns were used with a mobile phase flowrate of 0.5 ml/min. Initially, the dead volumes of the columns were estimated by injecting a small amount of Dihydroxyacetone. Thereafter, the total porosity of the columns were calculated from the resulting dead times (equation 3.16). The retention times of the three components in the two columns were similarly measured by injecting an infinitesimal amount of each substance. Analogous to equation 3.15, the first absolute moment of the resulting near symmetric peaks were taken as the corresponding retention times ($t_{r,i}$). The Henry coefficient of the components can then be calculated according to [5]:

$$a_i = \frac{t_{r,i} - t_0}{t_0 - t_{dead}} \left(\frac{\epsilon}{1 - \epsilon} \right) \quad (7.1)$$

where t_{dead} represents the corresponding plant dead time. Additionally, the plate numbers of each components were estimated in the two columns according to equation 3.18. The results are tabulated in table 7.1

The competitive Langmuir adsorption isotherms (equation 3.27) were chosen to model the equilibrium relationships. The inverse method introduced in section 3.2.3.4 was used to determine the parameters of the isotherm model. The objective function given by equation 3.33 was slightly modified in this case. Instead of the individual concentration profiles of each components, the total detector response (S) was used to compare the experimental and simulated profiles. Additionally, the parameter b_i for each component was replaced by a single saturation capacity (q_{sat} , equation 3.22). Thus, for the given ternary system with any of the two stationary phases, the minimization problem reduces to fitting four parameters, namely the Henry coefficients (a_i , $i \in \{C6, Ph, C7\}$) and the saturation capacity. Thus the modified problem can be written as:

$$\min_{a_i, q_{sat}} \left\| \frac{S_{sim} - S_{exp}}{S_{exp}^{max}} \right\| \quad (7.2)$$

subject to the model equations 3.10, the inlet condition 3.5, bounds on the variables and equilibrium relationships given by equations 3.27 and 3.22.

Table 7.1: Retention parameters of C6, Ph and C7 from single component injections on C18 and EPS stationary phases at $\dot{V}_f=0.5$ ml/min

Column		Zorbax Eclipse C18 XDB (C18)	Zorbax Bonus-RP (EPS)
L [cm]		25	25
d_c [cm]		0.46	0.46
t_0 [min]		4.85	4.98
ϵ [min]		0.5447	0.5616
$t_{r,i}$ [min]	C6	20.96	16.09
	Ph	23.96	28.82
	C7	42.58	28.89
a_i	C6	4.1863	3.009
	Ph	4.9683	6.4592
	C7	9.8569	6.4698
N_i	C6	9484	8429
	Ph	13654	15311
	C7	12716	12716
$\alpha_{Ph,C6}$		1.19	2.15
$\alpha_{C7,Ph}$		1.98	1.00

A noticeable aspect of the problem formulation of the type given by equation 7.2 is that, calibration factors corresponding to the detector response are needed for each component to generate the simulated response (S_{sim}). These linear factors for each components were determined using again pulse injections. More details on the calibration factors and linearity of the response can be found in Appendix A. The reference data (S_{exp}) needed for the inverse method were generated by injecting the ternary mixture with a preset injection amount well within the detector linearity range. With the experimental profiles thus generated, the minimization problem (equation 7.2) was solved using 'fmincon' optimization routine in MATLAB.

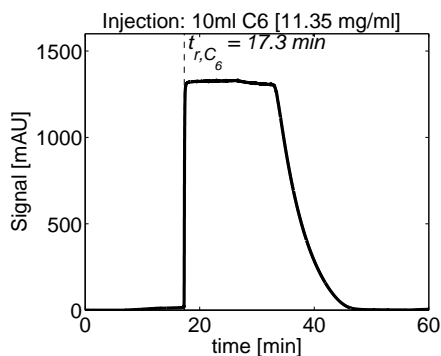


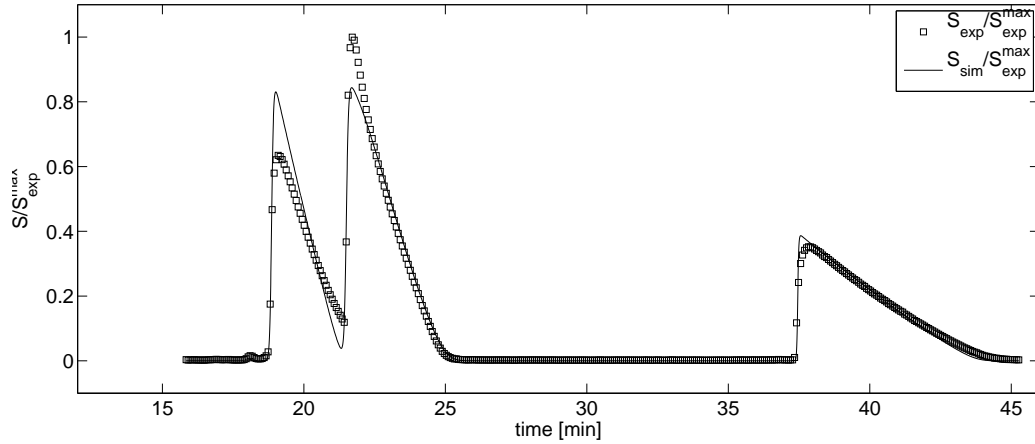
Figure 7.3: Breakthrough curve for C6 to determine initial values of q_{sat}

Table 7.2: Saturation capacity (q_{sat}) estimates [mg/ml] for initial values in the inverse method

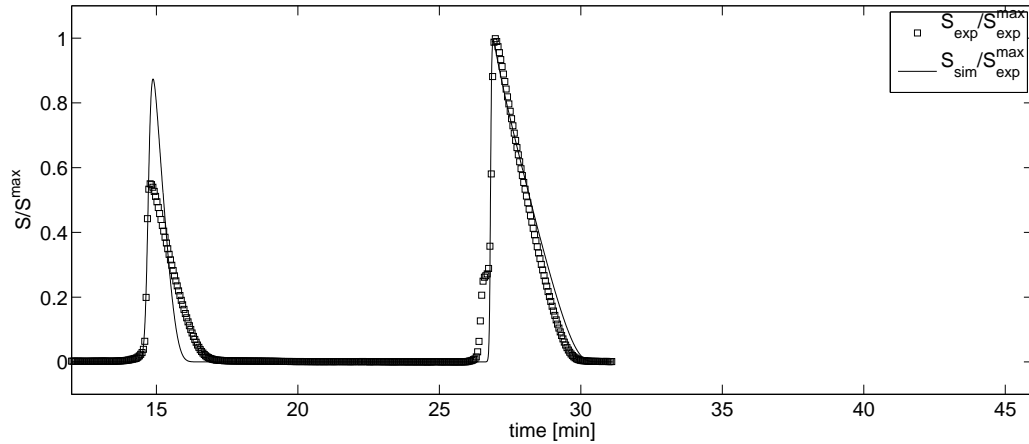
components	C18	EPS
C6	51.16	123.83
Ph	54.03	135.98
C7	79.62	168.92

However, the minimization problem of the type given above requires good starting values. The individual Henry coefficients found (a_i values in table 7.1) were used as the corresponding initial guesses for the competitive case. For q_{sat} values, breakthrough experiments were carried out for each component. For example, figure 7.3 shows one such a breakthrough curve for C6. From the resulting retention time of the shock front, the corresponding $\Delta q_i/\Delta C_i$ values can be deduced (see equation 3.23). With an empty column to begin with and a known injection concentration, good estimates of q_{sat} can be found this way. The saturation capacity estimates thus found are tabulated in table 7.2 for the two Zorbax columns. Their average values were taken as initial guesses for q_{sat} (61.60 mg/ml for C18 and 142.91 mg/ml for EPS).

Figure 7.4 shows the fitted experimental and simulated profiles for Zorbax C18 and EPS columns with the respective injection amounts. The column parameters (dimensions, total porosity, average plate numbers etc.) for the simulation were taken from table 7.1. Given the selectivity and retention differences (see table 7.1), C6 and Ph elute close together in C18 with C7 well separated. In the EPS column however, C6 with a lower retention time is well separated from the co-eluting pairs of Ph and C7. The quality of fit is relatively good for the C18 column except for a slight overshoot for C6 and an undershoot for Ph in the simulated profiles. In case of the EPS column



(a) Zorbax C18. Injection mixture : $40\mu\text{l}$ of C6 (24.10 mg/ml), Ph (25.31) and C7 (24.26 mg/ml)



(b) Zorbax EPS. Injection mixture : $60\mu\text{l}$ of C6 (20.07 mg/ml), Ph (19.75) and C7 (20.42 mg/ml)

Figure 7.4: Evaluation of isotherm parameters by inverse method: fit of experimental and simulated detector response for a flowrate of $\dot{V}_f=0.5$ ml/min

data, the discrepancy in simulated and experimental profiles are rather large for C6 part of the profile. Additionally, a displacement like effect seen experimentally on the sharp front of the Ph-C7 co-eluting pair is not captured by the method used. The resulting fitted parameters are tabulated in table 7.3.

In comparison with the initial a_i values of the C18 column considered for the fit from table 7.1, the corresponding fitted values do not show any major change. Besides, the predicted saturation capacity for C18 columns also lies very close to the initial guess. Suggesting that for relatively small injection volumes, single component adsorption isotherms would suffice to describe the multi-component ones. This however is not seen for the EPS column. The predicted q_{sat} value is significantly higher than the initial average used,

which renders the resulting chromatograms more towards linear regime. This is evident from the more symmetric peak of C6 in figure 7.4b. The Henry coefficients corresponding to the multi-component isotherms are again not significantly influenced.

The discrepancies seen in the experimental and simulated profiles of the EPS column could be a direct result of some phenomena far more complex than those assumed for the Langmuir model. Another possible source for inaccuracy (particularly in C18 column) could be due to the inaccuracies involved in the solution method of the ED model adopted (see section 3.3).

Table 7.3: Parameters determined by the inverse method, corresponding to figure 7.4, with $b_i = a_i/q_{sat}$

parameter	C18	EPS
q_{sat}	59.40	345.25
a_{C6}	4.5033	2.8275
a_{Ph}	5.2262	6.6133
a_{C7}	10.0493	6.6882
b_{C6}	0.0758	0.0082
b_{Ph}	0.0880	0.0192
b_{C7}	0.1692	0.0194

7.4.2 Application of adsorption isotherm parameters to determine sensitivity to non-linearities

The Henry coefficients determined in the previous section were used as a basis for studying the sensitivity of the relative segment length (x_{C18}) and the segment order to the non-linearity of the isotherm parameters. Using the a_i values from table 7.1, the saturation capacities (q_{sat}) were varied from a value of 25 mg/ml (highly non-linear) to 500 mg/ml (moderately non-linear) for C18 and EPS segments. The dimensions ($d_c = 0.3$ cm, variable length) and porosities ($\epsilon_{C18} = 0.6795$ and $\epsilon_{EPS} = 0.6576$) of the smaller segments were used to optimize $Pr_{Ph}Y_{Ph}$ for each combination of the saturation capacities for both segment orders C18-EPS and EPS-C18. A feed concentration of $C_{inj,i} = 20$ mg/ml was used for all three components. The extent of non-linearity can be assessed from the respective chromatogram non-linearity parameters $\bar{\lambda}_i$ introduced in section 3.2.2 (equation 3.25). In table 7.4, $\bar{\lambda}_i$ values corresponding to different saturation capacities in consideration are

tabulated for the two stationary phases. It can be seen that for a q_{sat} value of 500 mg/ml, the calculated parameters are close to the non-linearity limit ($\bar{\lambda}_i \geq 0.1 \rightarrow$ non-linearity). On the other hand, the $\bar{\lambda}_i$ values corresponding to saturation capacities of 25 ml/mg results in extreme non-linearity parameters (7-8 folds with respect to the limiting non-linearity factor). Optimization

Table 7.4: Isotherm parameter b_i [ml/mg] and chromatogram non-linearity parameter ($\bar{\lambda}_i$) of the ternary system for $C_{inj,i} = 20$ mg/ml

	C18		EPS	
$q_{sat}=25$	$b_{C6}=0.1801$	$\bar{\lambda}_{C6}=0.7827$	$b_{C6}=0.1131$	$\bar{\lambda}_{C6}=0.6934$
	$b_{Ph}=0.2090$	$\bar{\lambda}_{Ph}=0.8070$	$b_{Ph}=0.2645$	$\bar{\lambda}_{Ph}=0.8410$
	$b_{C7}=0.4020$	$\bar{\lambda}_{C7}=0.8894$	$b_{C7}=0.2675$	$\bar{\lambda}_{C7}=0.8425$
$q_{sat}=50$	$b_{C6}=0.0901$	$\bar{\lambda}_{C6}=0.6430$	$b_{C6}=0.0566$	$\bar{\lambda}_{C6}=0.5307$
	$b_{Ph}=0.1045$	$\bar{\lambda}_{Ph}=0.6764$	$b_{Ph}=0.1323$	$\bar{\lambda}_{Ph}=0.7257$
	$b_{C7}=0.2010$	$\bar{\lambda}_{C7}=0.8008$	$b_{C7}=0.1338$	$\bar{\lambda}_{C7}=0.7279$
$q_{sat}=100$	$b_{C6}=0.0450$	$\bar{\lambda}_{C6}=0.4739$	$b_{C6}=0.0283$	$\bar{\lambda}_{C6}=0.3612$
	$b_{Ph}=0.0523$	$\bar{\lambda}_{Ph}=0.5111$	$b_{Ph}=0.0661$	$\bar{\lambda}_{Ph}=0.5695$
	$b_{C7}=0.1005$	$\bar{\lambda}_{C7}=0.6678$	$b_{C7}=0.0669$	$\bar{\lambda}_{C7}=0.5722$
$q_{sat}=200$	$b_{C6}=0.0225$	$\bar{\lambda}_{C6}=0.3105$	$b_{C6}=0.0141$	$\bar{\lambda}_{C6}=0.2204$
	$b_{Ph}=0.0261$	$\bar{\lambda}_{Ph}=0.3432$	$b_{Ph}=0.0331$	$\bar{\lambda}_{Ph}=0.3981$
	$b_{C7}=0.0502$	$\bar{\lambda}_{C7}=0.5012$	$b_{C7}=0.0334$	$\bar{\lambda}_{C7}=0.4008$
$q_{sat}=500$	$b_{C6}=0.0090$	$\bar{\lambda}_{C6}=0.1526$	$b_{C6}=0.0057$	$\bar{\lambda}_{C6}=0.1016$
	$b_{Ph}=0.0105$	$\bar{\lambda}_{Ph}=0.1729$	$b_{Ph}=0.0132$	$\bar{\lambda}_{Ph}=0.2092$
	$b_{C7}=0.0201$	$\bar{\lambda}_{C7}=0.2867$	$b_{C7}=0.0134$	$\bar{\lambda}_{C7}=0.2111$

strategy explained in section 6.2.3 was used again here to maximize $Pr_{Ph}Y_{Ph}$. The results are tabulated in table 7.5.

In the C18 segment, the isotherm parameters are characterized by longer retention and better C6-Ph separation ($\alpha_{Ph,C6} = 1.19$). Whereas faster elution in EPS segment comes at the cost of nearly inseparable Ph-C7 pair ($\alpha_{C7,Ph} = 1.00$). The highest $Pr_{Ph}Y_{Ph}$ value is seen for the moderately non-linear case ($q_{sat,C18}=q_{sat,EPS}=500$ mg/ml). Additionally, the objective function increases with increasing q_{sat} (decreasing non-linearity in the given case). Trivially, moving away from extreme non-linear effects translates to lesser chromatogram overlap, thus resulting in higher yield of the target.

An important observation to be made here is that the optimal relative

length of C18 (x_{C18}) seem to depend only on the ratios of q_{sat} than their magnitudes. The cells corresponding to the first four rows and four columns in table 7.5 represents the q_{sat} combinations of 25, 50, 100 and 200 mg/ml. The tri-diagonal elements in this section (light gray, the middle and dark gray cells) represents configurations with fixed q_{sat} ratios (2, 1 and 0.5 respectively). The resulting optimal x_{C18} values corresponding to these cells seem to be consistent along the diagonals. This suggests that for the set of components with the kind of retention and selectivities considered, the optimal segment length ratio corresponding to the $Pr_{Ph}Y_{Ph}$ maximum depends greatly on the relative differences in segment non-linearities.

On the other hand, the segment order C18-EPS seem to dominate under the given separation factors in most of the cases. This in a way is related to the results found in section 6.3.1 (table 6.5), i.e. the improvement in the objective function noticed when the target in first segments co-elutes with its least retained neighbor. This dominance however is not seen in all cases (e.g. $q_{sat, EPS}=500$). This reverse order optima (EPS-C18) may be related to the faster retention and low non-linearity offered by the EPS segment.

7.5 Conclusions

It was attempted to identify a suitable experimental test system in order to elucidate the influence of using multiple stationary phases for preparative isolation of a target component from a multi-component mixture. The ternary system consisted of Cyclohexanone (C6), Phenol (Ph) and Cycloheptanone (C7). In all cases, a mobile phase composed of Methanol-Water (ratio 30-70) was used in combination with the classical C18 RP stationary phase and a similar alkyl-silica based phase consisting of an embedded amide group (EPS).

Basic trends seen from the theoretical results described in chapter 6 combining different stationary phases were demonstrated experimentally using the serial coupling concept. Preparative overloaded chromatograms using the two types of stationary phase showed considerable difference with change in segment lengths and order. In contrast, corresponding analytical separation profiles were hardly influenced by segment order.

Preliminary adsorption isotherm data of the components were estimated for both stationary phases. Using these data, the influence of isotherm non-linearities on the optimal coupling ratios and order of the preparative isolation of the intermediately eluting Phenol was analyzed. For the system considered, rather than the non-linearities expressed by columns saturation capacities themselves, their differences were found to significantly influence

Table 7.5: Dependency of optimal $P^{rPh}Y_{ph}$ [$\mu\text{g}/\text{cm}^2\text{min}$], V_{inj} [ml], x_{C18} and segment order isotherm non-linearities (q_{sat}). Light gray cells : $q_{sat,C18}/q_{sat,EPS} = 2$. Dark gray cells : $q_{sat,C18}/q_{sat,EPS} = 0.5$. See table 7.4 for the corresponding b_i values and chromatogram non-linearity parameters (λ_j).

$q_{sat,j}$ [mg/ml]	$q_{sat,EPS} = 25$ (highly non-linear)	$q_{sat,EPS} = 50$	$q_{sat,EPS} = 100$	$q_{sat,EPS} = 200$	$q_{sat,EPS} = 500$ (moderately non-linear)
$q_{sat,C18} = 25$ (highly non-linear)	$P^{rPh}Y_{ph} = 1933$ $V_{inj} = 0.014$ $x_{C18} = 0.455$ C18-EPS	$P^{rPh}Y_{ph} = 2316$ $V_{inj} = 0.016$ $x_{C18} = 0.515$ C18-EPS	$P^{rPh}Y_{ph} = 2582$ $V_{inj} = 0.037$ $x_{C18} = 0.739$ EPS-C18	$P^{rPh}Y_{ph} = 2696$ $V_{inj} = 0.026$ $x_{C18} = 0.725$ EPS-C18	$P^{rPh}Y_{ph} = 2860$ $V_{inj} = 0.019$ $x_{C18} = 0.496$ EPS-C18
	$P^{rPh}Y_{ph} = 2911$ $V_{inj} = 0.022$ $x_{C18} = 0.381$ C18-EPS	$P^{rPh}Y_{ph} = 3873$ $V_{inj} = 0.028$ $x_{C18} = 0.453$ C18-EPS	$P^{rPh}Y_{ph} = 4622$ $V_{inj} = 0.033$ $x_{C18} = 0.512$ C18-EPS	$P^{rPh}Y_{ph} = 5166$ $V_{inj} = 0.050$ $x_{C18} = 0.734$ EPS-C18	$P^{rPh}Y_{ph} = 5471$ $V_{inj} = 0.041$ $x_{C18} = 0.574$ C18-EPS
$q_{sat,C18} = 100$	$P^{rPh}Y_{ph} = 3869$ $V_{inj} = 0.031$ $x_{C18} = 0.296$ C18-EPS	$P^{rPh}Y_{ph} = 5802$ $V_{inj} = 0.044$ $x_{C18} = 0.369$ C18-EPS	$P^{rPh}Y_{ph} = 7606$ $V_{inj} = 0.056$ $x_{C18} = 0.451$ C18-EPS	$P^{rPh}Y_{ph} = 8984$ $V_{inj} = 0.064$ $x_{C18} = 0.514$ C18-EPS	$P^{rPh}Y_{ph} = 10599$ $V_{inj} = 0.099$ $x_{C18} = 0.725$ EPS-C18
$q_{sat,C18} = 200$	$P^{rPh}Y_{ph} = 5228$ $V_{inj} = 0.033$ $x_{C18} = 0.565$ C18-EPS	$P^{rPh}Y_{ph} = 7582$ $V_{inj} = 0.061$ $x_{C18} = 0.298$ C18-EPS	$P^{rPh}Y_{ph} = 11159$ $V_{inj} = 0.082$ $x_{C18} = 0.384$ C18-EPS	$P^{rPh}Y_{ph} = 14305$ $V_{inj} = 0.101$ $x_{C18} = 0.471$ C18-EPS	$P^{rPh}Y_{ph} = 17428$ $V_{inj} = 0.143$ $x_{C18} = 0.669$ EPS-C18
$q_{sat,C18} = 500$ (moderately non-linear)	$P^{rPh}Y_{ph} = 7730$ $V_{inj} = 0.048$ $x_{C18} = 0.593$ C18-EPS	$P^{rPh}Y_{ph} = 10962$ $V_{inj} = 0.068$ $x_{C18} = 0.569$ C18-EPS	$P^{rPh}Y_{ph} = 15332$ $V_{inj} = 0.097$ $x_{C18} = 0.533$ C18-EPS	$P^{rPh}Y_{ph} = 22183$ $V_{inj} = 0.157$ $x_{C18} = 0.400$ C18-EPS	$P^{rPh}Y_{ph} = 29334$ $V_{inj} = 0.195$ $x_{C18} = 0.5136$ C18-EPS

the optimal segment relative lengths. A theoretical analysis predicted that, with poor selectivity between Ph-C7 pairs in the EPS segment, not many optimal configurations were found with EPS as the preceding segment.

Another interesting concept would have been the combination of solvent and velocity gradients along with serial coupling of stationary phases. Analysis of such novel but rather sophisticated configurations including an experimental investigation is beyond the scope of this thesis. Using the generic analysis of the ternary system performed above and the tools developed, this work could serve as a base for further advanced investigations.

Chapter 8

Summary and conclusions

Preparative chromatographic separation of intermediately eluting components from multi-component mixtures are still a challenging task. Optimal production rates and yields are often insufficient or limited using conventional isocratic batch operations. In order to improve the performance, many alternate operating modes have been employed successfully by exploiting additional degrees of freedom. In this thesis, the potentials of few such configurations involving recycling chromatography, solvent gradients and multiple stationary phases were investigated. The theoretical studies involved were carried out primarily using ternary mixtures, representing multi-component separations in a generic way.

The quantitative evaluation of productivity or yield in preparative chromatography are critically dependent on the amount of target component collected, which in turn depend strongly on the fractionation times of the chromatogram. The focus in chapter 4, was on a general analysis of cut-time finding strategies for an intermediately eluting target. Two new cut-time optimization strategies were proposed, the first approach based on a continuous optimization (ContOpt) employed cubic splines to interpolate discrete chromatograms. The second strategy involved formulated the problem as a mixed integer non-linear programming problem (MINLP). The accuracy and efficiency of the two methods were compared with that of an established method based on evaluating local purities (LocPur). In case of a symmetric peaks, the LocPur and MINLP formulations yielded the same result, confirming the general validity of both approaches. In contrast, for complex cases involving non-linearities, the LocPur method resulted in suboptimal cut-time values. Irrespective of the drawback, the local purity based method benefits from its simplicity in implementation, resulting in the rapid estimation of sufficiently accurate cut-times. The discrete nature of the chromatograms imparts an equally discrete dependency of the estimated target mass on the grid size of the chromatograms. This characteristic is of crucial importance when gradient based optimizers are used later to maximize objective functions dependent on such cut-times. It was also found that the discontinuous dependencies can be eliminated to a certain extent by the ContOpt approach.

A new concept of combining gradient elution and closed-loop recycling (CLR-G) was introduced in chapter 5. Using the LocPur strategy introduced in chapter 4, the recovery yield and production rates of the intermediately eluting component of a ternary mixture were used as performance indices to compare the new method with conventional batch isocratic, gradient and isocratic closed-loop recycling (CLR-ISO) methods. By virtue of the recycling principle, larger amount of the target could be isolated using CLR-G and CLR-ISO schemes, resulting in better performance in comparison with the batch schemes. The CLR-G scheme also showed a distinct degree of outperformance over its closest competitor (CLR-ISO) when the separation factors between the target component and its two neighbors decreased with decreasing Henry coefficients as a result of increasing elution strength during the gradient. The improvement exploitable was found to depend strongly on the critically on the column regeneration time involved.

The study involving mobile phase gradients was followed by investigations on exploiting the separation potential of using multiple stationary phases. In chapter 6, the concept of coupling segments with different stationary phases in series has been extended to preparative separation using a theoretical study. By employing an objective function incorporating again both production rate and yield of intermediately eluting target components, the influence of segment order, relative lengths and injected sample volume has been studied. Owing to the underlying non-linearities, the segment order was found to have a profound influence on the objective function. Serial coupling was found to be particularly beneficial when the target nearly co-eluted with different neighbors in different segments. Further, placing the segment where the target co-elutes with the less retained neighbor before the segment with the opposite behavior, resulted in a noticeably higher separation performance. Even higher improvements in the objective functions were predicted by using an integrated approach of mechanically mixing stationary phases. The key parameter in such a configuration was the mixing ratio.

An experimental ternary test system consisting of two cycloketones and phenol was identified, which exhibited selectivity and retention difference on two alkyl-silica bonded phases. The general trends seen in serial coupling of stationary phases were demonstrated experimentally in chapter 7. Using adsorption isotherm data measured for the ternary system, the sensitivity of optimal relative length of segments on the isotherm non-linearities were analyzed. Rather than the degree of non-linearity of the isotherms of the stationary phases itself, their differences were found to influence the optimal segment orders and length significantly.

Exploring new operational concepts also leaves unanswered questions behind. The optimal cut-time finding algorithms in chapter 4 were evaluated

considering rather simple chromatograms. In more complex cases however, chromatograms could also exhibit multiple maxima in terms of local purities of the target. A wider comparison and development of the cut-time finding algorithms should consider this aspect. On the other hand, the complex separation scheme involving closed-loop recycling and an initial solvent gradient is open for experimental validation. It would also be worthwhile to investigate in future the preparative separation potential of a combined operational mode involving solvent and velocity gradients in addition to the specific degrees of freedom associated with multiple stationary phases. With this thesis, novel concepts were brought out for improved isolation of target components from multi-component mixtures using preparative chromatographic techniques.

Appendix A

Detector calibration and peak deconvolution

A.1 Detector calibration

Many isotherm determination methods including the inverse method and the frontal analysis require calibration factors. They are nothing but functional relationships between the detector response and the concentration of one or more substances in the detector flow cell. The relationship $C_i = f(S)$ although can any take form including non-linear ones, in this thesis, only linear relationships of the form [5]

$$C_i = k_{f,\lambda,i} S_\lambda \quad (\text{A.1})$$

are considered. In the above equation, $k_{f,\lambda,i}$ represents the calibration factor of a component i at a wavelength λ .

A.2 Finding calibration factors

Given this linear relationship holds, the $k_{f,i,\lambda}$ values are found from pulse injections of the individual components for each wavelengths. For example, figure A.1 shows detector responses at 287.4 and 302.6 nm for cyclohexanone (C6), phenol (Ph) and cycloheptanone (C7) pulse injections on the EPS column. $k_{f,i,\lambda}$ is then found from the chromatogram as per [5]:

$$k_{f,\lambda,i} = \frac{V_{inj} C_{inj,i}}{\dot{V}_f \cdot A_{\lambda,i}} \quad (\text{A.2})$$

where \dot{V}_f is the mobile phase flow rate. And $A_{\lambda,i}$, the peak area (of detector response) at a particular wavelength given by :

$$A_{\lambda,i} = \int_0^\infty S_\lambda \cdot t \quad (\text{A.3})$$

The linearity of the calibration found by equation A.2 can be checked by injecting the substance in incremental amounts and plotting the resulting peak area. Figure A.2 shows one such linearity plot (m_{inj} vs $A_{i,\lambda}$) for C6, Ph and C7. Out of the four wavelengths shown, the calibration factors are linear over the whole range for C7. Whereas for C6, wavelength 285.5 nm and 289.3nm are partially linear (upto $m_{inj} = 4$ mg). The response for phenol on the other hand is linear for the given wavelengths above 289.3 nm.

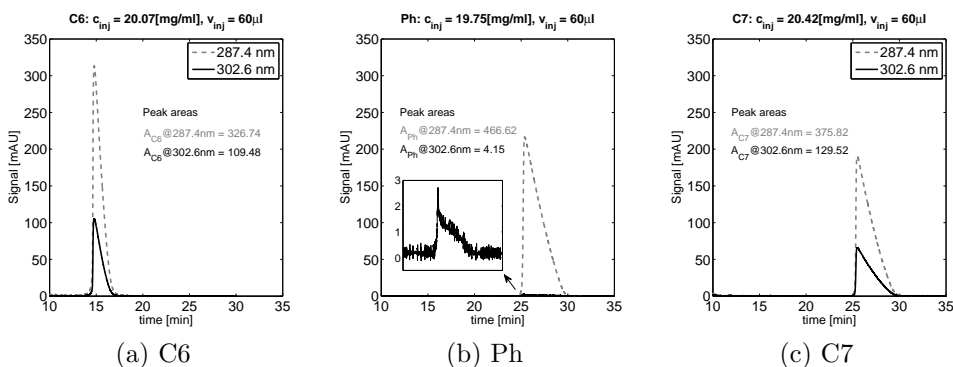


Figure A.1: Single component pulse injection responses for calculating $k_{f,i}$ on EPS column

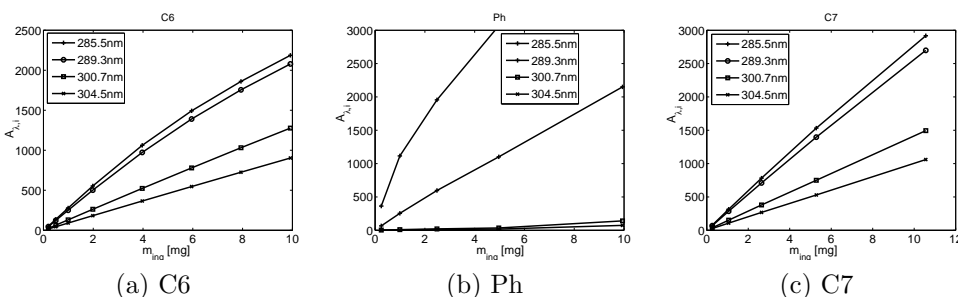


Figure A.2: Calibration curves at different wavelengths

A.3 Peak deconvolution

Examples in the previous section illustrate the fact that, under certain wavelengths, it is possible to disregard the response of one or more components. Given such a situation, selective component visibility or invisibility could be exploited to extract the individual concentration profiles of the components from the total detector signal.

Figure A.1 also shows the $A_{i,\lambda}$ values calculated (equation A.3) for $\lambda = 287.4$ and 302.6 nm respectively for C6, Ph and C7. It is important to note that phenol (Ph) has a very low detector response at $\lambda = 302.6$ nm. This is

characterized by a $A_{Ph,302.6}$ value of 4.15 [min.mAU] against its peak area at 287.4 nm (466.62 [min.mAU]). Since phenol elutes in between (C6 & C7) and as long as C6 and C7 do not overlap, this low detector response characteristic of Ph can be exploited to deconvolute the multi-component response.

Once the calibration factors $k_{f,i,\lambda}$ are known for each components at the two different λ s, a pre-determined volume of multi-component mixture with known concentration* can be injected to yield a multi-component response. Figure A.3a shows one such response for a 60 μ l injection at $\lambda = 287.4$ and 302.6 nm. The first well separated peak is the component C6 (appearing between 13 and 18 min). Whereas phenol and C7 peaks overlap entirely. Hence, calculation of the concentration vs time data for C6 is straight forward from the linear relationship given by equation A.1. Either of the $k_{f,i,\lambda}$ values could be used in this regard. The concentration profiles of Ph and C6 on the otherhand has to be calculated indirectly. Based on the fact that phenol is nearly invisible at 302.6 nm, C_{C7} can be calculated by :

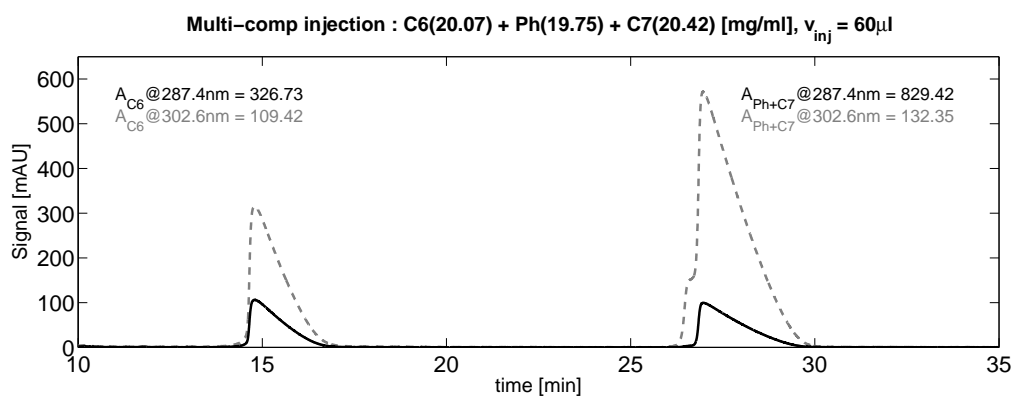
$$C_{C7} = k_{f,C7,302.6} \cdot S_{302.6} \quad (\text{A.4})$$

This newly found C7 profile could be used to calculate its contribution to signal at 287.4 nm (given by $C_{C7}/k_{f,C7,287.4}$). This value could in turn be subtracted from the total detector response at the same wavelength to deduce the response generated by phenol, which can then be used to calculate C_{Ph} . This step is given as :

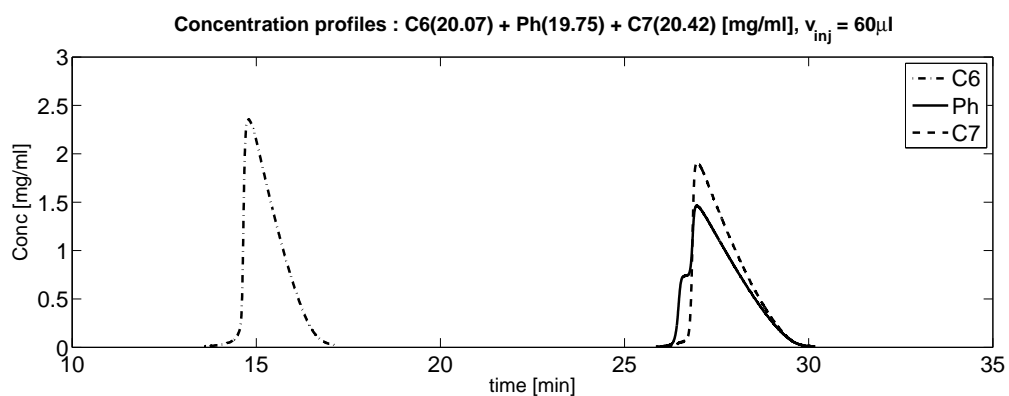
$$C_{Ph} = k_{f,Ph,287.4} \cdot \left(S_{287.4} - \frac{C_{C7}}{k_{f,C7,287.4}} \right) \quad (\text{A.5})$$

The resulting deconvoluted concentration profiles for the example shown in figures A.1 and A.3a is given in figure A.3b.

*Injected volume and concentrations has to be carefully chosen such that, the detector response is always in the linear range



(a) Detector response



(b) Deconvoluted concentration profiles

Figure A.3: An example of deconvolution of concentration profiles (three components) from total detector response

References

- [1] M. Tswett. Physikalisch-chemische Studien über das Chlorophyll. Die Adsorptionen. *Berichte der Deutschen Botanischen Gesellschaft*, 24: 316–323, 1906.
- [2] L. S. Ettre. *Chapters in the Evolution of Chromatography*. Imperial College Press, 2008.
- [3] L. R. Snyder, J. J. Kirkland, and J. W. Dolan. *Introduction to Modern Liquid Chromatography*. Wiley, 2009.
- [4] J. Cazes. *Encyclopedia of Chromatography 2004 Update Supplement*. CRC, 2004.
- [5] H. Schmidt-Traub. *Preparative Chromatography: of Fine Chemicals and Pharmaceutical Agents*. Wiley-VCH, 2005.
- [6] C. Horvath and H.J. Lin. Band spreading in liquid-chromatography - general plate height equation and a method for evaluation of individual plate height contributions. *Journal of Chromatography*, 149:43–70, 1978.
- [7] C. Horvath, W. Melander, and I. Molnar. Solvophobic interactions in liquid-chromatography with nonpolar stationary phases. *Journal of Chromatography*, 125(1):129–156, 1976.
- [8] K. J. Bombaugh and R. F. Levangie. High resolution preparative liquid chromatography using recycle. *Journal of Chromatographic Science*, 8: 560, 1970.
- [9] A. Seidel-Morgenstern and G. Guiochon. Theoretical study of recycling in preparative chromatography. *AIChE Journal*, 39:809–819, 1993.
- [10] J. Dingenen and J. N. Kinkel. Preparative chromatographic resolution of racemates on chiral stationary phases on laboratory and production scales by closed-loop recycling chromatography. *Journal of Chromatography A*, 666:627–650, 1994.
- [11] J. A. Biesenberger, M. Tan, I. Duvdevani, and T. Maurer. Recycle gel permeation chromatography. I. Recycle principle and design. *Journal of Polymer Science, Part B: Polymer Letters*, 9:353–357, 1971.

- [12] I. Duvdevani, J. A. Biesenberger, and M. Tan. Recycle gel permeation chromatography .3. Design modifications and some results with polycarbonate. *Journal of Polymer Science, Part B: Polymer Letters*, 9: 429, 1971.
- [13] C. Heuer, A. Seidel-Morgenstern, and P. Hugo. Experimental investigation and modeling of closed-loop recycling in preparative chromatography. *Chemical Engineering Science*, 50:1115–1127, 1995.
- [14] C. M. Grill. Closed-loop recycling with periodic intra-profile injection: a new binary preparative chromatographic technique. *Journal of Chromatography A*, 796:101–113, 1998.
- [15] H. K. Teoh, E. Sorensen, and N. Titchener-Hooker. Optimal operating policies for closed-loop recycling hplc processes. *Chemical Engineering Science*, 58:4145–4158, 2003.
- [16] M. Bailly and D. Tondeur. 2-way chromatography - flow reversal in non-linear preparative liquid-chromatography. *Chemical Engineering Science*, 36:455–469, 1981.
- [17] M. Bailly and D. Tondeur. Recycle optimization in non-linear productive chromatography .1. mixing recycle with fresh feed. *Chemical Engineering Science*, 37:1199–1212, 1982.
- [18] J. R. Crary, K. Cain-Janicki, and R. Wijayarathne. External recycle chromatography: A practical method for preparative purifications. *Journal of Chromatography A*, 462:85–94, 1989.
- [19] C. M. Grill and L. Miller. Separation of a racemic pharmaceutical intermediate using closed-loop steady state recycling. *Journal of Chromatography A*, 827:359–371, 1998.
- [20] C. A. Grill, L. Miller, and T. Q. Yan. Resolution of a racemic pharmaceutical intermediate - a comparison of preparative HPLC, steady state recycling, and simulated moving bed. *Journal of Chromatography A*, 1026:101–108, 2004.
- [21] J. H. Kennedy, M. D. Belvo, V. S. Sharp, and J. D. Williams. Comparison of separation efficiency of early phase active pharmaceutical intermediates by steady state recycle and batch chromatographic techniques. *Journal of Chromatography A*, 1046:55–60, 2004.
- [22] T. Q. Yan and C. Orihuela. Rapid and high throughput separation technologies - steady state recycling and supercritical fluid chromatography for chiral resolution of pharmaceutical intermediates. *Journal of Chromatography A*, 1156:220–227, 2007.

- [23] T. Sainio and M. Kaspereit. Analysis of steady state recycling chromatography using equilibrium theory. *Separation and Purification Technology*, 66:9–18, 2009.
- [24] J. W. Lee and P. C. Wankat. Optimized design of recycle chromatography to isolate intermediate retained solutes in ternary mixtures: Langmuir isotherm systems. *Journal of Chromatography A*, 1216:6946–6956, 2009.
- [25] F. Charton, M. Bailly, and G. Guiochon. Recycling in preparative liquid chromatography. *Journal of Chromatography A*, 687:13–31, 1994.
- [26] G. Cretier and J. L. Rocca. Gradient elution in preparative reversed-phase liquid chromatography. *Journal of Chromatography A*, 658:195–205, 1994.
- [27] A. Felinger and G. Guiochon. Optimizing experimental conditions in overloaded gradient elution chromatography. *Biotechnology Progress*, 12:638–644, 1996.
- [28] T. M. Phillips and P. M. Phillips. *Handbook of HPLC, Second Edition (Chromatographic Science Series)*. CRC Press, 2010.
- [29] G.A. Howard and A.J.P. Martin. The separation of the c-12-c-18 fatty acids by reversed-phase partition chromatography. *Biochemical Journal*, 46:532–538, 1950.
- [30] L. R. Snyder. Principles of gradient elution. *Chromatographic Reviews*, 7:1 – 51, 1965.
- [31] S. R. Gallant, S. Vunnum, and S. M. Cramer. Optimization of preparative ion-exchange chromatography of proteins: Linear gradient separations. *Journal of Chromatography A*, 725:295–314, 1996.
- [32] A. Felinger and G. Guiochon. Comparing the optimum performance of the different modes of preparative liquid chromatography. *Journal of Chromatography A*, 796:59–74, 1998.
- [33] P. Jandera, D. Komers, and G. Guiochon. Optimization of the recovery yield and of the production rate in overloaded gradient-elution reversed-phase chromatography. *Journal of Chromatography A*, 796:115–127, 1998.
- [34] P. Jandera. Simultaneous optimisation of gradient time, gradient shape and initial composition of the mobile phase in the high-performance liquid chromatography of homologous and oligomeric series. *Journal of Chromatography A*, 845:133–144, 1999.

- [35] Y. C. Shan and A. Seidel-Morgenstern. Optimization of gradient elution conditions in multicomponent preparative liquid chromatography. *Journal of Chromatography A*, 1093:47–58, 2005.
- [36] P. Jandera and J. Churáček. *Gradient elution in column liquid chromatography : theory and practice*. Elsevier, 1985.
- [37] C. T. Mant and R. S. Hodges. Mixed-mode hydrophilic interaction/cation-exchange chromatography (HILIC/CEX) of peptides and proteins. *Journal of Separation Science*, 31:2754–2773, 2008.
- [38] A. J. Alpert. Hydrophilic-interaction chromatography for the separation of peptides, nucleic-acids and other polar compounds. *Journal Of Chromatography*, 499:177–196, 1990.
- [39] E. Hartmann, Y. X. Chen, C. T. Mant, A. Jungbauer, and R. S. Hodges. Comparison of reversed-phase liquid chromatography and hydrophilic interaction/cation-exchange chromatography for the separation of amphipathic alpha-helical peptides with l- and d-amino acid substitutions in the hydrophilic face. *Journal of Chromatography A*, 1009:61–71, 2003.
- [40] J. R. Litowski, P. D. Semchuk, C. T. Mant, and R. S. Hodges. Hydrophilic interaction/cation-exchange chromatography for the purification of synthetic peptides from closely related impurities: serine side-chain acetylated peptides. *Journal of Peptide Research*, 54:1–11, 1999.
- [41] F. Erni and R. W. Frei. 2-dimensional column liquid-chromatographic technique for resolution of complex-mixtures. *Journal of Chromatography*, 149(FEB):561–569, 1978. 17.
- [42] D. R. Stoll, X. P. Li, X. O. Wang, P. W. Carr, S. E. G. Porter, and S. C. Rutan. Fast, comprehensive two-dimensional liquid chromatography. *Journal of Chromatography A*, 1168(1-2):3–43, October 2007.
- [43] M.M. Bushey and J.W. Jorgenson. Automated instrumentation for comprehensive 2-dimensional high-performance liquid-chromatography of proteins. *Analytical Chemistry*, 62:161–167, 1990.
- [44] P. Jandera. Stationary phases for hydrophilic interaction chromatography, their characterization and implementation into multidimensional chromatography concepts. *Journal of Separation Science*, 31(9):1421–1437, May 2008.
- [45] A.P. Kohne, U. Dornberger, and T. Welsch. Two-dimensional high performance liquid chromatography for the separation of complex mixtures of explosives and their by-products. *Chromatographia*, 48:9–16, 1998.

- [46] A.J. Link. Multidimensional peptide separations in proteomics. *Trends in Biotechnology*, 20:S8–S13, 2002.
- [47] H. J. Issaq, K. C. Chan, G. M. Janini, T. P. Conrads, and T. D. Veenstra. Multidimensional separation of peptides for effective proteomic analysis. *Journal of Chromatography B-Analytical Technologies in the Biomedical and Life Sciences*, 817(1):35–47, March 2005.
- [48] L. I. Mondello. *Multidimensional Chromatography*. Oxford University Press, Oxford Oxfordshire, 2002.
- [49] S. Nyiredy, Z. Szucs, and L. Szepesy. Stationary-phase optimized selectivity lc (sos-lc): Separation examples and practical aspects. *Chromatographia*, 63:S3–S9, 2006.
- [50] S. Nyiredy, Z. Szucs, and L. Szepesy. Stationary phase optimized selectivity liquid chromatography: Basic possibilities of serially connected columns using the "prisma" principle. *Journal of Chromatography A*, 1157:122–130, 2007.
- [51] K. Bischoff, S. Nyiredy, and Z. Szucs. Elements for separating substances by distributing between a stationary and a mobile phase, and method for the production of a separating device, 2006. WO/2006/125564; PCT/EP2006/004744.
- [52] G. Guiochon. Preparative liquid chromatography. *Journal of Chromatography A*, 965:129–161, 2002.
- [53] G. Guiochon and B. Lin. *Modeling for Preparative Chromatography*. Academic Press, Boston, 2003.
- [54] G. Guiochon, G. Shirazi, A. Felinger, and A. M. Katti. *Fundamentals of Preparative and Nonlinear Chromatography*. Academic Press Inc., U.S., 2006.
- [55] A. J. P. Martin and R. L. M. Synge. A new form of chromatogram employing two liquid phases i. a theory of chromatography 2. application to the micro-determination of the higher monoamino-acids in proteins. *Biochemical Journal*, 35:1358–1368, 1941.
- [56] L. C. Craig. Identification of small amounts of organic compounds by distribution studies II. Separation by counter-current distribution. *J. Biol. Chem.*, 155:519–534, 1944.
- [57] S. Golshan-Shirazi and G. Guiochon. Comparison of the various kinetic models of non-linear chromatography. *Journal of Chromatography A*, 603:1–11, 1992.
- [58] J. C. Giddings. *Dynamics of Chromatography*. Dekker, New York, 1965.

- [59] J. C. Giddings and H. Eyring. A molecular dynamic theory of chromatography. *Journal of Physical Chemistry*, 59(5):416–421, 1955.
- [60] F. Dondi and M. Remelli. The characteristic function-method in the stochastic-theory of chromatography. *Journal of Physical Chemistry*, 90(9):1885–1891, April 1986.
- [61] A. Seidel-Morgenstern. *Mathematische Modellierung der präparativen Flüssigchromatographie*. Deutscher Universitätsverlag, Wiesbaden, 1995.
- [62] P. Rouchon, M. Schonauer, P. Valentin, and G. Guiochon. Numerical-simulation of band propagation in nonlinear chromatography. *Separation Science and Technology*, 22:1793–1833, 1987.
- [63] J.J. Vandemter, F.J. Zuiderweg, and A. Klinkenberg. Longitudinal diffusion and resistance to mass transfer as causes of nonideality in chromatography. *Chemical Engineering Science*, 5:271–289, 1956.
- [64] D. Ruthven. *Principles of Adsorption and Adsorption Processes*. Wiley, 1984.
- [65] K. Mihlbachler, K. Kaczmarski, A. Seidel-Morgenstern, and G. Guiochon. Measurement and modeling of the equilibrium behavior of the troger’s base enantiomers on an amylose-based chiral stationary phase. *Journal of Chromatography A*, 955:35–52, 2002.
- [66] A. Seidel-Morgenstern. Experimental determination of single solute and competitive adsorption isotherms. *Journal of Chromatography A*, 1037:255–272, 2004.
- [67] D. Antos and A. Seidel-Morgenstern. Application of gradients in the simulated moving bed process. *Chemical Engineering Science*, 56:6667–6682, 2001.
- [68] D. Antos and A. Seidel-Morgenstern. Two-step solvent gradients in simulated moving bed chromatography - numerical study for linear equilibria. *Journal of Chromatography A*, 944:77–91, 2002.
- [69] E. Soczewinski. Solvent composition effects in thin-layer chromatography systems of type silica gel-electron donor solvent. *Analytical Chemistry*, 41:179, 1969.
- [70] O. Lisec, P. Hugo, and A. Seidel-Morgenstern. Frontal analysis method to determine competitive adsorption isotherms. *Journal of Chromatography A*, 908:19–34, 2001.
- [71] F. G. Helfferich and P. W. Carr. Nonlinear-waves in chromatography .1. waves, shocks, and shapes. *Journal of Chromatography*, 629:97–122, 1993.

- [72] C. T Kelley. *Iterative Methods for Linear and Nonlinear Equations*. Society for Industrial Mathematics, 1987.
- [73] S.K. Godunov. A finite difference method for the numerical computation and discontinuous solutions of the equations of fluid dynamics. *Matematicheskii Sbornik*, 47:271–306, 1959. In Russian.
- [74] S. Golshan-Shirazi and G. Guiochon. *Theoretical Advancement in Chromatography and Related Separation Techniques*, volume 383 of *NATO ASI, Series C*. Kluwer, Dordrecht, 1992.
- [75] Anurag Rathore. *Scale-up and Optimization in Preparative Chromatography: Principles and Biopharmaceutical Applications*. Marcel Dekker Inc, New York, 2002.
- [76] A Felinger and G Guiochon. Optimization of the experimental conditions and the column design parameters in overloaded elution chromatography. *Journal of Chromatography*, 591:31–45, 1992.
- [77] J. Nocedal. *Numerical Optimization*. Springer Science+Business Media, LLC, Norwell, 2006.
- [78] L. T. Biegler, O. Ghattas, M. Heinkenschloss, D. Keyes, and B. van Bloemen Waanders. *Real-Time PDE-Constrained Optimization (Computational Science and Engineering)*. Society for Industrial and Applied Mathematics, Philadelphia, PA, USA, 2007.
- [79] M. Fisher, J. Nocedal, Y. Tremolet, and S. J. Wright. Data assimilation in weather forecasting: a case study in pde-constrained optimization. *Optimization and Engineering*, 10:409–426, 2009.
- [80] S. Hazra. *Large-Scale Pde-Constrained Optimization in Applications*. Springer, Berlin, 2010.
- [81] M. Hinze. *Optimization with Pde Constraints*. Springer, Berlin, 2008.
- [82] K. Morton. *Numerical Solution of Partial Differential Equations*. Cambridge University Press, Cambridge, 1994.
- [83] L. T. Biegler, O. Ghattas, M. Heinkenschloss, and B. van Bloemen Waanders. *Large-Scale PDE-Constrained Optimization*. Springer, Berlin, 2003.
- [84] A. Nebro, E. Alba, and F. Luna. Multi-objective optimization using grid computing. *Soft Computing - A Fusion of Foundations, Methodologies and Applications*, 11:531–540, 2007.
- [85] A. Felinger and G. Guiochon. Optimizing preparative separations at high recovery yield. *Journal of Chromatography A*, 752:31–40, 1996.

- [86] B. Sreedhar and A. Seidel-Morgenstern. Preparative separation of multi-component mixtures using stationary phase gradients. *Journal of Chromatography A*, 1215:133 – 144, 2008.
- [87] K. Lee. *Modern Heuristic Optimization Techniques*. IEEE Press, New York, 2008.
- [88] I.S. Osman and J.P. Kelly. *Meta-Heuristics: Theory and Applications*. Springer, 1996.
- [89] D. Nagrath, A. Messac, B. W. Bequette, and S. M. Cramer. A hybrid model framework for the optimization of preparative chromatographic processes. *Biotechnology Progress*, 20:162–178, 2004.
- [90] G. Ziomek and D. Antos. Stochastic optimization of simulated moving bed process - sensitivity analysis for isocratic and gradient operation. *Computers & Chemical Engineering*, 29:1577–1589, 2005.
- [91] G Ziomek, D Antos, L Tobiska, and A Seidel-Morgenstern. Comparison of possible arrangements of five identical columns in preparative chromatography. *Journal of Chromatography A*, 1116:179–188, 2006.
- [92] G Ziomek, M Kaspereit, JJ Jezowski, A Seidel-Morgenstern, and D Antos. Effect of mobile phase composition on the smb processes efficiency stochastic optimization of isocratic and gradient operation. *Journal of Chromatography A*, 1070:111–124, 2005.
- [93] B. Sreedhar, A. Damtew, and A. Seidel-Morgenstern. Theoretical study of preparative chromatography using closed-loop recycling with an initial gradient. *Journal of Chromatography A*, 1216:4976 – 4988, 2009.
- [94] Y. Kawajiri and L.T. Biegler. Optimization strategies for simulated moving bed and powerfeed processes. *AIChE Journal*, 52:1343–1350, 2006.
- [95] Y. C. Shan and A. Seidel-Morgenstern. Analysis of the isolation of a target component using multicomponent isocratic preparative elution chromatography. *Journal of Chromatography A*, 1041:53–62, 2004.
- [96] L. Lapidus and N.R. Amundson. The rate-determining steps in radial adsorption analysis. *Journal of Physical Chemistry*, 56:373–383, 1952.
- [97] G Houghton. Band shapes in non-linear chromatography with axial dispersion. *Journal of Physical Chemistry*, 67:84, 1963.
- [98] P.C. Haarhoff and H.J. Van der Linde. Concentration dependence of elution curves in non-ideal gas chromatography. *Analytical Chemistry*, 38:573, 1966.

- [99] S. Golshan-shirazi and G. Guiochon. Solutions of the equilibrium and semiequilibrium models of chromatography. *Journal of Chromatography*, 506:495–545, 1990.
- [100] V.B. Marco and G.G. Bombi. Mathematical functions for the representation of chromatographic peaks. *Journal of Chromatography A*, 931:1–30, 2001.
- [101] C. de Boor. *A Practical Guide to Splines*. Springer, Berlin, 2001.
- [102] A. Felinger. *Data Analysis and Signal Processing in Chromatography*. Elsevier, Amsterdam, 1998.
- [103] R.D.B. Fraser and E. Suzuki. Resolution of overlapping absorption bands by least squares procedures. *Analytical Chemistry*, 38:1770, 1966.
- [104] A.V. Pirogov, O.N. Obrezkov, and O.A. Shpigun. Chromatogram generator chromatogram modeling software. *Journal of Chromatography A*, 706:31–36, 1995.
- [105] R. Davies. *Statistical Models of Shape*. Springer, Berlin, 2008.
- [106] Neos server for optimization. <http://www-neos.mcs.anl.gov/>.
- [107] R. Fourer, D.M. Gay, and B.W. Kernighan. *AMPL: A Modeling Language for Mathematical Programming*. Thomson/Brooks/Cole, South Melbourne, 2003.
- [108] T. Lastusilta, M. R. Bussieck, and T. Westerlund. An experimental study of the gams/alphaecp minlp solver. *Industrial & Engineering Chemistry Research*, 48:7337–7345, 2009.
- [109] P. Jandera. A method for characterization and optimization of reversed-phase liquid-chromatographic separations based on the retention behavior in homologous series. *Chromatographia*, 19:101–112, 1984.
- [110] M. Kele and G. Guiochon. Repeatability and reproducibility of retention data and band profiles on reversed-phase liquid chromatography columns iii. results obtained with kromasil c-18 columns. *Journal of Chromatography A*, 855:423–453, 1999.
- [111] J. J. Gilroy, J. W. Dolan, and L. R. Snyder. Column selectivity in reversed-phase liquid chromatography - iv. type-b alkyl-silica columns. *Journal of Chromatography A*, 1000:757–778, 2003.
- [112] S. Kayillo, G. R. Dennis, and R. A. Shalliker. An assessment of the retention behaviour of polycyclic aromatic hydrocarbons on reversed phase stationary phases: Selectivity and retention on c18 and phenyl-type surfaces. *Journal of Chromatography A*, 1126:283–297, 2006.

- [113] J. Y. Wu, W. G. Bicker, and W. G. Lindner. Separation properties of novel and commercial polar stationary phases in hydrophilic interaction and reversed-phase liquid chromatography mode. *Journal of Separation Science*, 31:1492–1503, 2008.
- [114] D. Goldberg. *Genetic Algorithms in Search, Optimization, and Machine Learning*. Addison-Wesley, Boston, 1989.
- [115] G. Vivo-Truyols, J.R. Torres-Lapasio, and M.C. Garcia-Alvarez-Coque. A hybrid genetic algorithm with local search: I. discrete variables: optimisation of complementary mobile phases. *Chemometrics and Intelligent Laboratory Systems*, 59:89–106, 2001.
- [116] Z.Y. Zhang, K. Hidajat, A.K. Ray, and M. Morbidelli. Multiobjective optimization of smb and varicol process for chiral separation. *AIChE Journal*, 48:2800–2816, 2002.
- [117] T. Zhang and E. Francotte. Chromatographic properties of composite chiral stationary phases based on cellulose derivatives. *Chirality*, 7: 425–433, 1995.
- [118] M. De Beer, F. Lynen, K. Chen, P. Ferguson, M. Hanna-Brown, and P. Sandra. Stationary-phase optimized selectivity liquid chromatography: Development of a linear gradient prediction algorithm. *Analytical Chemistry*, 82:1733–1743, 2010.
- [119] M. De Beer, F. Lynen, M. Hanna-Brown, and P. Sandra. Multiple step gradient analysis in stationary phase optimised selectivity lc for the analysis of complex mixtures. *Chromatographia*, 69:609–614, 2009.

Curriculum Vitae

Personal details

Name	• Balamurali Sreedhar
Date of birth	• 12 February 1982
Place of birth	• Thiruvalla-Kerala, India
Address	• Rogätzerstr. 5a, 39106 Magdeburg
Nationality	• Indian
Marital status	• Married

Schooling

06/1987-03/1997	• Christian High School, Udupi, India
08/1997-03/1999	• Milagres College, Kallianpur, India

Education

10/1999-06/2003	• Bachelor of Engineering in Chemical Engineering, R.V. College of Engineering, Bangalore, India
10/2004-01/2007	• Master of Science in Chemical and Process Engineering, Otto von Guericke University, Magdeburg

Work Experience

10/2003-08/2004	• On contract for National Bureau of Soil Survey and Land Use Planning, Bangalore, India
03/2007-01/2011	• Max Planck Institute for Dynamics of Complex Technical Systems